

การศึกษาแบบเฟสตัดัพรินซิเพิลของความบกพร่องแบบซับซ้อนที่คัดเลือก
ในสารกึ่งตัวนำ

นายภาคภูมิ เรือนจันทร์

วิทยานิพนธ์นี้เป็นส่วนหนึ่งของการศึกษาตามหลักสูตรปริญญาวิทยาศาสตรดุษฎีบัณฑิต
สาขาวิชาฟิสิกส์
มหาวิทยาลัยเทคโนโลยีสุรนารี
ปีการศึกษา 2552

**FIRST-PRINCIPLES STUDY OF SELECTED DEFECT
COMPLEXES IN SEMICONDUCTORS**

Pakpoom Reunchan

**A Thesis Submitted in Partial Fulfillment of the Requirements for the
Degree of Doctor of Philosophy in Physics
Suranaree University of Technology
Academic Year 2009**

FIRST-PRINCIPLES STUDY OF SELECTED DEFECT COMPLEXES IN SEMICONDUCTORS

Suranaree University of Technology has approved this thesis submitted in partial fulfillment of the requirements for the Degree of Doctor of Philosophy.

Thesis Examining Committee

(Asst. Prof. Dr. Chinorat Kobdaj)

Chairperson

(Prof. Dr. Sukit Limpijumnong)

Member (Thesis Advisor)

(Dr. Anderson Janotti)

Member

(Dr. Malliga Suewattana)

Member

(Dr. Saroj Rujirawat)

Member

(Prof. Dr. Pairote Sattayatham)

Vice Rector of Academic Affairs

(Assoc. Prof. Dr. Prapun Manyum)

Dean of Institute of Science

ภาคภูมิ เรือนจันทร์ : การศึกษาแบบเฟิสต์พริ้นซิเพิลของความบกพร่องแบบซับซ้อนที่
คัดเลือกในสารกึ่งตัวนำ (FIRST-PRINCIPLES STUDY OF SELECTED DEFECT
COMPLEXES IN SEMICONDUCTORS)

อาจารย์ที่ปรึกษา : ศาสตราจารย์ ดร. ชูกิจ ลิ้มปิงานงค์, 173 หน้า.

ความบกพร่องมูลฐานแบบเฉพาะที่ สารเจือ และความบกพร่องแบบซับซ้อนที่รวมความ
บกพร่องมูลฐานและสารเจือ มีบทบาทสำคัญอย่างยิ่งในสารกึ่งตัวนำ ในวิทยานิพนธ์นี้ ได้มี
การศึกษาความบกพร่องแบบซับซ้อนหลายแบบในสารกึ่งตัวนำหลายชนิดเชิงทฤษฎีโดยอาศัยการ
คำนวณแบบเฟิสต์พริ้นซิเพิลบนพื้นฐานของวิธีฟังก์ชันนัลของความหนาแน่น สมบัติหลักของความ
บกพร่องที่ศึกษาได้แก่ เสถียรภาพทางพลังงาน โครงสร้างสถานะพลังงานอิเล็กทรอนิกส์ และในบาง
กรณีได้ศึกษาสมบัติทางพลศาสตร์ด้วย ระบบความบกพร่องแบบซับซ้อนที่ได้ทำการศึกษาได้แก่
(1) ความบกพร่องแบบซับซ้อนระหว่างอะตอม Zn แบบเกิน และ อะตอม N แบบแทนที่ ในผลึก
ZnO ซึ่งความบกพร่องแบบซับซ้อนดังกล่าว มีสมบัติสอดคล้องกับโดเนอร์ที่พบในตัวอย่างที่ผ่าน
การยิงด้วยอิเล็กตรอนพลังงานสูง (2) ความบกพร่องชนิดซับซ้อนระหว่างซิลิกอน และ ไนโตรเจน
ในไดลูตไนไตรด์ ($\text{GaAs}_{1-x}\text{N}_x$) (การคำนวณพบว่าอะตอมของ Si และ N ชอบที่จะจับตัวกันในรูปแบบ
ชนิดสปลิท-อินเตอร์สติเชียล ซึ่งสอดคล้องกับการทดลองที่พบว่า Si และ N หักล้างผลซึ่งกันและ
กัน) (3) ความบกพร่องชนิดซับซ้อนระหว่างคาร์บอน และ ไนโตรเจน ในผลึก GaAs และ GaP
(ความถี่การสั่นที่ได้จากการคำนวณของโมเลกุล CN ที่แทนที่แอนไอออน สอดคล้องกับสเปกตรัม
แสงใต้แดงที่ได้จากการทดลอง)

PAKPOOM REUNCHAN : FIRST-PRINCIPLES STUDY OF SELECTED
DEFECT COMPLEXES IN SEMICONDUCTORS. THESIS ADVISOR :
PROF. SUKIT LIMPIJUMNONG, Ph.D. 173 PP.

FIRST-PRINCIPLES/DEFECTS/SEMICONDUCTORS

Native point defects, impurities and also their complexes play a crucial role in semiconductors. In this thesis, several defect complexes in a number of semiconductors were theoretically studied using first-principles methods based on density functional theory. The main properties studied include energetic stability, electronic structures, and in some cases the dynamic behaviors. The studied defect systems are: (1) the complex between Zn interstitial and N substitution in ZnO which is consistent with the donor observed in electron irradiated ZnO samples, (2) the split-interstitial Si-N complex in dilute nitrides ($\text{GaAs}_{1-x}\text{N}_x$) (The Si-N in the split-interstitial form is consistent with the mutual passivation experiments), (3) carbon-nitrogen complex in GaAs and GaP (The calculated vibration frequencies of substitutional CN molecule is consistent with the observed infrared spectroscopy).

School of Physics

Academic Year 2009

Student's Signature _____

Advisor's Signature _____

ACKNOWLEDGEMENTS

First of all, I am very grateful to my advisor Prof. Dr. Sukit Limpijumnong for his great advisory, kind patience, inspiration, and fruitful instructions to me as a young student since six years ago. He and his wife Rissada always have friendship and kindly support for me. I would like to thank Prof. Dr. Chris Van de Walle for his kindness accepting me to join his group for almost a year where I learn, be encouraged and obtain great knowledge. I also thank Dr. Anderson Janotti very much for his great advices and educations both in academic research and living. He also made my day easier when I was struggling in something back in USA and even Thailand. I would like to thank Asst. Prof. Dr. Chinorat Kobdaj, Dr. Saroj Rujirawat and Dr. Malliga Suewattana for contributing as my advisory committee members. Part of this work was performed during my visit at Materials department and Material Research Laboratory (MRL), University of California Santa Barbara. I also want to thank California NanoSystems Institute (CNSI), MRL and Synchrotron Light Research Institute, Thailand (SLRI) for their hospitality and computational resources. I am deeply grateful to Development and Promotion of Science and technology Talents project (DPST) and Royal Golden Jubilee program Ph.D. (RGJ) for their funding supports. I also appreciate friendship from J. Weber and J. Varley when I was in the states. Importantly, my study would not be completed with out supports and warm advices from the faculties of the School of Physics, Suranaree University of Technology. I also thank to all of my good friends back in high school, undergrad and especially members in our research group: Dr. Sirichok Jungthawan, Dr. Kanoknan

Sarasamak, Dr. Jiraroj T.-Theinprasert, and Sutassana Na-Phattalung. Most importantly, without great support from my dad, mom, sisters and Szu-Yin Yeh, I probably stuck in somewhere on my way to accomplish the degree, thank all.

Pakpoom Reunchan

CONTENTS

	Page
ABSTRACT IN THAI.....	IV
ABSTRACT IN ENGLISH	V
ACKNOWLEDGEMENTS.....	VI
CONTENTS.....	VIII
LIST OF TABLES.....	XII
LIST OF FIGURES	XIV
LIST OF ABBREVIATIONS.....	XX
CHAPTER	
I INTRODUCTION.....	1
II THEORETICAL METHODS	7
2.1 Many Electrons Problems in Solids.....	7
2.2 Density Functional Theory	9
2.2.1 The Hohenberg-Kohn (HK) theorem.....	9
2.2.2 The Kohn-Sham (KS) equations.....	10
2.3 The Exchange Correlation Energy.....	13
2.3.1 The local density approximation (LDA).....	14
2.3.2 The generalized gradient approximation (GGA)	15
2.3.3 LDA+ U	16
2.4 Plane Wave Pseudopotential Method	18
2.4.1 Norm-conserving pseudopotential.....	22

CONTENTS (Continued)

	Page
2.4.2 Ultrasoft pseudopotential (USPP).....	23
2.4.3 Projector augmented-wave method (PAW)	23
2.5 Force Acting on Nuclei	24
2.6 Periodic Boundary Conditions and Brillouin Zone Sampling	25
III CALCULATION METHODS FOR DEFECTS IN	
SEMICONDUCTORS	28
3.1 Defect Concentration	28
3.2 Defect Formation Energy	30
3.3 Chemical Potentials	31
3.4 Supercell Approach.....	33
3.4.1 Supercell for the wurtzite structure.....	33
3.4.2 Supercell for the zincblende structure.....	35
3.4.3 Finite-size corrections	36
3.5 Defect Transition Levels.....	37
3.5.1 Thermodynamic transition levels.....	37
3.5.2 Optical transition levels	39
3.6 Formation of Defect Complexes	41
3.7 Diffusivity, Migration and Minimum Energy Paths.	42
IV NATIVE-DEFECT-RELATED COMPLEX DONORS IN	
<i>n</i>-TYPE ZnO	44
4.1 Introduction.....	44

CONTENTS (Continued)

		Page
4.2	Computational Method	46
4.3	Results and Discussion	48
4.3.1	Defect structure and formation energy	48
4.3.2	Defect concentration analysis	53
4.4	Summary	58
V	MUTUAL PASSIVATION OF ELECTRICALLY ACTIVE AND	
	ISOVALENT IMPURITIES IN DILUTE NITRIDES.....	60
5.1	Introduction.....	60
5.2	Computational Approach.....	64
5.3	Results and Discussion	66
5.3.1	Group-IV donors and isovalent N in GaAs.....	67
5.3.2	Former model: (X) _{Ga} -N _{As} complexes	68
5.3.3	Proposed model: Split-interstitial complex.....	74
5.4	Summary	83
VI	CARBON-NITROGEN MOLECULES IN GALLIUM ARSENIDE	
	AND GALLIUM PHOSPHIDE.....	84
6.1	Introduction.....	84
6.2	Computational Method	86
6.3	Results and Discussion	89
6.3.1	Substitutional CN molecules (CN _{As})	91
6.3.2	Interstitial CN molecules (CN _i)	98

CONTENTS (Continued)

	Page
6.3.3 General trends of the bond length and the vibrational frequency.....	100
6.3.4 Discussion and comparison with experiment	104
6.4 Conclusions.....	106
VII SUMMARY AND POTENTIAL FUTURE RESEARCH	108
7.1 Brief Summary of Studied Defect Complexes.....	108
7.1.1 Zn _i -N _O complex in ZnO	108
7.1.2 Silicon-nitrogen complex in dilute nitrides.....	109
7.1.3 Carbon-nitrogen complexes in GaAs and GaP	109
7.2 Potential Future Research	109
REFERENCES	111
APPENDIX.....	127
CURRICULUM VITAE.....	152

LIST OF TABLES

Table		Page
2.1	Calculated optical dielectric constant ε^∞ , atomic electron correlation energy U^{at} for Zn, Cd, Ga and In. The on-site Coulomb interaction energy U is also listed for ZnO, CdO, GaN and InN. These values are from Ref. (Janotti, <i>et al.</i> , 2006).....	18
4.1	Calculated formation energies (at $E_F=0$, referenced to the VBM) for Zn_i , N_O , and $\text{Zn}_i\text{-N}_\text{O}$ in ZnO, under zinc-rich and oxygen-rich conditions.....	52
5.1	Calculated binding energies of $X_{\text{Ga}}\text{-N}_{\text{As}}$ ($X = \text{Si}$ and Ge) in the neutral and positive charge states. The binding energies, derived using GaAs CBM and GaAsN alloy CBM are listed in the columns marked as “ref. GaAs” and “ref. GaAsN”, respectively.....	73
5.2	Calculated $(X\text{-N})_{\text{As}}$ bond lengths and the bond lengths between the surrounding Ga atoms and $(X\text{-N})_{\text{As}}$. The displacements of the surrounding Ga atoms from original sites are given in terms of percentages of equilibrium Ga-As bond length..	77
5.3	Calculated stretch mode vibrational frequencies of $(\text{Si-N})_{\text{As}}$ and $(\text{Ge-N})_{\text{As}}$ split interstitial in neutral and 1– charge states	82

LIST OF TABLES (Continued)

Table	Page
6.1 Calculated bond lengths $d_{\text{C-N}}$, stretching frequencies ω , and formation energies E^f (for the Fermi level at the VBM) of CN molecules in GaAs in the symmetric (asymmetric in parentheses) configurations. For each charge state, the lower energy configuration is shown in boldface.	95
6.2 Calculated bond lengths $d_{\text{C-N}}$, stretching frequencies ω , and formation energies E^f (for the Fermi level at the VBM) of CN molecules in GaP in the symmetric (asymmetric in parentheses) configurations. For each charge state the lower energy configuration is shown in boldface.	96

LIST OF FIGURES

Figure		Page
2.1	Schematic illustration of the replacement of the all-electron wave function and core potential (solid curves) by a pseudo-wave function and pseudopotential (dashed curves). The figure is a reproduction of Figure 3.1 in Ref. (Singh and Nordstrom, 2006)	21
3.1	Schematic illustration of the wurtzite structure, the c -axis ([0001] direction) is perpendicular to the paper. The large circles represent cations, small circles anions. The shaded area shows the primitive unit cell. The arrows represent the translation vectors of each cell (as labeled). The dashed lines serve as the guide to an eye for the shape of the supercells.....	34
3.2	Schematic configuration coordinate diagram of an acceptor A in negative charge state A^- and neutral charge state A^0 with the presence of an electron in the bottom of conduction band. It is illustrating the difference between thermal and optical ionization energies for an acceptor A . E_{rel} is the energy gained by the relaxation of negative charge state A^- from A^0 equilibrium configuration to its equilibrium configuration, called “Frank-Condon shift”	39
4.1	Local atomic geometry of $(\text{Zn}_i\text{-N}_\text{O})^+$. (a) Side view (perpendicular to the c axis). (b) Top view (parallel to the c axis)	49

LIST OF FIGURES (Continued)

Figure	Page
4.2	Calculated formation energy as a function of the Fermi level for N_O , Zn_i , and the Zn_i - N_O complex under Zn-rich conditions and N_2 precipitation limits. The Fermi level is referenced to the valence band maximum. The slope of each line indicates the charge states. The solid brown line is the calculated formation energy of the same supercell contained both Zn_i and N_O but at a distance far away from each other. The dashed line denotes to the sum of energy between isolated Zn_i and N_O50
4.3	Concentrations of Zn_i , N_O , and Zn_i - N_O as a function of nitrogen chemical potential μ_N . The Zn-rich growth condition and growth temperature of 950°C are assumed. The dash lines are to guide the eyes for the μ_N at nitrogen concentration at 10^{17} cm^{-3} . N_2 precipitation limit is set at $\mu_N = 0$54
4.4	The Fermi energy as a function of μ_N for the calculations of defect concentration plotted in Figure 4.3. The Fermi energies are calculated with the consideration of the charge neutrality during the growth processes55

LIST OF FIGURES (Continued)

Figure		Page
4.5	Ratio of the concentration of Zn_i-N_O complex to the total concentration of Zn_i as a function of temperature. The dashed line represents thermal equilibrium condition while the solid line represents results in the event that the total concentration of Zn_i and N_O are determined by thermal equilibrium and kept fixed during the cool down to the room temperature.	57
5.1	Local lattice structure of (a) $(Si_{Ga}-N_{As})^+$ and (b) $(Si-N)_{As}^-$. In the $Si_{Ga}-N_{As}$ configuration, Si_{Ga} is a nearest neighbor of N_{As} . In the $(Si-N)_{As}$ configuration, Si and N share an As site.....	67
5.2	Formation energy under Ga-rich conditions as a function of Fermi energy for (a) Si_{Ga} and (b) Ge_{Ga} in GaAs. Both Si_{Ga} and Ge_{Ga} always have 1+ charge state.....	69
5.3	Calculated bandstructures of (a) defect-free GaAs (presented in a 64-atom supercell BZ) and (b) GaAs containing Si_{Ga}	70
5.4	Calculated bandgap of $GaAs_{1-x}N_x$ alloys as a function of N fraction. The black solid dots represent the calculated bandgap of $GaAs_{1-x}N_x$ at mol % N = 0.00, 0.93, 1.56 and 3.13. The calculations were performed by replacing an As atom by a N atom in 216-, 128- and 64-atom supercell respectively. The dashed line serves as a guide to the eye	71

LIST OF FIGURES (Continued)

Figure	Page
5.5 Calculated bandstructures of (a) 64-atom GaAsN supercell and (b) the same supercell containing a $\text{Si}_{\text{Ga}}\text{-N}_{\text{As}}$ pair	74
5.6 Formation energies as a function of Fermi level of (a) $\text{Si}_{\text{Ga}}\text{-N}_{\text{As}}$ and $(\text{Si-N})_{\text{As}}$ and (b) $\text{Ge}_{\text{Ga}}\text{-N}_{\text{As}}$ and $(\text{Ge-N})_{\text{As}}$ in GaAsN under Ga-rich conditions. The plots show the Fermi level in the range 0-1.25 eV which corresponds to the bandgap of GaAsN alloys with the N concentration of ~1%	76
5.7 Calculated projected density of states of Si (or Ge) and N <i>p</i> -orbitals for (a) $(\text{Si-N})_{\text{As}}$ (b) $(\text{Ge-N})_{\text{As}}$. The grey shaded area present the summation of projected density of states of host atoms. Density of state plots of <i>p</i> -orbitals scaled up for clarity. Dashed lines indicate the range of GaAs experimental bandgap	78
5.8 Calculated bandstructure of a 64-atom GaAsN supercell containing a $(\text{Si-N})_{\text{As}}$	79
5.9 Charge density plots of the (a) bonding and (b) antibonding states associated with $(\text{Si-N})_{\text{As}}$. The structure in (b) has been rotated with respect to (a) to improve the virsualization.....	80
5.10 Schematic illustrations of the absorption and luminescencence energies for (a) $(\text{Si-N})_{\text{As}}$ and (b) $(\text{Ge-N})_{\text{As}}$	81

LIST OF FIGURES (Continued)

Figure	Page
6.1 Local atomic geometry of a CN molecule substituting on an As site in GaAs: (a) symmetric configuration, CN_{As} , and (b) asymmetric configuration, CN_{As} (asym). Both are shown for the 2+ charge state.	89
6.2 Schematic illustrations of the $pp\pi^*$ single-particle energy levels of the CN molecule in the GaAs band gap. (a) Substituting on an As site (CN_{As}) and (b) CN on an interstitial site (CN_i). The solid dots show the electron occupation for the neutral charge state.	90
6.3 (a) Charge density of the $pp\pi^*$ states of CN_{As} that are located in the GaAs band gap. (b) Contour plot of one of the states in (a) in a (001) plane cutting through the CN molecule. (c) Charge density of one of the $pp\pi$ states of CN_{As} that resides below the valence-band maximum. (d) The corresponding contour plot of (c)	91
6.4 Calculated energy of $\text{CN}_{\text{As}}^{2+}$ as the CN molecule rotates from asymmetric to symmetric and back to an equivalent asymmetric configuration. The symmetric configuration is the saddle point along this path.....	93
6.5 Formation energies of CN molecules in GaAs as a function of the Fermi energy. The solid lines and dashed lines represent the asymmetric and symmetric configurations, respectively.	98

LIST OF FIGURES (Continued)

Figure	Page
6.6 Local atomic geometry of interstitial CN molecules in GaAs: (a) CN_i^+ (sym), (b) CN_i^+ (asym), and (c) CN_i^0 (asym)	99
6.7 Calculated energy of CN_i^{1+} as the CN molecule rotates from a symmetric to an asymmetric configuration. The rotation occurs without any barrier and lowers the energy by almost 0.6 eV	101
6.8 (a) Calculated vibration frequencies and (b) C-N bond distances for various configurations of a CN molecule in GaAs and GaP as a function of charge Δq inserted into the molecule, which are measured relative to a neutral free CN molecule with nine electrons. The solid symbols are for interstitial CN and the open symbols are for substitutional CN. The colors code the host materials (red for GaAs and green for GaP), whereas the symbols are used to distinguish the symmetric (circle) from asymmetric (triangle) configurations. The CN molecules is characterized as triply, doubly, or singly bonded for $\Delta q = -1, -3$, and -5 , respectively. The dashed lines are linear fits to all of the data points	103

LIST OF ABBREVIATIONS

BLYP	=	Becke-Lee-Yang-Parr
CBM	=	Conduction Band Minimum
DFT	=	Density Functional Theory
DLST	=	Deep-Level Transient Spectroscopy
EPR	=	Electron Paramagnetic Resonance
GGA	=	Generalized Gradient Approximation
HK	=	Hohenberg-Kohn
KS	=	Kohn-Sham
LAPW	=	Linearized Augmented Plane-Wave
LDA	=	Local Density Approximation
LHS	=	Left Hand Side
MER	=	Minimum Energy Path
NEB	=	Nudge Elastic Band
OPW	=	Orthogonalized Plane Wave
PAW	=	Projector Augmented Wave
PBE	=	Perdew-Burke-Ernzerhof
PEB	=	Plain Elastic Band
PL	=	Photoluminescence
PP	=	Pseudo Potential
RHS	=	Right Hand Side

LIST OF ABBREVIATIONS (Continued)

RTA	=	Rapid Thermal Annealing
SCVT	=	Seeded Chemical Vapor Transport
USPP	=	Ultra Soft Pseudo Potential
UV	=	Ultra Violet
VASP	=	Vienna Ab-initio Simulation Package
VBM	=	Valence Band Maximum

CHAPTER I

INTRODUCTION

Crystalline solids can be classified based on their electrical conductivity into following categories: metal, semimetal, semiconductor, and insulator. Among the four classes of materials, semiconductors are the most important for new technological devices. The main reason is that their electrical properties can be tuned and controlled in a wide range. Their conductivity can be significantly altered in different ways. This is in contrast to other three classes of solids where their conductivity cannot be easily altered. The elemental semiconductors, silicon (Si) and germanium (Ge) are studied and developed into devices with the bandgap of less than 1 eV. During the past few decades, binary compounds and alloys of elements in group-IV, group II-VI and group III-V have been studied and investigated intensively. These new generation semiconductors offer a wide range of properties with improved efficiency and thermal stability, benefiting from wider bandgaps.

To utilize semiconductors, one needs to increase their electrical conductivity. Generally, this is done by doping with impurities. For instance, doping bulk silicon (group IV element) with group V element such as phosphorus (P) turns silicon into *n*-type material. An extra electron from P is loosely bounded and can be thermally excited from the donor level to the bottom of the conduction band. The donor level is introduced just below the bottom of conduction band. These excited electrons make the material electrically active. Si can also be doped with group III element such as

boron (B) which turns Si into *p*-type semiconductor. Because the doping element lacks one electron, a hole in silicon lattice is created. The acceptor level locates just above the valence band maximum (Ashcroft and Mermin, 1976). The electrons in valence band can be thermally excited to the acceptor level, leaving holes in the valence band. The holes are free to move, making the material electrical conductive with *p*-type carriers. In very much the same way, binary compound semiconductors and their alloys can be doped into *n*-type and *p*-type as well. For example, to dope gallium arsenide (GaAs) *n*-type there are two approaches, the first approach is by replacing gallium (Ga) which is group III element with group IV element such as silicon (Si) or carbon (C). The second approach is by replacing arsenic (As) which is group V element with group VI element such as selenium (Se) or sulfur (S). Similarly, in principle, *p*-type GaAs can be achieved by either replacing Ga with group II element such as zinc (Zn) and beryllium (Be) or by replacing As with group IV element such as Si. However, in real systems, Si can be both donor (if it replaces Ga) and acceptor (if it replaces As). As a result, it is called “amphoteric” dopant.

In the beginning of semiconductors age, the elementary semiconductors, i.e., Si and Ge were widely used. Many decades later, these prototypical semiconductors are still being studied and used in a vast number of technological important applications. Driven by the needs to keep up with the emerging technology, new classes of semiconductors such as gallium arsenide (GaAs) have been discovered. Some of their electronic properties are superior to Si. For instance, its higher bandgap leads to higher breakdown voltage. In addition, GaAs has direct gap, making it suitable for optoelectronic applications. On the other hand, Si and Ge have indirect gap, making them unsuited for such applications. Moreover, alloying binary

compounds allows additional degree of freedom to engineer the bandgap or other properties. Such alloys are for examples, $\text{In}_x\text{Ga}_{1-x}\text{As}$ and $\text{Al}_x\text{Ga}_{1-x}\text{As}$ alloys.

Electrons in the valence bands can be thermally or optically excited into the conduction bands, contributing to electrical conductivity. The size of the bandgap determines both the thermal stability of carrier concentrations and the optical excitation profile. If the bandgap of a semiconductor is too narrow, the carrier concentration can be greatly affected by temperature. Devices fabricated from semiconductors with too small bandgap would not sustain high temperature. The bandgap of semiconductors also determines the photon energy of optoelectronic devices. For instance, to have optoelectronic devices in the blue light region, the semiconductor must have a bandgap exceeding 2.5 eV. The need for devices that can be operated reliably at high temperature combined with the need for blue light to UV optoelectronic devices, leads to substantial interests in wide bandgap semiconductors. Wide bandgap semiconductors, for e.g. SiC, GaN, In_2O_3 , SnO_2 and ZnO, are required for high power electronics and blue-to-UV optoelectronic devices, such as blue-LEDs and blue laser diodes (Morkoc, Strite, Gao, Lin, Sverdlov and Burns, 1994; Look, 2001). However, the semiconductor has to be dopable into both “*n*-type” and “*p*-type”. Unfortunately, among those aforementioned wide gap semiconductors, only GaN and SiC have been successfully doped into both *n*- and *p*-type to the level required for the device applications. Other wide gap materials are under intensive investigations.

Generally, there are many kinds of point defects in semiconductors, including native ones (such as vacancies, interstitials, and antisites) and impurities. Defects can greatly influence optical and electronic properties of semiconductors. To make the

high quality semiconductors, it is necessary to reduce the unintentional active defects (both native defects and unintentional impurities) while optimizing the incorporation of the wanted defects (i.e. dopants). The knowledge on the formation processes and defect energies in different growth conditions can greatly help to choose the growth/doping environments. Since some defects can bind to each other, forming defect complexes thus it is important to identify and study possible complexes of defects in semiconductors. Many defect complexes have been theoretically proposed and experimentally investigated. For example, a recent first- principles study of defects in ZnO shows that defect complexes in the form of diatomic molecules NO, NC, CO, N₂, and O₂ substituting on an O site can be very stable and have adverse effects on nitrogen doping in ZnO (Limpijumnong, Li, Wei and Zhang, 2005). For another example, a complex involving a donor and two acceptors ($\text{As}_{\text{Zn}}\text{-}2V_{\text{Zn}}$) has been studied theoretically (Limpijumnong, Zhang, Wei and Park, 2004) and found to have low energy. The defect was proposed to be the cause of recent success in As-doped *p*-type ZnO (Look, Renlund, Burgener II and Sizelove, 2004). Subsequently, experimental evidence, that As is indeed substituted on the Zn site, has been reported (Wahl, Rita, Correia, Marques, Alves and Soares, 2005).

Defect complexes in semiconductors can be categorized into three classes based on the constituent defects. 1) Complexes between native defects such as vacancy-antisite complexes in GaAs (Chadi and Zhang, 1990), zinc vacancy-antisite complexes in ZnO (Chen, Betsuyaku and Kawasuso, 2008), a pair between interstitial and vacancy namely, “Frenkel pair” that are expected to exist in a substantial amount after an electron irradiation experiments (Linde, Uftring, Watkins, Härle and Scholz, 1997; Look, Reynolds, Hemsky, Sizelove, Jones and Molnar, 1997), and complexes

between zinc interstitial and oxygen vacancy in ZnO that is recently studied and proposed as important source for *n*-type conductivity (Kim and Park, 2009). 2) Complexes between native defects and impurities, such as complexes between oxygen and arsenic vacancy in GaAs (Skowronski, 1992), complex of gallium vacancy and a carbon atom (Ogino and Aoki, 1980), the complex between V_{Ga} and oxygen (Neugebauer and Van de Walle, 1996), complex between arsenic on zinc site and two zinc vacancy ($\text{As}_{\text{Zn}}\text{-}2V_{\text{Zn}}$), and complex between zinc interstitial and nitrogen substituted oxygen $\text{Zn}_i\text{-N}_\text{O}$ (Look, Farlow, Reunchan, Limpijumnong, Zhang and Nordlund, 2005). 3) Complex between impurities, such as complex between hydrogen and dopant atoms in which they are widely studied in several semiconductors, such as, GaAs, GaN and ZnO. Another example is the complex between low-*Z* atoms, in diatomic molecule or in split-interstitial forms. As part of this thesis, we have studied silicon-nitrogen complex $(\text{Si-N})_{\text{As}}$ in diluted nitride alloys (Janotti, Reunchan, Limpijumnong and Van de Walle, 2008) and complexes between carbon and nitrogen in GaAs and GaP (Limpijumnong, Reunchan, Janotti and Van de Walle, 2008).

Since most of the electronic properties of semiconductors are sensitive to the detailed atomic geometry of defects. It is therefore important to understand defect complexes in addition to basic native point defects. To investigate those mentioned defects, the first-principles approach is employed. Density functional theory is a powerful and widely used method to study materials down to the fundamental quantum mechanic level. Based on this approach, the electron eigenfunctions and eigenenergies are obtained. From the wavefunctions other material properties, such as electronic structures and total energies can be calculated. Advance computing

technologies and efficient numerical schemes enabled us to study more complicated structures.

This thesis is organized as following. Chapter II briefly describes the density functional theory and some other theoretical methods used in this work. Chapter III describes the theoretical approaches used in calculations of defects and complexes in semiconductors. Chapter IV is dedicated to Zn_i-N_O complex in ZnO. Although, Zn_i is believed to have high formation energy making them unlikely to exist in a meaningful amount, we have showed that in nitrogen doped ZnO Zn_i-N_O complex has a reasonably low energy and can be formed. Chapter V and Chapter VI focus on the defect complexes in GaAs and GaP. In chapter V, the split-interstitial $(Si-N)_{As}$ defects in GaAs are studied. The defect can explain the mutual passivation of shallow donor Si (or Ge) and isovalent N. In chapter VI, diatomic molecules in GaAs and GaP are studied. The calculations show that the CN molecule favors the substitution an anion site over being an interstitial. Chapter VII is dedicated to summarize all accomplished works in this dissertation. Some potential directions in this research area are suggested.

CHAPTER II

THEORETICAL METHODS

2.1 Many Electrons Problems in Solids

In order to elucidate the behaviors of electrons in solid, quantum mechanics approaches are needed. The wave functions of electrons in the system can be obtained by solving Schrödinger equation,

$$\hat{H}\Psi_n(\mathbf{R}, \mathbf{r}) = \varepsilon_n \Psi_n(\mathbf{R}, \mathbf{r}), \quad (2.1)$$

where ε_n are energy eigenvalues and $\Psi_n(\mathbf{R}, \mathbf{r})$ are the corresponding eigenfunctions.

The Hamiltonian of the system of atomic nuclei and electrons interacting through Coulombic electrostatic forces can be written as

$$\begin{aligned} \hat{H} = & -\sum_{I=1}^P \frac{\hbar^2}{2M_I} \nabla_I^2 - \sum_{i=1}^N \frac{\hbar^2}{2m} \nabla_i^2 + \frac{e^2}{2} \sum_{I=1}^P \sum_{J \neq I}^P \frac{Z_I Z_J}{|\mathbf{R}_I - \mathbf{R}_J|} \\ & + \frac{e^2}{2} \sum_{i=1}^N \sum_{j \neq i}^N \frac{1}{|\mathbf{r}_i - \mathbf{r}_j|} - e^2 \sum_{I=1}^P \sum_{i=1}^N \frac{Z_I}{|\mathbf{R}_I - \mathbf{r}_i|}, \end{aligned} \quad (2.2)$$

in which the terms on the right-hand-side (RHS) can be denoted as

$$\hat{H} = T_N + T_e + V_{NN} + V_{ee} + V_{Ne}, \quad (2.3)$$

where $\mathbf{R} = \{\mathbf{R}_I, I = 1, \dots, P\}$ is a set of P nuclear coordinates, and $\mathbf{r} = \{\mathbf{r}_i, i = 1, \dots, N\}$ is a set of N electronic coordinates. M_I and m are the mass of nucleus and electron, respectively. Z_I denotes the nuclear atomic number. The kinetic energy of nuclei and electrons are represented by operators T_N and T_e . V_{NN} , V_{ee} and V_{Ne} are

Coulombic electrostatic operators of nucleus-nucleus, electron-electron repulsion energy, and nucleus-electron attraction energy, respectively. An attempt to ease this full quantum mechanic equation was proposed by Born and Oppenheimer (Born and Oppenheimer, 1927) based on the observation that the time scale associated with motion of nuclei is usually much larger than that associated with electrons. In addition, a proton is 1839 times heavier than an electron. As a result to the electrons, the nuclei are essentially stationary. From the ions viewpoint, they see only a time-average adiabatic electronic potential. This is called “Born-Oppenheimer or adiabatic approximation”. The electronic Hamiltonian can be written as

$$\hat{h}_e = \hat{T} + \hat{U}_{ee} + \hat{V}_{ne}, \quad (2.4)$$

where \hat{T} is the electronic kinetic energy operator, \hat{U}_{ee} is the electron-electron interaction, and \hat{V}_{ne} is the electron-nuclei interaction. Hence, the electronic Schrödinger equation can be written as

$$\hat{h}_e \Phi(\mathbf{R}, \mathbf{r}) = \varepsilon(\mathbf{R}) \Phi(\mathbf{R}, \mathbf{r}), \quad (2.5)$$

where $\Phi(\mathbf{R}, \mathbf{r})$ is the many-electron wavefunction, and $\varepsilon(\mathbf{R})$ is the eigenvalue parameterized by nuclear coordinate \mathbf{R} .

The early approach to reduce many electron problems into solvable ones was raised by Hatree (Hartree, 1928). It is assumed that a many-electron wavefunction can be written as a product of one-electron orbitals. The Slater determinant is used to construct a many-electron wave function where Pauli’s exclusion principle is included. This approach is known as “Hartree-Fock approximation”. These days, it becomes an approach by choice, especially for molecular systems.

For a small number of interacting particles, such as a hydrogen atom, the many-body Schrödinger equation can provide the exact eigenstates and eigenvalues of electrons. However, in reality we need to deal with systems that are composed of several electrons. Even in a small molecule there are already several interacting electrons. In solids, numbers of electrons are in the order of 10^{23} . It is impossible to directly solve traditional many-body Schrödinger equation. Several approaches have been proposed to simplify this problem.

2.2 Density Functional Theory

Because solving many-body Schrödinger equation of many electrons is extremely difficult or even impossible, the effective methods to reduce computational cost to the computable level are needed. In 1920s, Thomas (Thomas, 1927) and Fermi (Fermi, 1928) independently proposed an idea for calculating the energy of electronic systems in terms of electron density distribution. Thomas-Fermi theory led to the hypothesis that the ground state density for any electronic system uniquely determines the system. This became the starting point for density functional theory (DFT).

Next, we will briefly describe the formulation of DFT proposed by Hohenberg and Kohn (Hohenberg and Kohn, 1964) subsequently fulfilled by Kohn and Sham (Kohn and Sham, 1965).

2.2.1 The Hohenberg-Kohn (HK) theorem

Theorem 1: The density as the basic variable

The ground state density $n(\mathbf{r})$ of a bound interacting electrons system in some external potential determines this potential uniquely. In other word, it cannot be

external potential $v_{\text{ext}}(\mathbf{r}) \neq v'_{\text{ext}}(\mathbf{r})$ that gives the same ground state density $n(\mathbf{r})$, unless they differ by a trivial additive constant.

Theorem 2: The Hohenberg-Kohn variational principle

In the variational principle, the energy of an electronics system can be calculated, using normalized trial wave function $\tilde{\Psi}$. This theorem proposes the formulation of variational principle in terms of trial density $\tilde{n}(\mathbf{r})$ rather than trial wave function $\tilde{\Psi}$. The variational energy E_v , which is functional of the density is defined as

$$E_v[\tilde{n}(\mathbf{r})] = F[\tilde{n}(\mathbf{r})] + \int \tilde{n}(\mathbf{r}) v_{\text{ext}}(\mathbf{r}) d\mathbf{r}, \quad (2.6)$$

with

$$F[\tilde{n}(\mathbf{r})] = \langle \Psi[\tilde{n}] | \hat{T} + \hat{U}_{ee} | \Psi[\tilde{n}] \rangle. \quad (2.7)$$

Here $\Psi[\tilde{n}]$ denotes to the ground state of a potential which has $\tilde{n}(\mathbf{r})$ as its ground state density. So that $E_0 = E_v[n(\mathbf{r})]$, where E_0 is ground state energy, verifies

$$E_0 < E_v[\tilde{n}(\mathbf{r})] \quad (2.8)$$

for any $\tilde{n}(\mathbf{r}) \neq n(\mathbf{r})$.

The formulation of the ground state energies is entirely in terms of the density distribution $\tilde{n}(\mathbf{r})$ and of well defined but not explicitly known functional of the density $F[\tilde{n}(\mathbf{r})]$.

2.2.2 The Kohn-Sham (KS) equations

A practical scheme following HK formulation has been introduced by Kohn and Sham (Kohn and Sham, 1965). It is currently the most utilized formalism for DFT based applications. The KS scheme regards an electron as a particle moving in an

effective single-particle potential. For a non-interacting electron system, a set of self-consistent Hartree equations can be constructed. The Hartree single particle equations are

$$\left(-\frac{1}{2}\nabla^2 + V_H(\mathbf{r}) - E_j \right) \psi_j(\mathbf{r}) = 0, \quad (2.9)$$

where j denotes both spatial and spin quantum numbers. $V_H(\mathbf{r})$ is Hartree effective potential defined as

$$V_H(\mathbf{r}) = -\frac{Z}{r} + \int \frac{n(\mathbf{r}')}{|\mathbf{r} - \mathbf{r}'|} d\mathbf{r}'. \quad (2.10)$$

The first term on the RHS is the potential due to the nucleus of the atom with atomic number Z . The second term is the potential due to the average electronic distribution $n(\mathbf{r})$. $n(\mathbf{r})$ is given by

$$n(\mathbf{r}) = \sum_{j=1}^N |\psi_j(\mathbf{r})|^2. \quad (2.11)$$

In ground state, the sum runs over the N states with the lowest eigenvalues. For an interaction electron system, the universal functional $F[\tilde{n}(\mathbf{r})]$ can be written as

$$F[\tilde{n}(\mathbf{r})] \equiv T_s[\tilde{n}(\mathbf{r})] + \frac{1}{2} \int \frac{\tilde{n}(\mathbf{r})\tilde{n}(\mathbf{r}')}{|\mathbf{r} - \mathbf{r}'|} d\mathbf{r}d\mathbf{r}' + E_{xc}[\tilde{n}(\mathbf{r})], \quad (2.12)$$

where $T_s[\tilde{n}(\mathbf{r})]$ is the kinetic energy functional for non-interacting electrons.

$E_{xc}[\tilde{n}(\mathbf{r})]$ is the exchange-correlation energy functional. The HK variational principle for interacting electron can be written as

$$E_v[\tilde{n}(\mathbf{r})] \equiv \int v(\mathbf{r})\tilde{n}(\mathbf{r})d\mathbf{r} + T_s[\tilde{n}(\mathbf{r})] + \frac{1}{2} \int \frac{\tilde{n}(\mathbf{r})\tilde{n}(\mathbf{r}')}{|\mathbf{r} - \mathbf{r}'|} d\mathbf{r}d\mathbf{r}' + E_{xc}[\tilde{n}(\mathbf{r})] \geq E_0. \quad (2.13)$$

The corresponding Euler-Lagrange equations, for a given total number of electrons has the form

$$\delta E_\nu[\tilde{n}(\mathbf{r})] \equiv \int \delta \tilde{n}(\mathbf{r}) \left\{ V_{\text{eff}}(\mathbf{r}) + \frac{\delta}{\delta \tilde{n}(\mathbf{r})} T_s[\tilde{n}(\mathbf{r})] \Big|_{\tilde{n}(\mathbf{r})=n(\mathbf{r})} - \varepsilon \right\} d\mathbf{r} = 0, \quad (2.14)$$

where ε is a Langrange multiplier to assure particle conservation. The electron density $n(\mathbf{r})$ can be obtained by solving the single particle equation

$$\left(-\frac{1}{2} \nabla^2 + V_{\text{eff}}(\mathbf{r}) - E_j \right) \psi_j(\mathbf{r}) = 0, \quad (2.15)$$

where

$$V_{\text{eff}}(\mathbf{r}) = V(\mathbf{r}) + \int \frac{n(\mathbf{r}')}{|\mathbf{r} - \mathbf{r}'|} d\mathbf{r}' + V_{\text{XC}}(\mathbf{r}), \quad (2.16)$$

and

$$V_{\text{XC}}(\mathbf{r}) \equiv \frac{\delta E_{\text{XC}}[\tilde{n}(\mathbf{r})] \Big|_{\tilde{n}(\mathbf{r})=n(\mathbf{r})}}{\delta \tilde{n}(\mathbf{r})}. \quad (2.17)$$

The solution to equation (2.15) gives

$$n(\mathbf{r}) = \sum_{j=1}^N |\psi_j(\mathbf{r})|^2. \quad (2.18)$$

The self-consistent equations [Eq. (2.15)-(2.18)] are Kohn-Sham (KS) equations which have the ground state energy as

$$E = \sum_{j=1}^N E_j + E_{\text{XC}}[n(\mathbf{r})] - \int V_{\text{XC}}(\mathbf{r}) n(\mathbf{r}) d\mathbf{r} - \frac{1}{2} \int \frac{n(\mathbf{r}) n(\mathbf{r}')}{|\mathbf{r} - \mathbf{r}'|} d\mathbf{r} d\mathbf{r}' \quad (2.19)$$

If $E_{\text{XC}}[n(\mathbf{r})]$ and $V_{\text{XC}}(\mathbf{r})$ are neglected, the KS equations are reduced to self-consistent Hartree equations. Many body effects are included in the E_{XC} and V_{XC} . In practice, the simple approximations for exchange correlation energy $E_{\text{XC}}[n(\mathbf{r})]$ are used.

2.3 The Exchange Correlation Energy

For systems of many interacting particles, in a particular case, a system is with repulsive electron-electron interactions. In such system, an electron at point \mathbf{r} in space prevents other electrons from approaching this location. Thus, the probability of finding an electron at point \mathbf{r} depends on location of other electrons in system. This leads to the correlation function $g_c(\mathbf{r}, \mathbf{r}')$. Another important interaction is the exchange interaction from Pauli's exclusion principle. It states that if two electrons have parallel spins then they are not allowed to be at the same position at the same time. This gives the effective repulsion between electrons with parallel spins denoted by $g_x(\mathbf{r}, \mathbf{r}')$.

The exchange correlation energy can be described using the Coulomb interaction between the electronic density and the displaced charge density. The exchange correlation hole can be defined as

$$n_{xc}(\mathbf{r}, \mathbf{r}') = n(\mathbf{r}')[g(\mathbf{r}, \mathbf{r}') - 1], \quad (2.20)$$

where

$$g(\mathbf{r}, \mathbf{r}') = g_x(\mathbf{r}, \mathbf{r}') + g_c(\mathbf{r}, \mathbf{r}'). \quad (2.21)$$

The exchange correlation energy can be written as

$$E_{xc}[n(\mathbf{r})] = \frac{1}{2} \iint \frac{n(\mathbf{r})n_{xc}(\mathbf{r}, \mathbf{r}')}{|\mathbf{r} - \mathbf{r}'|} d\mathbf{r} d\mathbf{r}'. \quad (2.22)$$

Sometimes E_{xc} is divided into two term E_x and E_c . The main reason that makes density functional theory useful is the effective and accurate approximations of exchange and correlation energy. Next, we describe the most widely used approximations to the exchange and correlation energy in DFT.

2.3.1 The local density approximation (LDA)

The most used approximation to the exchange correlation energy is the local density approximation. The main idea is to consider a general inhomogeneous electronic system as locally homogeneous. The exchange-correlation energy can be written as

$$E_{\text{XC}}^{\text{LDA}}[n(\mathbf{r})] = \int n(\mathbf{r}) \varepsilon_{\text{XC}}^{\text{LDA}}[n(\mathbf{r})] d\mathbf{r}, \quad (2.23)$$

where $\varepsilon_{\text{XC}}^{\text{LDA}}(n)$ is the exchange-correlation energy per particle of a uniform electron gas of density n .

The exchange-correlation energy within LDA is basically calculated through (2.21), using $\varepsilon_{\text{XC}}^{\text{LDA}}(n) = \varepsilon_{\text{X}}^{\text{LDA}}(n) + \varepsilon_{\text{C}}^{\text{LDA}}(n)$. $\varepsilon_{\text{X}}^{\text{LDA}}(n)$ and $\varepsilon_{\text{C}}^{\text{LDA}}(n)$ are the exchange energy and correlation energy per particle, respectively. The exchange energy is given by Dirac's expression (Dirac, 1930)

$$\varepsilon_{\text{X}} = -\frac{3}{4} \left(\frac{3}{\pi} \right)^{1/3} n^{1/3} = -\frac{3}{4} \left(\frac{9}{4\pi^2} \right)^{1/3} \frac{1}{r_s} = -\frac{0.458}{r_s} \text{ a.u.}, \quad (2.24)$$

where $r_s = [(3/4\pi n)]^{1/3}$ is the mean interelectronic distance expressed in atomic unit.

The correlation part was first estimated by E. P. Wigner (Wigner, 1938) as

$$\varepsilon_{\text{C}}(n) = -\frac{0.44}{r_s + 7.8}. \quad (2.25)$$

Afterward, a more accurate approximation was made by Ceperly and Alder (Ceperley and Alder, 1980) based on the quantum Monte Carlo simulations and has been parameterized by Perdew and Zunger (Perdew and Zunger, 1981).

2.3.2 The generalized gradient approximation (GGA)

To improve the LDA, the inhomogeneity of density is taken into account. This can be done by expanding E_{xc} as a series in terms of the density and its gradient. This approach is known as gradient expansion. The exchange-correlation energy can be written in the following form

$$E_{xc}[n] = \int n(\mathbf{r}) \varepsilon_{xc}[n(\mathbf{r})] F_{xc}[n(\mathbf{r}), \nabla n(\mathbf{r}), \nabla^2 n(\mathbf{r}), \dots] d\mathbf{r}, \quad (2.26)$$

where the function F_{xc} is a factor for modifying LDA expressions according to the density variation at the considered point. The second order gradient expansion corresponds to an expression of the type

$$E_{xc}[n] = \int A_{xc}[n] n(\mathbf{r})^{4/3} d\mathbf{r} + \int C_{xc}[n] |\nabla n(\mathbf{r})|^2 / n(\mathbf{r})^{4/3} d\mathbf{r}. \quad (2.27)$$

The only first term corresponds to only the local density.

However it provides no systematic improvement. In addition, it exhibits singularities and violates sum rules. It is therefore unphysical and provides worsen result than the LDA.

To solve this problem, Perdew shown that imposing the exact condition required for exchange and correlation holes, such as the normalization conditions. The negativity of the exchange density can remarkably improve the quality of exchange energy. His function has named as generalized gradient approximations (GGAs). A number of modified gradient have been subsequently proposed. Langreth-Mehl functional (Langreth and Mehl, 1983), BLYP functional (Becke, 1988; Lee, Yang and Parr, 1988; Miehlich, Savin, Stoll and Preuss, 1989), PBE functional (Perdew, Burke and Ernzerhof, 1996) and Perdew-Wang functional (Perdew, 1991).

2.3.3 LDA+ U

For the transition metal oxides and rare-earth metal compounds for example ZnO, LDA and GGA have problems describing the well-localized d and f states. Some insulators appear to be metals in the calculations due to these problems. LDA and GGA cannot adequately describe the strong Coulombic repulsions between $3d$ or $4f$ electrons localized on some metal ions. Recently, Anisimov and co-workers (Anisimov and Gunnarsson, 1991) introduced an orbital dependent term “ U ”, following the work of Hubbard (Hubbard, 1965). “ U ” is the energy penalized for adding another electron to the same occupied particular site of an electron. It acts only on localized d or f states, as a Hubbard-type onsite repulsion term. This approach combined with density functional theory is known as LDA+ U (or GGA+ U) method (Anisimov and Gunnarsson, 1991). The splitting of Hubbard sub-bands is produced. It qualitatively produces the behavior of Mott-Hubbard insulator, where the strong correlations induce the opening of the energy gap. A number of approaches have been developed based on the Hubbard “ U ” model. In the rotationally invariant form by Liechtenstein *et al.*, (Liechtenstein, Anisimov and Zaanen, 1995), the total energy is given by

$$E_{\text{tot}}^{\text{LDA}+U}[n(\mathbf{r}), \{f\}] = E_{\text{tot}}^{\text{LDA}}[n(\mathbf{r})] + E^U(\{f\}) - E_{dc}(\{f\}). \quad (2.28)$$

The second term $E^U(\{f\})$ is the on-site Coulomb interaction given the Hatree-Fock-like interactions. The last term $E_{dc}(\{f\})$ is the correction for the double counting of electron-electron Coulomb interaction. $\{f\}$ is the occupation matrix with the elements $f_{\alpha,\beta}^{t,\sigma}$, where t and σ denote the site and spin direction and α and β denote angular momentum quantum numbers. If we neglect the effects associated with

higher-multipolar terms in the Coulomb interaction and assume no effective exchange splitting, the total energy can be written as

$$E_{\text{tot}}^{\text{LDA}+U}[n(\mathbf{r}), \{f\}] = E_{\text{tot}}^{\text{LDA}}[n(\mathbf{r})] + \sum_t \frac{U}{2} \left\{ \sum_{\alpha, \sigma} f_{\alpha, \alpha}^{t, \sigma} - \sum_{\alpha, \beta, \sigma} f_{\alpha, \beta}^{t, \sigma} f_{\beta, \alpha}^{t, \sigma} \right\}. \quad (2.29)$$

The Kohn-Sham energies in LDA+ U associated with the narrow bands are shifted with respect to their respective LDA energies according to

$$\varepsilon_{\alpha}^{\text{LDA}+U} = \frac{\partial E_{\text{tot}}^{\text{LDA}+U}}{\partial f_{\alpha, \alpha}} = \varepsilon_{\alpha}^{\text{LDA}} + U \left(\frac{1}{2} - f_{\alpha, \alpha} \right). \quad (2.30)$$

The result of applying on-site Coulomb interaction is to shift these fully occupied narrow bands down in energy by $\sim U/2$ with respect to other bands.

There are many methods to calculate U parameters. One of the systematic and general approaches to calculate U parameter based on first-principle calculations has been proposed by Janotti *et al.* (Janotti, Segev and Van de Walle, 2006). In order to obtain the improvement over LDA description for real systems by using LDA+ U approach, the choice of the U parameter is important. U is defined as the Coulomb interaction between d electrons on the same atom. Consequently, the atomic correlation energy U^{at} can be defined from the energy difference between the addition and the removal of an electron from the atomic d subshell as follows

$$U^{\text{at}} = [E_{\text{tot}}(d^{n+1}) - E_{\text{tot}}(d^n)] - [E_{\text{tot}}(d^n) - E_{\text{tot}}(d^{n-1})], \quad (2.31)$$

where $E_{\text{tot}}(d^n)$ is the total energy of an isolated atom with n electrons occupying the d sub-shell. The $n = 9$ is used as reference because most of atomic d sub-shell in metal species in semiconductors are completely occupied.

Table 2.1 Calculated optical dielectric constant ϵ^∞ , atomic electron correlation energy U^{at} for Zn, Cd, Ga and In. The on-site Coulomb interaction energy U is also listed for ZnO, CdO, GaN and InN. These values are from Ref. (Janotti, *et al.*, 2006)

	U^{at} (eV)	ϵ^∞	U (eV)
ZnO	18.0	3.8	4.7
CdO	13.8	6.7	2.1
GaN	19.6	5.0	3.9
InN	14.4	7.6	1.9

When these atoms are in a solid, the atomic Coulomb correlation interaction is screened by the optical dielectric constant ϵ^∞ , resulting in a Hubbard-like Coulomb interaction

$$U = \frac{U^{\text{at}}}{\epsilon^\infty}. \quad (2.32)$$

Table 2.1 shows the calculated values of the optical dielectric constant ϵ^∞ , the atomic Coulomb correlation energy, U^{at} , for d states, and the screened Coulomb correlation energy U (Janotti, *et al.*, 2006).

Most of the calculations in this thesis are performed within LDA approximations. The calculations that use LDA+ U method are explicitly declared.

2.4 Plane Wave Pseudopotential Method

The Kohn-Sham formulation of density functional theory leads us to the mathematical problem of solving the equation

$$\left\{ -\frac{1}{2}\nabla^2 + V_{\text{eff}}(\mathbf{r}) \right\} \psi_i(\mathbf{r}) = E_i \psi_i(\mathbf{r}), \quad (2.33)$$

where the effective potential $V_{\text{eff}}(\mathbf{r})$ includes all interactions acting on an electron.

The electronic density $n(\mathbf{r})$ is given by

$$n(\mathbf{r}) = \sum_{i=1}^N f_i |\psi_i(\mathbf{r})|^2, \quad (2.34)$$

where N is the number of electrons, and f_i is the step function in which its value depends on occupation number. The solutions to the Kohn-Sham equations need two important things: first is the treatment of electron-nucleus interaction, and the second is a mathematical way to represent the single-particle orbitals.

For periodic systems in solid crystals, Bloch's theorem states that the wavefunction of an electron in a periodic potential $V(\mathbf{r} + \mathbf{a}_i) = V(\mathbf{r})$ can be written as a plane wave times a periodic function $u_{\mathbf{k}}(\mathbf{r})$, i.e.,

$$\psi_{\mathbf{k}}(\mathbf{r}) = e^{i\mathbf{k}\cdot\mathbf{r}} u_{\mathbf{k}}(\mathbf{r}), \quad (2.35)$$

$u_{\mathbf{k}}(\mathbf{r})$ has the same periodicity as that of the potential, i.e., $u_{\mathbf{k}}(\mathbf{r}) = u_{\mathbf{k}}(\mathbf{r} + \mathbf{a}_i)$, where \mathbf{a}_i ($i = 1, 2, 3$) are the primitive vectors of the crystal. Bloch's theorem points out that the wave functions composed of a phase factor and a periodic part. This naturally well described by the plan waves basis sets. Using the Fourier transform, the wavefunction can be expressed as

$$\psi^{(\mathbf{k})}(\mathbf{r}) = \frac{e^{i\mathbf{k}\cdot\mathbf{r}}}{\sqrt{\Omega}} \sum_{\mathbf{G}=0}^{\infty} C_{\mathbf{k}}(\mathbf{G}) e^{i\mathbf{G}\cdot\mathbf{r}}, \quad (2.36)$$

where \mathbf{G} are the reciprocal lattice vectors and $C_{\mathbf{k}}(\mathbf{G})$ are the Fourier coefficient. In principle, an infinite number of vectors is required to perfectly represent the wave function. In practice, we can limit the plane waves expansion to a finite number of \mathbf{G} . This limits the plane waves in the expansion to those with kinetic energy lower than the energy cutoff E_{cut} , following by the condition

$$\frac{\hbar}{2m}|\mathbf{k} + \mathbf{G}|^2 < E_{\text{cut}}. \quad (2.37)$$

If there is no atomic potential, the plane waves are the exact solutions. In the region far away from the nuclei where the potential is reasonably smooth, the potential can be reasonably treated as a perturbation to the free electron case. However, in the region near the nuclei, the atomic potential is very strong, making the wave functions very complicated. Such wave functions require a very large number of plane waves to describe, making it computationally impractical.

To overcome this problem, the pseudopotential (PP) was introduced. The main idea of pseudopotential as well as projector augmented wave method (PAW) is originated from the orthogonalized plane wave (OPW) approach, proposed by Herring (Herring, 1940). In this approach, the valence wave functions are constructed as a linear combination of plane wave and core wave functions. The plane wave expansions orthogonalized to the core states by choosing appropriate expansion coefficient. Then, the core states are eliminated by replacing the potential with an effective potential.

Within the spirit of OPW method and base on the observation that 1) core states are not essential to describe the chemical bonding and 2) the valence wavefunctions inside the core region are not need to be accurately described. The wavefunction near the core regions can be replaced with a smoother pseudo-wavefunction. Philips and Kleinman (Phillips and Kleinman, 1959) showed that one can construct a smooth valence-wavefunction $\tilde{\psi}_v$ that is not orthogonalized to the core states ψ_c as following

$$|\tilde{\psi}_v\rangle = |\psi_v\rangle + \sum_c \alpha_{cv} |\psi_c\rangle, \quad (2.38)$$

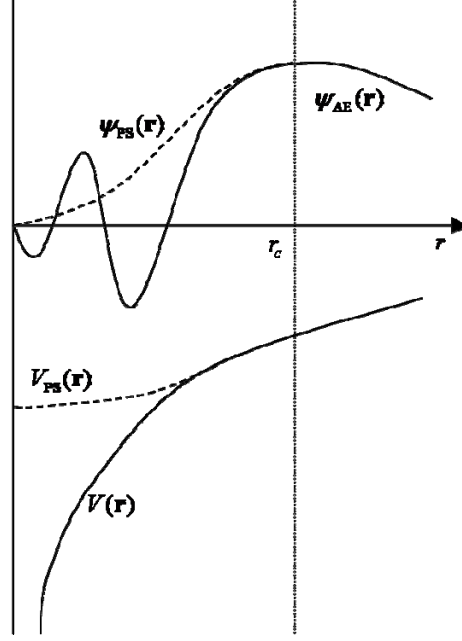


Figure 2.1 Schematic illustration of the replacement of the all-electron wave function and core potential (solid curves) by a pseudo-wave function and pseudopotential (dashed curves). The figure is a reproduction of Figure 3.1 in Ref. (Singh and Nordstrom, 2006)

where $\alpha_{cv} = \langle \psi_c | \tilde{\psi}_v \rangle \neq 0$. The reformulation of this pseudo-wavefunction with modified Schrödinger equation leads to a pseudo-Hamiltonian

$$\hat{H}_{\text{PS}} = \hat{H} + \sum_c (\varepsilon_v - \varepsilon_c) |\psi_c\rangle \langle \psi_c|, \quad (2.39)$$

where $\hat{H} = \hat{T} + \hat{V}$. $\hat{V} = (Z_c / r) \hat{I}$ is the bare potential of nuclei, where \hat{I} is the identity operator. This pseudo-Hamiltonian provides the same eigenvalues as that of the original one. However, its wavefunction is smoother and nodeless. The associated potential is

$$\hat{V}_{\text{PS}} = \frac{Z_c}{r} \hat{I} + \sum_c (\varepsilon_v - \varepsilon_c) |\psi_c\rangle \langle \psi_c|. \quad (2.40)$$

The potential is called pseudopotential. Its most general form can be written as

$$\hat{V}_{\text{ps}}(\mathbf{r}) = \sum_{l=0}^{\infty} \sum_{m=-l}^l v_{\text{ps}}^l(r) |lm\rangle \langle lm| = \sum_{l=0}^{\infty} v_{\text{ps}}^l(r) \hat{P}_l, \quad (2.41)$$

where $v_{\text{ps}}^l(r)$ is the pseudopotential associated with an angular component l and the

operator $\hat{P} = \sum_{m=-l}^l |lm\rangle \langle lm|$ is a projection operator of the l^{th} angular momentum.

2.4.1 Norm-conserving pseudopotential

The construction of pseudopotential is an inverse problem to give the well-behave pseudo wave functions outside the core regions. This requires the pseudo-wavefunctions to decay exactly as the all-electron wave functions beyond some radius r_c . In addition, the eigenvalues of a pseudo Hamiltonian are the same as those of all-electron Hamiltonian. To obtain such pseudopotential, the inversion of a radial Schrödinger equation

$$\left\{ -\frac{\hbar^2}{2m} \frac{d^2}{dr^2} + \frac{l(l+1)}{2r^2} + v(r) \right\} rR(\varepsilon, r) = \varepsilon rR(\varepsilon, r) \quad (2.42)$$

is needed. If ε is fixed, its solution is uniquely determined by the value of the wave function $R(\varepsilon, r)$ and its derivative $R'(\varepsilon, r)$ at any given point r_0 . If the all-electron potential and the pseudopotential are the same outside some radius r_c , then the all-electron and pseudo-wave functions are proportional when the corresponding logarithmic derivatives are the same. The proportionality becomes an equality when the norm inside the cutoff radius is preserved following the condition

$$\int_0^{r_c} r^2 [R_{\text{ps}}^l(\varepsilon, r)]^2 dr = \int_0^{r_c} r^2 [R_{\text{AE}}^l(\varepsilon, r)]^2 dr, \quad (2.43)$$

which is called norm-conservation property. This was first introduced by Hamann, Schlüter, and Chiang (Hamann, Schlüter and Chiang, 1979).

2.4.2 Ultrasoft pseudopotential (USPP)

The concept of the ultrasoft pseudopotential was first introduced by Vanderbilt (Vanderbilt, 1990). This offers a possibility to resolve the plane-wave convergence problem. In ultrasoft pseudopotential approach, the norm-conservation constraints are relaxed by generalizing the sum rule. By relaxing these constraints, all the wave functions at their reference energies can be transferred into pseudo-wave functions, requiring only the matching of the logarithmic derivative at the cutoff radius. This allows large cutoff radius can be chosen quite large beyond the maximum of the radial wavefunctions, resulting in smoother pseudo-wave functions.

2.4.3 Projector augmented-wave method (PAW)

To improve the pseudopotential approach, the PAW method was introduced by Blöchl (Blöchl, 1994). The approach combines the idea of ultrasoft pseudopotential and linearized augmented plane-waves (LAPW) method. It retains all-electron characters by decomposing the all-electron wavefunctions in terms of a smooth pseudo-wave function outside the core region and a rapid varying contribution localized within the core region. The all-electron and pseudo-wave functions are related by the following equation

$$|\psi_{\text{AE}}^n\rangle = |\psi_{\text{PS}}^n\rangle + \sum_{I=1}^P \sum_{l,m} \sum_i (|\phi_{\text{AE}}^{illm}\rangle - |\phi_{\text{PS}}^{illm}\rangle) \langle \tilde{p}_i^{llm} | \psi_{\text{PS}}^n \rangle, \quad (2.44)$$

where $\phi_{\text{AE}}^{illm}(\mathbf{r})$ are all-electron partial wavefunctions centering on atom I . $\phi_{\text{PS}}^{illm}(\mathbf{r})$ are pseudo-atomic partial wavefunctions that match the all-electron ones outside a cutoff

radius. \tilde{p}_i^{ilm} is the projector functions with the relation $\langle \tilde{p}_i^{ilm} | \psi_{\text{PS}}^n \rangle = \delta_{ij}$. In Eq. (2.44), the sums run over all the atomic sites I , angular momentum (l,m) , and the projector function i . From Eq. (2.44), the electronic density can be divided into three contributions. A soft pseudo-charge density from ψ_{PS}^n and two localized charge densities relating to $\phi_{\text{AE}}^{ilm}(\mathbf{r})$ and $\phi_{\text{PS}}^{ilm}(\mathbf{r})$. PAW method freezes the core orbitals and adjusts only the valence wavefunctions as the same way as the pseudopotential method. PAW is currently one of the most powerful approaches combining the efficiency of pseudopotential plane-wave method with the accuracy of augmentation method.

2.5 Force Acting on Nuclei

The forces acting on nuclei can be calculated by Hellman-Feynman theorem which was proved independently by Hellmann (Hellmann, 1937) and Feynman (Feynman, 1939). It states that the derivative of the total energy with respect to a parameter is the expectation value of the derivative of the Hamiltonian with respect to the parameter, i.e.,

$$\frac{\partial E}{\partial \lambda} = \langle \psi(\lambda) | \frac{\partial H}{\partial \lambda} | \psi(\lambda) \rangle. \quad (2.45)$$

If the parameters are the coordinates of nuclei, the derivatives become the force. This formalism allows the calculations of the forces from the derivatives of the Hamiltonian. Because only the potential terms in the Hamiltonian depend on coordinates, the RHS of Eq. (2.45) is actually just the derivatives of the potentials.

2.6 Periodic Boundary Conditions and Brillouin Zone Sampling

To directly solve the Kohn-Sham equations of crystalline solids without utilizing the crystal symmetries and periodicities, the calculations of vitally infinite atoms are needed. By applying the periodic boundary conditions, the problem is dramatically reduced. In this concept, a unit cell (a box) containing atom(s) is created and repeated in all appropriated directions. The symmetry and the structure of the unit cell correspond to the actual crystal geometry. The Bloch's theorem states that the wavefunctions obey,

$$\psi_{\mathbf{k}}(\mathbf{r} + \mathbf{a}_i) = e^{i\mathbf{k} \cdot \mathbf{a}_i} \psi_{\mathbf{k}}(\mathbf{r}), \quad (2.46)$$

where \mathbf{a}_i are translation lattice vectors. Note that, for a special case where $\mathbf{k} = 0$, the wavefunctions have the same periodicity as the unit cell.

For a larger cell, composed of several unit cells, the relationship

$$\psi_{\mathbf{k}}(\mathbf{r} + n\mathbf{a}_i) = e^{in\mathbf{k} \cdot \mathbf{a}_i} \psi_{\mathbf{k}}(\mathbf{r}) \quad (2.47)$$

is also hold if $\mathbf{k} \cdot \mathbf{a}_i = 2\pi m / n$ where m and n are integers. As a consequence, the non-equivalent \mathbf{k} -vectors that are compatible with periodic boundary condition in repeated cell consist of n replicas of the unit cell along the lattice vector \mathbf{a}_i are

$$\mathbf{k} = 0, \pm \frac{\mathbf{b}_i}{n}, \pm \frac{2\mathbf{b}_i}{n}, \dots, \pm \frac{(n/2-1)\mathbf{b}_i}{n}, \frac{\mathbf{b}_i}{2}. \quad (2.48)$$

The electronic charge density in a periodic lattice system can be described as

$$n(\mathbf{r}) = \sum_{\mathbf{k} \in \text{BZ}} \omega_{\mathbf{k}} |\psi_{\mathbf{k}}(\mathbf{r})|^2, \quad (2.49)$$

where the sum runs over all \mathbf{k} -vectors in the Brillouin zone. The weight factors $\omega_{\mathbf{k}}$, depend on the symmetries of the unit cell. Beside electronic charge density many

other, such as energy and density of states, can be obtained. For example, density of states per unit energy $n(\varepsilon)$ can be evaluated by the following expression

$$n(\varepsilon) = \frac{1}{\Omega_{\text{BZ}}} \int_{\text{BZ}} \delta(\varepsilon_{nk} - \varepsilon) d\mathbf{k}, \quad (2.50)$$

where ε_{nk} is the energy of the n^{th} electron, ε is the Fermi energy and Ω_{BZ} is volume of the Brillouin zone. To evaluate computationally, the integral in Eq. (2.50) can be changed to the weighted sum over a set of discrete k-points in Brillouin zone, i.e.,

$$\frac{1}{\Omega_{\text{BZ}}} \int_{\text{BZ}} d\mathbf{k} \rightarrow \sum_{\mathbf{k}} \omega_{\mathbf{k}} \quad (2.51)$$

The number of points required for well-converged wavefunction depends on a unit cell and the system details. The approach to accelerate the number of points convergence of Brillouin zone summation have been proposed by Baldereschi (Baldereschi, 1973) and Chadi and Cohen (Chadi and Cohen, 1973). However, the more general scheme proposed by Monkhorst and Pack (Monkhorst and Pack, 1976) is used in this thesis. The scheme divides the Brillouin zone into equally-spaced mesh with the special k -points

$$\mathbf{k} = n_1 \mathbf{b}_1 + n_2 \mathbf{b}_2 + n_3 \mathbf{b}_3, \quad (2.52)$$

where the integers n_i are given by $n_i = (2r - q - 1) / 2q$ and $r = 1, 2, \dots, q$. \mathbf{b}_i are reciprocal lattice vectors and q is the number of k-points in i direction.

In order to obtain a faster convergence of the integrations, Dirac-delta function for the occupation is replaced by smoother function. One of such functions is Fermi-Dirac function:

$$f\left(\frac{\varepsilon_{nk} - \varepsilon}{\sigma}\right) = \frac{1}{\exp\left(\frac{\varepsilon_{nk} - \varepsilon}{\sigma}\right) + 1}, \quad (2.53)$$

where σ is a smearing parameter. The entropy of the non-interacting at finite temperature can be also obtained.

CHAPTER III

CALCULATION METHODS FOR DEFECTS IN SEMICONDUCTORS

In this chapter, the methodologies needed for investigating defects in semiconductors are described. First-principles calculations enable us to investigate their behaviors and properties. Based on first-principles calculations, one can investigate several properties, e.g. local geometry of defects, x-ray absorption characteristics, and defect infrared spectroscopy signatures. The defect formation energy can also be obtained. The formation energy can be used to estimate the defect concentration. For the calculations, we use a plane-wave pseudopotential code called “Vienna *Ab-initio* Simulation Package (VASP)” (Kresse and Furthmüller, 1996b; Kresse and Furthmüller, 1996a).

3.1 Defect Concentration

For a system with N possible sites incorporating by n impurities, the impurity concentration is assumed to be sufficiently low such that interactions between defects can be ignored. The free energy of the system is defined as $F = E - TS$, where T is the temperature. The entropy is defined as $S = k \ln \Omega$, where k is the Boltzmann’s constant. Ω is the number of microstates which is equal to the number of possible ways to place n impurities on N sites. For instance $\Omega = N! / n!(N - n)!$. Stirling’s

formula is used when N and n are large, for e.g., $\ln N! \approx N(\ln N - 1)$ (Abramowitz and Stegun, 1965). Under thermodynamic equilibrium, the most stable state of the system is when the free energy is the lowest. Regarding the number of defects, the lowest free energy occurs when, $\frac{\partial F}{\partial n} \approx \frac{\partial E}{\partial n} - kT \ln(N/n) = 0$. This gives $n = N \exp[-(\partial E / \partial n) / kT]$, where $\partial E / \partial n$ is energy per impurity, i.e., formation energy E^f .

Under thermal equilibrium, the concentration of each defect depends on its formation energy, site occupation, and temperature. The concentration c of a defect is given by

$$c = N_{\text{sites}} N_{\text{degeneracy}} \exp(-E^f / kT), \quad (3.1)$$

where N_{sites} is the number of possible defect sites per unit volume in the lattice, k is the Boltzmann's constant, and T is the temperature. $N_{\text{degeneracy}}$ is the number of possible ways to arrange a defect on one site. For instance, number of different orientations that a defect can have at a particular site. In actual non-equilibrium growth processes, the concentrations could deviate greatly from the values obtained using Eq. (3.1).

How well Eq. (3.1) describes the actual growth process, depends on many factors. Generally, it is valid when the mobility of a relevant defect is sufficiently high to allow them to equilibrate at the temperature of interest (Van de Walle and Neugebauer, 2004).

3.2 Defect Formation Energy

The formation energy of a defect is defined as (Zhang and Northrup, 1991; Van de Walle and Neugebauer, 2004)

$$E^f(X^q) = E_{\text{tot}}(X^q) - E_{\text{tot}}(\text{bulk}) - \sum_i n_i \mu_i + q(E_F + E_v + \Delta V), \quad (3.2)$$

where $E_{\text{tot}}(X)$ is the total energy of a supercell containing a defect X (X can be a defect or a defect complex). $E_{\text{tot}}(\text{bulk})$ is the total energy of the same supercell containing no defect. n_i is the number of atoms of specie i (host atoms or impurity atoms) that are added to (positive) or removed from (negative) the supercell to create the defect. μ_i is the chemical potential of atom i . E_F is the Fermi level, referenced to the valence band maximum in the bulk, E_v . There is also a correction term ΔV needed to align the potential in the supercell containing defect with that in the bulk. This is because the calculations of the supercell containing a defect and of the bulk are separated calculations and used different potential energies. ΔV aligns the electrostatic potential at the point far from the defect with that of the bulk.

For shallow defects, there is another correction needed to improve the value of the calculated ionization energy. For a shallow acceptor, the acceptor level exhibits a similar dispersion to the uppermost of valence band. In the negative charge state, this level is filled (assumed that it is a single acceptor). For a real isolated acceptor, which is corresponding to a calculation using an infinitely large supercell, this electron would be removed from the top of valence band at the Γ point. However, in the actual calculations, where the supercell size is limited, the electron is removed from the highest occupied Kohn-Sham level at the special k-points. The correction energy (E_{corr}) is defined as the energy difference between the highest occupied state at Γ

point and that at special k-points. The magnitude of this correction can be sizeable, depending on the supercell size. In Ref. (Van de Walle, Limpijumnong and Neugebauer, 2001), the correction energy for the case of Be_{Ga} in GaN is illustrated as

$$E^f(\text{Be}_{\text{Ga}}^0) = E_{\text{tot}}(\text{Be}_{\text{Ga}}^0) - E_{\text{tot}}(\text{GaN, bulk}) - \mu_{\text{Be}} + \mu_{\text{Ga}} - E_{\text{corr}}. \quad (3.3)$$

For shallow donors, E_{corr} is also needed. For donors, it is the energy difference between the lowest occupied state at the Γ point and that at the special k-points.

The formation energy can be used to predict the stable defects and charge states under a given growth condition. Moreover, it is very useful for predicting the electrical properties of those defects.

3.3 Chemical Potentials

The formation energy of a defect depends strongly on the availability (partial pressure) of each constituent element in the growth process. For instance, the high partial pressure of Ga can help to suppress the formation of Ga vacancies. However, the condition would increase the chance of N vacancy formation. In the calculations, the partial pressure influences the formation energy through the chemical potential μ_i . In order for the crystal to grow in equilibrium (gradually grown), the partial pressure of each elemental component has to be in balance. For instance, in the case of GaN, the balance conditions between the chemical potential of Ga and N are described by

$$\mu_{\text{Ga}} + \mu_{\text{N}} = E_{\text{tot}}(\text{GaN}), \quad (3.4)$$

where $E_{\text{tot}}(\text{GaN})$ is the total energy of GaN per molecular formula. If the sum on the left hand side (LHS) of Eq. (3.4) is higher than $E_{\text{tot}}(\text{GaN})$, then GaN will quickly grow and the quality of the crystal will be poor. On the other hand, if the sum on the

LHS is lower than $E_{\text{tot}}(\text{GaN})$, the crystal will disintegrate. The natural phases of Ga and N, i.e. metal Ga and N_2 molecule, set the upper limit of the chemical potentials. Under the extreme Ga-rich condition, the value of μ_{Ga} is equal to its upper limit $\mu_{\text{Ga}} = \mu_{\text{Ga}[\text{bulk}]}$. This gives the lower μ_{N} limit,

$$\mu_{\text{N}}^{\text{min}} = E_{\text{tot}}(\text{GaN}) - \mu_{\text{Ga}[\text{bulk}]} \quad (3.5)$$

If μ_{Ga} is pushed higher than this limit, the crystal will not grow smoothly because the metal phase of Ga will start to form (Tarsa, Heying, Wu, Fini, DenBaars and Speck, 1997). Similarly, the upper limit for N-rich condition is $\mu_{\text{N}} = \mu_{\text{N}[\text{N}_2 \text{ molecule}]}$ which result the lower limit on μ_{Ga} ,

$$\mu_{\text{Ga}}^{\text{min}} = E_{\text{tot}}(\text{GaN}) - \mu_{\text{N}[\text{N}_2 \text{ molecule}]} \quad (3.6)$$

The total energy of GaN can be expressed in terms of chemical potentials as

$$E_{\text{tot}}(\text{GaN}) = \mu_{\text{Ga}[\text{bulk}]} + \mu_{\text{N}[\text{N}_2 \text{ molecule}]} + \Delta H_f(\text{GaN}), \quad (3.7)$$

where $\Delta H_f(\text{GaN})$ is the enthalpy of formation or heat of formation of GaN.

When an impurity x is incorporated to the materials, its solubility also depend on the corresponding chemical potential μ_x . The lower bound of μ_x is $-\infty$. This is the case that there is no impurity x in the growth environment. The upper bound of μ_x is generally defined as the formation energy of natural phase of x . For example, the upper bound of chemical potential $\mu_{\text{Mg}} = \mu_{\text{Mg}[\text{bulk}]}$. However, sometimes an additional bounds introduced by others phases are considered. For example, when Mg is incorporating in GaN, the Mg can interact with N and form Mg_3N_2 with an equilibrium condition

$$3\mu_{\text{Mg}} + 2\mu_{\text{N}} = 3\mu_{\text{Mg}[\text{bulk}]} + 2\mu_{\text{N}[\text{N}_2 \text{ molecule}]} + \Delta H_f(\text{Mg}_3\text{N}_2), \quad (3.8)$$

where $\Delta H_f(\text{Mg}_3\text{N}_2)$ is the enthalpy of formation of Mg_3N_2 . This gives

$$3\mu_{\text{Mg}} + 2\mu_{\text{N}} = E_{\text{tot}}(\text{Mg}_3\text{N}_2), \quad (3.9)$$

Equation (3.9) gives the relationship between μ_{Mg} and μ_{N} which sometimes post on additional constrain on μ_{Mg} .

3.4 Supercell Approach

Our calculations of defects and impurities are performed with the supercell approach. The name “supercell” refers to a cell that composed of several primitive unit cells. The model of a defect or an impurity can be made by adding, substituting, or removing atoms in the supercell. Generally defect in real materials are exist in a low concentration, for e.g., in the order of 10^{17} per cm^3 . This corresponds to a defect in $\sim 10^6$ atoms of host material. Although, a large supercell should be used to study isolated defects, in practice, a supercell containing 10^6 atoms is too big for first-principle calculations. This is because computation time goes as $N^2 \ln N$ where N is the number of atoms in supercell. It is thus important to choose the smallest cell size that gives reliable results for the system under investigation. In practice, a convergence of the results with respect to different supercell sizes should be carefully checked.

3.4.1 Supercell for the wurtzite structure

The primitive unit cell of the wurtzite structure (containing four atoms) has the lattice translation vectors $\mathbf{a}_1 = (a/2, -\sqrt{3}a/2, 0)$, $\mathbf{a}_2 = (a/2, \sqrt{3}a/2, 0)$, and $\mathbf{a}_3 = (0, 0, c)$, where a and c are the lattice parameters. If each translation vector of this

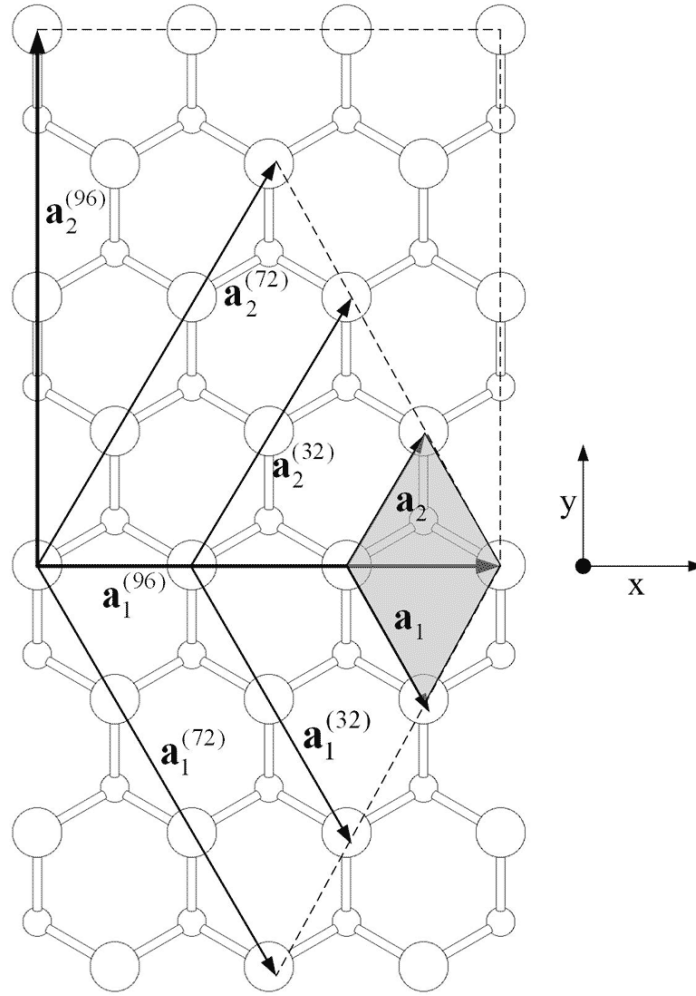


Figure 3.1 Schematic illustration of the wurtzite structure, the c-axis ([0001] direction) is perpendicular to the paper. The large circles represent cations, small circles anions. The shaded area shows the primitive unit cell. The arrows represent the translation vectors of each cell (as labeled). The dashed lines serve as a guide to the eye for the shape of the supercells.

basic unit cell is doubled then the translation vectors of 32-atom supercell (composed of eight primitive unit cell of the wurtzite structure) are obtained. This gives $\mathbf{a}_i^{(32)} = 2\mathbf{a}_i$ where $a_i = 1, 2, 3$. To create a 72-atom supercell, the primitive unit cell is

repeated three times along two directions on the basal-plane and twice in c -axis direction, so that the translation vectors are $\mathbf{a}_1^{(72)} = 3\mathbf{a}_1$, $\mathbf{a}_2^{(72)} = 3\mathbf{a}_2$, and $\mathbf{a}_3^{(72)} = 2\mathbf{a}_3$. In Figure 3.1, the shapes of 32- and 72-atom supercells are shown. Although, these supercells are easy to create, they are not very efficient for defect calculations. This is because the lengths of the three translation vectors are quite different (by 23% for 32-atom cell and 4% for 72-atom cell). As a result, the distances between defects in neighboring supercell images are unbalanced along each direction. To avoid this underlying problem, the 96-atom supercell is used. For the 96-atom cell, the translation vectors are mutually perpendicular, leading to a supercell with orthorhombic symmetry. The translation vectors of 96-atom supercell are $\mathbf{a}_1^{(96)} = 3\mathbf{a}_1 + 3\mathbf{a}_2$, $\mathbf{a}_2^{(96)} = 2\mathbf{a}_2 - 2\mathbf{a}_1$, and $\mathbf{a}_3^{(96)} = 2\mathbf{a}_3$, resulting in $\mathbf{a}_1^{(96)} = (3a, 0, 0)$, $\mathbf{a}_2^{(96)} = (0, 2\sqrt{3}a, 0)$, and $\mathbf{a}_3^{(96)} = (0, 0, 2c)$ as illustrated in Figure 3.1. The lengths of the translation vectors of 96-atom cell are quite similar (different by only 5%)

3.4.2 Supercell for the zincblende structure

The primitive unit cell of the zincblende structure has a face-center-cubic (fcc) symmetry. The cell (containing two atoms) has the translation vectors $\mathbf{a}_1 = (a/2, a/2, 0)$, $\mathbf{a}_2 = (0, a/2, a/2)$, and $\mathbf{a}_3 = (a/2, 0, a/2)$. The two most common supercells are 32- and 64-atom supercell that have a body-center-cubic and simple-cubic symmetry, respectively. For the 32-atom supercell, the translation vectors are $\mathbf{a}_1^{(32)} = 3\mathbf{a}_2 - \mathbf{a}_3 - \mathbf{a}_1 = (-a, a, a)$, $\mathbf{a}_2^{(32)} = 3\mathbf{a}_3 - \mathbf{a}_1 - \mathbf{a}_2 = (a, -a, a)$, and $\mathbf{a}_3^{(32)} = 3\mathbf{a}_1 - \mathbf{a}_2 - \mathbf{a}_3 = (a, a, -a)$. In this thesis, we mostly use the 64-atom supercell. The translation vectors of the 64-atom supercell are $\mathbf{a}_1^{(64)} = 2\mathbf{a}_1 - 2\mathbf{a}_2 + 2\mathbf{a}_3$,

$\mathbf{a}_2^{(64)} = 2a_2 - 2a_3 + 2a_1$, and $\mathbf{a}_3^{(64)} = 2a_2 - 2a_3 + 2a_1$. The simpler form of these vectors are $\mathbf{a}_1^{(64)} = (2a, 0, 0)$, $\mathbf{a}_2^{(64)} = (0, 2a, 0)$, and $\mathbf{a}_3^{(64)} = (0, 0, 2a)$.

3.4.3 Finite-size corrections

In the supercell approach, there are undesired interactions between defects and their images in periodic neighboring supercell. These interactions cause errors in the calculations. One of the errors is due to the elastic interactions. It is the leading error for uncharged defects and causes an overestimation in formation energy. The strain energy of a point defect falls off roughly with L^{-3} , where L is the linear dimension of the supercell, according to the elastic continuum theory (Grecu and Dederichs, 1971; Dederichs and Pollmann, 1972). We can therefore get rid of the elastic energy by performing the calculations with a few supercell sizes and extrapolating to the dilute limit ($L \rightarrow \infty$).

For charged defects, the calculations apply a uniform background charge (jellium) to counter part the defect avoiding the divergence of long-range Coulomb terms. Makov and Payne (Makov and Payne, 1995) mentioned that the energy of this system will converge very slowly as a function of the supercell size if the charge on the defect is assumed to be a point charge. This is because of the electrostatic interactions between the periodic arrangements of monopoles with compensated background converge as $1/\varepsilon L$, where ε is the static dielectric constant. Makov and Payne proposed a correction term which is derived from the multipole expansion. The first-order correction term is $-q^2\alpha/2\varepsilon L$, where q is charge and α is the Madelung constant of the supercell. This is sizeable for highly charged defects. However, this correction tends to work well for charged atomic or molecular systems with very

localized charge. However, it has been found to lead to an overestimation for defects in semiconductors (Van de Walle and Neugebauer, 2004) where the charge is generally not very localized. Often, the correction of defects in semiconductors worsens the results (Segev and Wei, 2003). We therefore do not apply this correction to the results reported in this thesis.

3.5 Defect Transition Levels

Some of point defects and impurities introduce levels in the bandgap of semiconductors. Electrons can be excited to and from these levels, allowing experimental detections. For examples, they can be detected by using deep-level transient spectroscopy (DLST) or photoluminescence (PL) experiments (Troxell and Watkins, 1980). In addition, for shallow defects, the level could be determined from an analysis of temperature-dependence Hall data (Chand, Henderson, Klem, Masselink, Fischer, Chang and Morko , 1984). It is also beneficial to carry out the calculation of these levels.

3.5.1 Thermodynamic transition levels

This type of levels would be observed in experiments where the final charge state has time to relax to its equilibrium configuration. Let the initial state with charge q_1 transforms to the final state with charge q_2 . Such transition would be able to be observed in DLST experiments. In the cases of shallow centers, such level could be derived from analyzing of temperature-dependent Hall data. The thermodynamic transition level $\varepsilon(q_1/q_2)$ is defined as the Fermi-level position where the charge

states q_1 and q_2 have an equal formation energy. Base on Eq. (3.2), $\varepsilon(q_1/q_2)$ can be obtained from

$$\varepsilon(q_1/q_2) = \frac{E^f(X^{q_1}; E_F = 0) - E^f(X^{q_2}; E_F = 0)}{q_2 - q_1}, \quad (3.10)$$

where $E^f(X^q; E_F = 0)$ is the formation energy of defect X in charge state q when the Fermi level is located at the valence band maximum ($E_F = 0$). If the Fermi level of the system lies below $\varepsilon(q_1/q_2)$, charge state q_1 is stable. On the other hand, if the Fermi level lies above $\varepsilon(q_1/q_2)$, charge state q_2 is stable. If a $\varepsilon(q_1/q_2)$ is located near the Fermi level such that the defect is likely to be thermally ionized at room temperature. It is called a shallow level. On the other, hand if it is unlikely to be ionized at room temperature, it is called a deep level.

For example, Be_{Ga} in GaN is found to be a shallow acceptor (Van de Walle, *et al.*, 2001). The relevant charge states in this case are $q_1 = 0$ and $q_2 = -1$. The thermodynamic transition level $\varepsilon(0/-1) = 170 \text{ meV} = E_A$ is called “the thermal ionization energy or acceptor ionization energy”. It is defined as

$$E^f(\text{Be}_{\text{Ga}}^-)(E_F = E_A) = E^f(\text{Be}_{\text{Ga}}^0). \quad (3.11)$$

From definition of formation energy in Eq. (3.2), E_A can be written as

$$E_A = E^f(\text{Be}_{\text{Ga}}^-)(E_F = 0) - E^f(\text{Be}_{\text{Ga}}^0). \quad (3.12)$$

Based on the definition of the thermal ionization energy, the atomic structure used to calculate each E^f in Eq. (3.12) is relaxed to its equilibrium configuration. The atomic positions in these equilibrium configurations are not necessarily the same for both charge states.

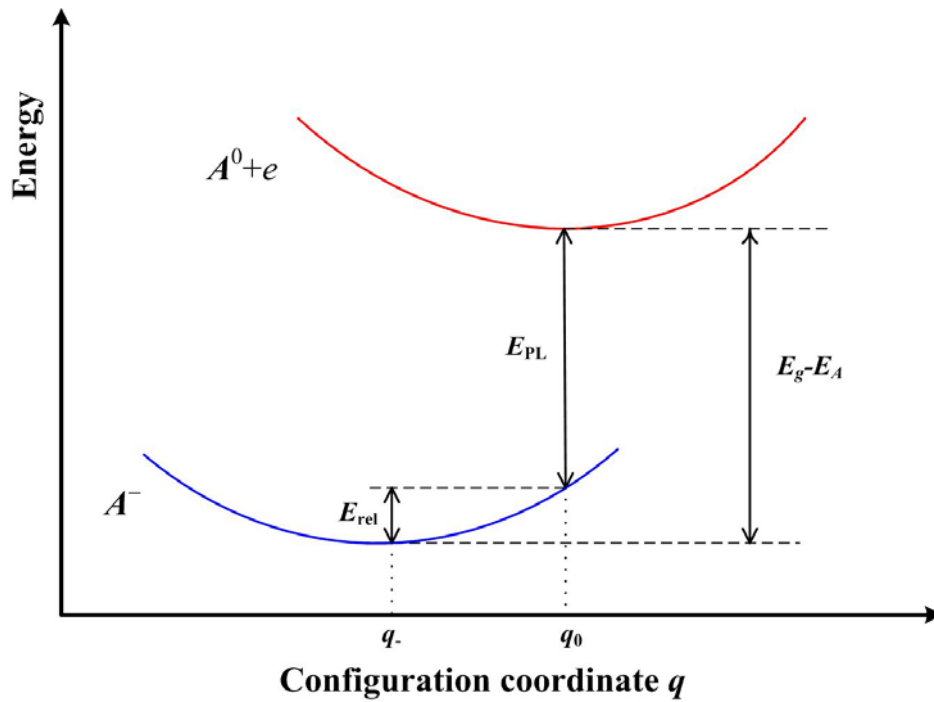


Figure 3.2 Schematic configuration coordinate diagram of an acceptor A in negative charge state A^- and neutral charge state A^0 with the presence of an electron in the bottom of conduction band. It is illustrating the difference between thermal and optical ionization energies for an acceptor A . E_{rel} is the energy gained by the relaxation of negative charge state A^- from A^0 equilibrium configuration to its equilibrium configuration, called “Frank-Condon shift”.

3.5.2 Optical transition levels

If the occupied levels are excited by photons, the transition of electrons between charge states q_1 and q_2 can occur, corresponding to the optical level $\varepsilon^{opt}(q_1/q_2)$. The optical transition levels can be defined in the same way as thermodynamic transition level except that the final state q_2 does not have time to relax from the q_1 state’s configuration. An example of an experiment that measures the optical transition levels

is the photoluminescence (PL) experiments. To elucidate this process, we consider an acceptor impurity, denoted by “ A ”. An exciting photon creates an electron-hole pair where the hole can be trapped at an A^- center and turns it into A^0 . An electron can be transferred to the bottom of the conduction band. The equilibrium configuration of the $A^0 + e$ state (where e is an electron at the bottom of conduction band) is higher in energy than the equilibrium configuration of A^- , $E_g - E_A$, as illustrated in Figure 3.2. E_g and E_A are the bandgap energy and the thermal ionization energy. Adding and subtracting the bandgap energy E_g to the ionization energy, we get $E_A = E^f[A^-](E_F = 0) - \{E^f[A^0] + E_g\} + E_g$, where the term $\{E^f[A^0] + E_g\}$ is the energy of $A^0 + e$. This gives $E_g - E_A = E^f[A^0 + e] - E^f[A^-](E_F = 0)$.

When an electron in the conduction band recombines with a hole on the acceptor, a photon with energy E_{PL} is emitted as illustrate in Figure 3.2. During this emission process, the atomic configuration of the acceptor remains fixed. The difference in energy between the negative charge acceptor A^- in q_0 configuration and its equilibrium configuration is the relaxation energy E_{rel} (Frank-Condon shift). $E_{PL} = E_g - E_A - E_{rel}$ as shown in Figure 3.2. The optical ionization energy, E_A^{opt} , is defined as the energy difference between the bandgap and the E_{PL} , i.e, $E_A^{opt} = E_g - E_{PL} = E_A + E_{rel}$. The ionization energy derived from an optical-related experiment is larger than the thermal ionization energy by an amount E_{rel} , which can be sizable depending on the difference in the atomic configuration between the two charge states.

3.6 Formation of Defect Complexes

Beside isolated point defects and impurities, the complexes between them can form. In order for two isolated defects to form a defect complex, one of the requirements is that the overall energy must be reduced after the complex is formed, i.e. the formation energy of the defect complex must be lower than the sum of formation energies of original defects. For example, defect A and defect B could combine to form a defect complex AB and release energy E_b , illustrated by the chemical reaction



The energy released (E_b) can be calculated from the formation energies

$$E_b = E^f(A) + E^f(B) - E^f(AB). \quad (3.14)$$

Defects A and B are bound and prefer to combine together to form defect complex AB only when E_b is positive. However, having a positive binding energy is not a guarantee that the complex will form. The actual formation of a defect complex depends on various factors. These include, but are not limited to, the absolute formation energies of each of the individual defects and the defect complex, the temperature, charge balance, and diffusivity of the defects involved. In order to achieve a larger concentration of complex than its constituents, the formation energy of the complex should be lower than both $E^f(A)$ and $E^f(B)$ in an essential amount. The concentration of complex will be small unless its binding energy is comparable to the formation energy of the constituents. This is because the complexes usually have a much more smaller configuration entropy. For example, a complex that consists of two constituents can be formed in $N_{\text{site}} N_{\text{degeneracy}}$ different configurations. However, if

the two constituents are independently formed, they can be produced in N_{site}^2 configurations. Note that $N_{\text{degeneracy}}$ is much smaller than N_{site} . It is therefore important to look at both complex binding energy and the configuration entropy when investigating complex defects.

3.7 Diffusivity, Migration and Minimum Energy Paths

Point defects may be mobile, depending on many factors, e.g., local bond strength, size of the diffusion atoms, and temperature. The diffusion properties of defects are essential to understand their incorporation during growth or processing. Experimentally, the dynamics of point defects can be studied by several techniques, for e.g., the electron paramagnetic resonance (EPR) and positron annihilation measurements. In experiments, the migration barriers are estimated based on the observations of the temperature at which the defects become mobile. Therefore, the calculations of defect migration barriers are important. A method to find the lowest energy path and the saddle point for a migration of an atom from a configuration to another, called “nudge elastic band (NEB)” method (Jónsson, Mills and Jacobsen, 1998) is used in this thesis. NEB is widely used in both chemistry and condensed matter physics. NEB method was originally formulated from chain of states method where several images (or states) of the system are connected together by virtual springs. The object function of system consist of P images can be constructed as

$$S^{PEB}(\mathbf{R}_1, \dots, \mathbf{R}_{P-1}) = \sum_{i=0}^P V(\mathbf{R}_i) + \sum_{i=1}^P \frac{Pk}{2} (\mathbf{R}_i - \mathbf{R}_{i-1})^2, \quad (3.15)$$

where \mathbf{R}_i is the reaction coordinate where some subset of the coordinates in the system is used to define a progress variable. $V(\mathbf{R}_i)$ is a potential function and k is

the spring constant. One could imagine minimizing this object function to find a minimum energy path (MEP) with respect to the intermediate images while fixing the end point images. This method is referred as “plain elastic band (PEB)” where the force acting on image i is

$$\mathbf{F}_i = -\nabla V(\mathbf{R}_i) + \mathbf{F}_i^s, \quad (3.16)$$

where

$$\mathbf{F}_i^s = k_{i+1}(\mathbf{R}_{i+1} - \mathbf{R}_i) - k_i(\mathbf{R}_i - \mathbf{R}_{i-1}). \quad (3.17)$$

The PEB method has its own fundamental problems. One problem is the corner cutting problem. This problem is resulted from a component of the spring force, which tends to pull images off the MEP. Another is the sliding down problem which results from the component of the true force $\nabla V(\mathbf{R}_i)$ in the direction of the path [see Fig. 3 in chapter 16 of the book by H. Jónsson *et al.* (Jónsson, *et al.*, 1998)]. In the NEB method, these problems are solved by projecting out the perpendicular component of the spring force and the parallel component of the true force when minimizing of an elastic band. Therefore, the force acting on image i becomes

$$\mathbf{F}_i^0 = -\nabla V(\mathbf{R}_i)|_{\perp} + \mathbf{F}_i^s \cdot \hat{\tau}_{\parallel} \hat{\tau}_{\parallel}, \quad (3.18)$$

where $\hat{\tau}_{\parallel}$ is the unit tangent to the path and $\nabla V(\mathbf{R}_i)|_{\perp} = \nabla V(\mathbf{R}_i) - \nabla V(\mathbf{R}_i) \cdot \hat{\tau}_{\parallel} \hat{\tau}_{\parallel}$. This projection of the perpendicular component of $\nabla V(\mathbf{R}_i)$ and the parallel component of the spring force is referred as “nudging”. NEB method is one of the most effective tools to find the MEP. NEB can find the energy barrier rather accurately, especially when sufficient images are included in the chain. The implementation of NEB method in the VASP code allows us to carry out MEPs and activation energy barriers for defect diffusions in solids.

CHAPTER IV

NATIVE-DEFECT-RELATED COMPLEX DONORS IN

n-TYPE ZnO

In this chapter, we present the results, focusing on theoretical part, of $\text{Zn}_i\text{-N}_\text{O}$ complex in ZnO. This work was a collaboration with experimentalist groups and has been published in 2005 (Look, *et al.*, 2005).

4.1 Introduction

ZnO is one of the transparent conducting oxide materials which has generated great interest since the past decade. This is because of the advances in bulk and epitaxial growth techniques make it possible to grow high quality ZnO crystal. ZnO is a potential material for new photonic and electronic application devices, such as UV light emitting diodes and transparent transistors (Look, 2001; Pearton, Norton, Ip, Heo and Steiner, 2005). As grown ZnO are *n*-type. The dominant donors were characterized to have activation energies of between 30 and 60 meV (Wagner and Helbig, 1974; Look, Reynolds, Sizelove, Jones, Litton, Cantwell and Harsch, 1998). Because the growth conditions were typically Zn-rich, the dominant donors were proposed to be either oxygen vacancy V_O or zinc interstitial Zn_i (Kröger, 1964; Look, Hemsky and Sizelove, 1999a). In 2000, Kohan *et al.* (Kohan, Ceder, Morgan and Van de Walle, 2000) showed that both V_O and Zn_i have high formation energies in *n*-type ZnO based on first-principles calculations. In addition, they showed that both native

defects are deep donors. However, recent computational work found that Zn_i is actually a shallow donor (Oba, Nishitani, Isotani, Adachi and Tanaka, 2001; Zhang, Wei and Zunger, 2001), as has also been suggested by electron-irradiation experiments (Look, *et al.*, 1999a). However, its high formation energy would still limit its formation in *n*-type ZnO. V_{O} is theoretically suggested as a deep donor (Janotti and Van de Walle, 2005; Janotti and Van de Walle, 2007b). Hydrogen is proposed to be one of the causes for *n*-type in ZnO by Van de Walle. Van de Walle's theoretical results (Van de Walle, 2000) show that interstitial hydrogen is always a donor, easily to ionize, and has a low formation energy. In addition to interstitial H, in a more recent work, Janotti and Van de Walle theoretically show that hydrogen substitution oxygen is also a potentially source of *n*-type carriers in ZnO and other metal oxides, (Janotti and Van de Walle, 2007a). Many experiments have confirmed that a shallow donor, with characters similar to those proposed to be H exists in commercial ZnO and can contribute significantly to the conductivity (Cox, Davis, Cottrell, King, Lord, Gil, Alberto, Vilão, Piroto Duarte, Ayres de Campos, Weidinger, Lichti and Irvine, 2001; Hofmann, Hofstaetter, Leiter, Zhou, Henecker, Meyer, Orlinskii, Schmidt and Baranov, 2002; Shimomura, Nishiyama and Kadono, 2002; Ip, Overberg, Heo, Norton, Pearson, Stutz, Luo, Ren, Look and Zavada, 2003; Nickel and Fleischer, 2003; Strzhemechny, Mosbacker, Look, Reynolds, Litton, Garces, Giles, Halliburton, Niki and Brillson, 2004). This fact, coupled with the theoretical evidence of high formation energies for the native defects led to believe that native donors are unlikely to be the source of the conductivity in as-grown ZnO (Kohan, *et al.*, 2000; Janotti and Van de Walle, 2007b).

In contrary, there are experimental evidence suggesting that native defect-related donors can contribute to the conductivity in *n*-type ZnO (Look, *et al.*, 2005). A molecular dynamic simulation by Nordlund also suggested that in a 1-MeV electron irradiation experiment, Zn_i is a much better candidate for irradiation donor than V_O . There is also an evidence that isolated Zn_i is mobile at room temperature (Coşkun, Look, Farlow and Sizelove, 2004; Gorelkinskii and Watkins, 2004). As a result, Zn_i has to form a complex to be stable.

Nitrogen is a highly plausible candidate to form complex with Zn_i . In many cases, nitrogen was introduced during the annealing processes. N can substitute O because of their covalent radii are comparable. N concentration is observed to be about 10^{17} cm^{-3} in ZnO sample used in the experiment by Look *et al.* (Look, Reynolds, Litton, Jones, Eason and Cantwell, 2002). We studied the Zn_i-N_O complex, using first-principles calculations based on density functional theory (DFT) and pseudopotentials. The formation energy and binding energy of the complex are calculated. The calculation shows that Zn_i-N_O complex is a shallow donor with the donor transition level shallower than that of Zn_i . The complex is thermodynamically stable compared to isolated Zn_i and N_O with a high binding energy. An estimation of defect concentrations is carried out.

4.2 Computational Method

The calculations are performed based on density functional theory with the local density approximations (LDA) (Hohenberg and Kohn, 1964; Kohn and Sham, 1965). The Vanderbilt-type ultrasoft pseudopotentials are used as implemented in the Vienna *ab-initio* simulation package (VASP) (Kresse and Furthmüller, 1996a; Kresse

and Furthmüller, 1996b). The Zn 3*d* electrons are treated as valence electrons. The cut-off energy of plane-wave basis set is set at 300 eV. The calculated lattice constant a of wurtzite ZnO of 3.205 Å and c/a of 1.60 are in good agreement with the experimental values of 3.249 Å and 1.602, respectively (Madelung, 1996). To study defects, i.e., Zn_{*i*}, N_O, and Zn_{*i*}-N_O, the supercell approach is employed. The supercell used in this work consists of 96 atoms (48 Zn atoms and 48 O atoms) or contains 24 primitive unit cells of wurtzite structure. The shifted 1×1×1 k -point grid for Brillouin zone integration is used; following the Monkhorst-Pack scheme (Monkhorst and Pack, 1976). All atoms are allowed to relax until the Hellmann-Feynman forces less than 0.1 eV/Å. For charged defects, the jellium background is used to neutralize the system.

The formation energy of Zn_{*i*}^{*q*}, N_O^{*q*}, and (Zn_{*i*}-N_O)^{*q*} where q is the charge state are defined as

$$E^f(\text{Zn}_i^q) = E_{\text{tot}}(\text{Zn}_i^q) - E_{\text{tot}}(\text{bulk}) - \mu_{\text{Zn}} + qE_F, \quad (4.1)$$

$$E^f(\text{N}_O^q) = E_{\text{tot}}(\text{N}_O^q) - E_{\text{tot}}(\text{bulk}) - \mu_{\text{N}} + \mu_{\text{O}} + qE_F, \quad (4.2)$$

and

$$E^f(\text{Zn}_i - \text{N}_O)^q = E_{\text{tot}}(\text{Zn}_i - \text{N}_O)^q - E_{\text{tot}}(\text{bulk}) - \mu_{\text{Zn}} - \mu_{\text{N}} + \mu_{\text{O}} + qE_F, \quad (4.3)$$

respectively. $E_{\text{tot}}(\text{Zn}_i^q)$, $E_{\text{tot}}(\text{N}_O^q)$, and $E_{\text{tot}}(\text{Zn}_i - \text{N}_O)^q$ are the total energies of the supercell containing Zn_{*i*}, N_O, and Zn_{*i*}-N_O in charge state q , respectively.

$E_{\text{tot}}(\text{bulk})$ is the total energy of the defect-free supercell. For defects in charge state q , electrons are removed (or added) to the Fermi energy of the system. μ_{Zn} , μ_{O} , and μ_{N} are the chemical potentials of the Zn atom, O atom, and N atom, respectively. In

this study, we focus our attentions on the Zn-rich conditions where μ_{Zn} is given by the energy of a Zn atom in the bulk zinc ($\mu_{\text{Zn}} = -1.87$ eV). This sets the oxygen chemical potential $\mu_{\text{O}} = E_{\text{tot}}(\text{ZnO}) - \mu_{\text{Zn}[\text{bulk}]} = -8.79$ eV. This is based on the calculated heat of formation of ZnO defined as $\Delta H_f(\text{ZnO}) = E_{\text{tot}}(\text{ZnO}) - \mu_{\text{Zn}[\text{bulk}]} - \mu_{\text{O}[\text{O}_2 \text{ molecule}]} = -3.58$ eV. The experimental value of ZnO heat of formation is 3.61 eV (Dean, 1992). The energy of half N_2 molecule is used for μ_{N} .

The concentration of each defect under thermodynamic equilibrium conditions at a finite temperature depends on its formation energy. The concentration can be expressed as

$$c = N_{\text{sites}} N_{\text{degeneracy}} \exp(-E^f / kT), \quad (4.4)$$

where N_{sites} is the number of sites in the ZnO lattice per unit volume that defect can occupy. For ZnO, the N_{sites} value for Zn site (or O site) is $\sim 4.28 \times 10^{22} \text{ cm}^{-3}$. $N_{\text{degeneracy}}$ is the number of equivalent configurations in which defects can be incorporated. For Zn_i and N_O , $N_{\text{degeneracy}}$ is 1. For $\text{Zn}_i - \text{N}_\text{O}$, $N_{\text{degeneracy}}$ is 3.

4.3 Results and Discussion

4.3.1 Defect structure and formation energy

There are two interstitial sites in wurtzite structure, the tetrahedral site and the octahedral site. For ideal structure ZnO, the tetrahedral site has four Zn and four O as nearest-neighbor atoms. Zinc atom occupied at this site is severely suffered from geometrical constraints. The octahedral site is in the hexagonal channel along the c axis where it is surrounded by three Zn and three O atoms. One therefore would

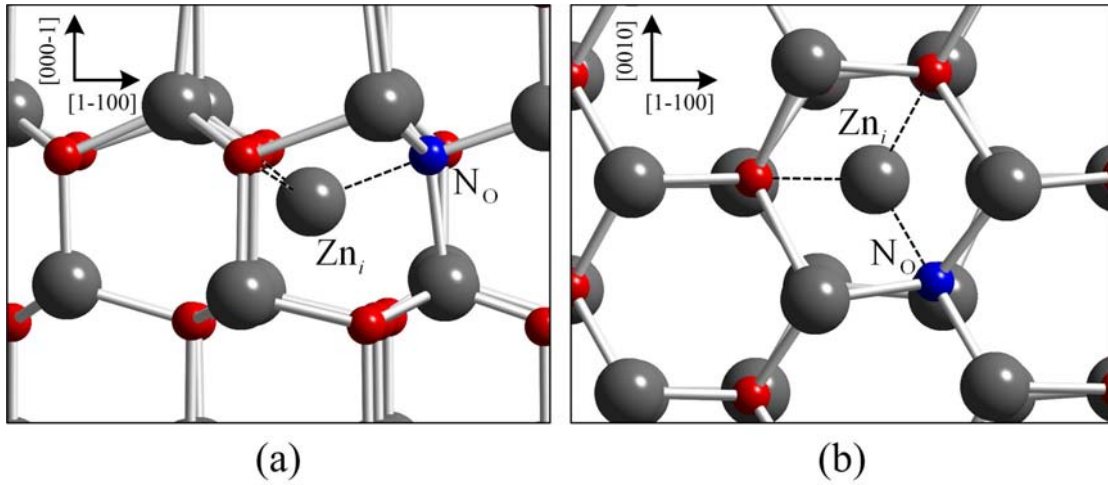


Figure 4.1 Local atomic geometry of $(\text{Zn}_i\text{-N}_\text{O})^+$. (a) Side view (perpendicular to the c axis). (b) Top view (parallel to the c axis).

expect that Zn interstitial will prefer the octahedral site over the tetrahedral site because the site has less geometrical constrain. Similar to the work of Janotti and Van de Walle (Janotti and Van de Walle, 2007b), we found that Zn_i at the tetrahedral site is unstable. It spontaneously relaxes to the octahedral site.

Under the presence of N_O , the complex of Zn_i and N_O can be formed. N prefers to occupy on the oxygen site due to the similar covalent radius between O and N (N is only $\sim 2.7\%$ larger in radius). There are also a number of experimental and theoretical works suggested that N is in the form of N_O in ZnO as well as substitutional diatomic molecule $(\text{N}_2)_\text{O}$ (Limpijumnong, *et al.*, 2005; Perkins, Lee, Li, Asher and Coutts, 2005; Fons, Tampo, Kolobov, Ohkubo, Niki, Tominaga, Carboni and Friedrich, 2007). For N_O , the averaged bond length between N and four surrounding Zn (Zn-N bond) is slightly smaller than typical Zn-O bond by $\sim 3.2\%$, indicating a small strains. The complex between Zn_i and N_O in the simplest form would be a pair between Zn_i at octahedral site and N substituting at one of nearest

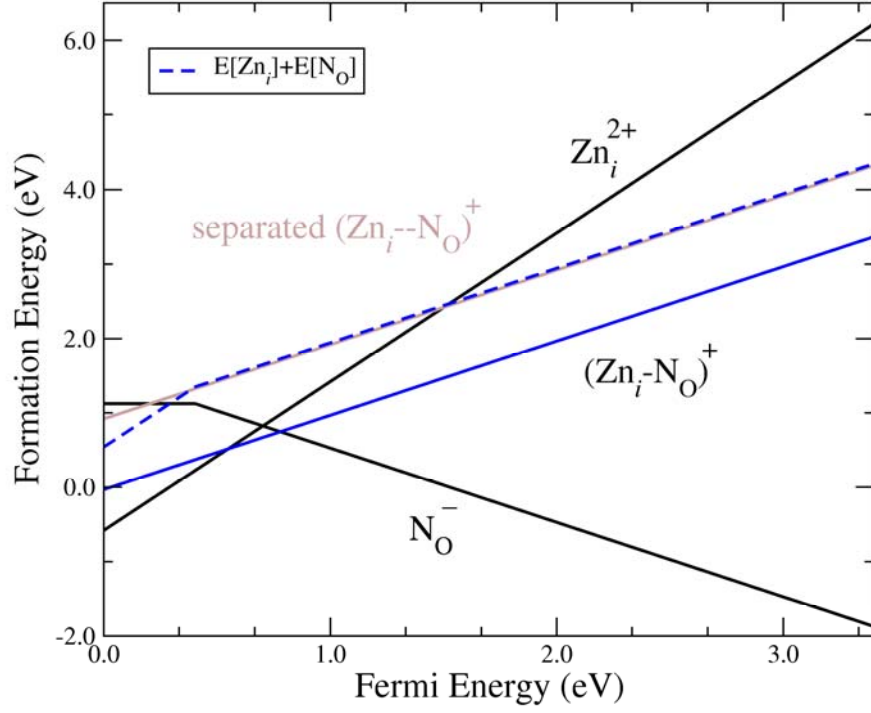


Figure 4.2 Calculated formation energy as a function of the Fermi level for N_O , Zn_i , and the Zn_i-N_O complex under Zn-rich conditions and N_2 precipitation limits. The Fermi level is referenced to the valence band maximum. The slope of each line indicates the charge states. The solid brown line is the calculated formation energy of the same supercell contained both Zn_i and N_O but at a distance far away from each other. The dashed line denotes to the sum of energy between isolated Zn_i and N_O .

oxygen sites as illustrated in Figure 4.1. We find that the detailed configurations of Zn_i and N_O in Zn_i-N_O complex distorted only slightly from their isolated forms.

Figure 4.2 shows the calculated formation energies for Zn-rich conditions. The condition is the most favorable condition for the formation of Zn_i and N_O . We find that Zn_i acts as a double donor with high formation energy under n -type condition, i.e., at the Fermi energy near the bottom of the conduction band. Zinc interstitial is

therefore unlikely be a dominant donor for typical *n*-type ZnO. However, the low formation energy of Zn_i^{2+} , under *p*-type conditions, indicates that it can be a source of compensation in *p*-type ZnO. Substitutional nitrogen N_O is a deep acceptor with $\varepsilon(0/-)$ transition level occurs at ~ 0.4 eV above the VBM. Base on the formation energies plots in Figure 4.2, at N_2 precipitation limit, N_O should act as a leading acceptor, due to its low formation energy under *p*-type conditions. If both Zn_i^{2+} and N_O^- are formed in the same system, they would be bind to each other forming $(\text{Zn}_i-\text{N}_\text{O})^+$ complex. We find that $\text{Zn}_i-\text{N}_\text{O}$ does not introduce a defect level induced in the calculated bandgap. This can be explained by the repulsion between the defect levels induced by Zn_i and N_O . $\text{Zn}_i-\text{N}_\text{O}$ is, therefore, exclusively occurred in 1+ charge state and acts as a donor in ZnO.

The calculated electronic transition energy of $\text{Zn}_i-\text{N}_\text{O}$ is underestimated due to well-known LDA gap problems. However, our calculations show that the donor level of $\text{Zn}_i-\text{N}_\text{O}$ is shallower than that of isolated Zn_i , which is argued to be a shallow donor (Oba, *et al.*, 2001; Zhang, *et al.*, 2001). In addition, a wavefunction analysis of Zn_i shows a high degree of delocalization, which is a characteristic of a shallow level. Although the $(0/+)$ transition energy of $\text{Zn}_i-\text{N}_\text{O}$ cannot be accurately calculated, it is entirely consistent with the observed value of 30 meV level (Look, *et al.*, 2005).

The binding energy can be calculated from a difference of energy between a supercell containing $\text{Zn}_i-\text{N}_\text{O}$ complex and another supercell containing separated Zn_i and N_O (the energy difference between the solid blue line and the solid brown line). The binding energy can also be calculated from a difference between the formation energy of $\text{Zn}_i-\text{N}_\text{O}$ and the sum of formation energy between Zn_i and N_O ; defined as

Table 4.1 Calculated formation energies (at $E_F=0$, referenced to the VBM) for Zn_i , N_O , and Zn_i-N_O in ZnO, under zinc-rich and oxygen-rich conditions.

Defect	Charge state	Formation energy (eV)	
		Zn rich	O rich
Zn_i	2+	-0.58	3.00
	+	1.90	5.48
	0	4.25	7.83
N_O	0	1.12	4.70
	-	1.53	5.11
Zn_i-N_O	2+	0.12	7.27
	+	-0.03	7.12
	0	2.71	9.86

$E_b = E^f(Zn_i - N_O) - [E^f(Zn_i) + E^f(N_O)]$. Both methods qualitatively give similar binding energy of ~ 0.95 eV.

It is also interesting to compare the 0.95 eV binding energy with the activation energy for irradiated-defect annealing in ZnO, of 1.7 eV (Look, Reynolds, Hemsky, Jones and Sizelove, 1999b). The difference between these two energies, $1.70 - 0.95 = 0.75$ eV, is a reasonable value for the migration barrier of Zn_i . The value is consistent with a recent migration barrier calculation for Zn_i in ZnO of 0.6 eV (Janotti and Van de Walle, 2007b).

4.3.2 Defect concentration analysis

The formation energy of Zn_i , N_O , and $\text{Zn}_i\text{-N}_\text{O}$ in ZnO depend on the Fermi energy and the partial pressure of the elements or, in other words, the chemical potentials. A secondary-ion mass measurement (Look, *et al.*, 2002) found a N concentration of about $1 \times 10^{17} \text{ cm}^{-3}$. In order to estimate the chemical potential of N (μ_N) during growth process, we assumed Zn-rich growth conditions with growth temperature $\sim 950^\circ\text{C}$. We find that Zn_i is the main donor native defect to be considered. Although, oxygen vacancy V_O^{2+} has slightly lower formation energy than Zn_i^{2+} , it is a deep donor. In addition, V_O is not expected to form in a high concentration under 1 MeV electron-irradiation. Native defects, that are acceptors such as V_Zn and O_i have high formation energies under Zn rich conditions. They are, thus, not expected to form in a reasonable concentration. Based on the formation energies plots in Figure 4.2, at N_2 -rich, N_O^- acts as leading acceptor indicating $(\text{Zn}_i\text{-N}_\text{O})^+$ acts as a leading donor with the Fermi level pinned at $\sim 0.8 \text{ eV}$, satisfying charge neutrality condition. However, this condition would produce the nitrogen concentration around 10^{20} cm^{-3} , calculated from the formation energy of N_O^- of $1.53 - 0.80 = 0.73 \text{ eV}$, $N_\text{sites} = 4.28 \times 10^{22} \text{ cm}^{-3}$ and $T = 1230 \text{ K}$. This suggested that the chemical potential which produces nitrogen concentration of 10^{17} cm^{-3} should be lower than those of N_2 -rich condition. The analysis of Zn_i , N_O , and $\text{Zn}_i\text{-N}_\text{O}$ concentration as a function of μ_N is performed. Figure 4.3 shows the concentration of Zn_i , N_O , and $\text{Zn}_i\text{-N}_\text{O}$ as a function of μ_N where $\mu_\text{N} = 0$ is referenced to the N_2 precipitation limit. Because the charge neutrality is assumed, the Fermi level of the

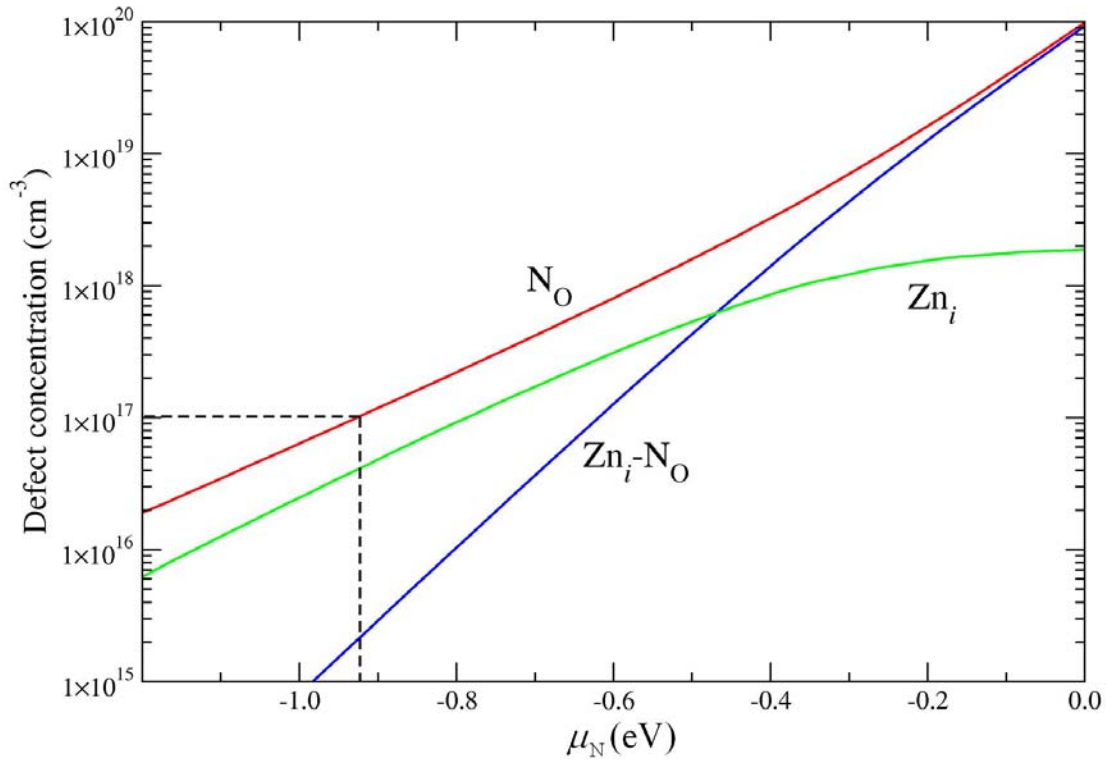


Figure 4.3 Concentrations of Zn_i , N_O , and Zn_i-N_O as a function of nitrogen chemical potential μ_N . The Zn-rich growth condition and growth temperature of 950°C are assumed. The dash lines are to guide the eyes for the μ_N at nitrogen concentration at 10^{17} cm^{-3} . N_2 precipitation limit is set at $\mu_N = 0$.

system depends on the concentration of N_O . The plot of Fermi level as a function of μ_N is shown in Figure 4.4.

Because the as-grown sample has a nitrogen concentration of $1 \times 10^{17} \text{ cm}^{-3}$, we can estimate μ_N to be about 0.92 eV below the N_2 precipitation limit. The μ_N at this nitrogen concentration is shown by a dashed line in Figure 4.3. At this point, the Fermi level of system is pinned at about 1.0 eV as shown in Figure 4.4. Using $\mu_N = -0.92 \text{ eV}$ and Fermi energy of 1.0 eV, the calculated formation energy of Zn_i-N_O is

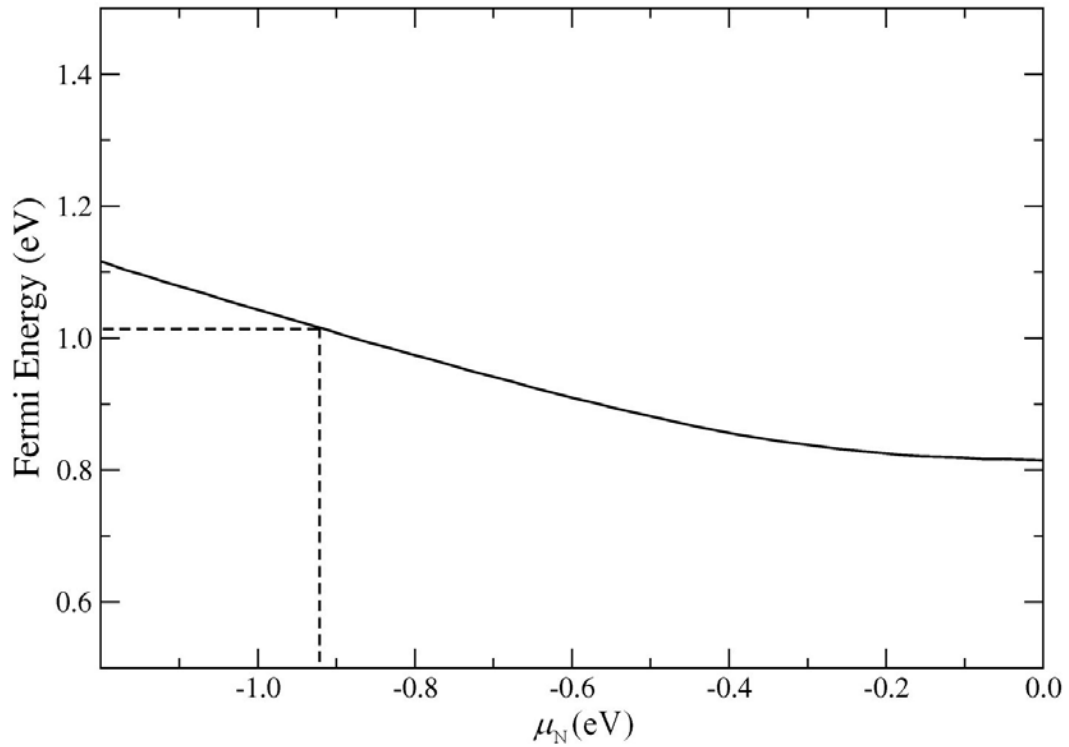


Figure 4.4 The Fermi energy as a function of μ_N for the calculations of defect concentration plotted in Figure 4.3. The Fermi energies are calculated with the consideration of the charge neutrality during the growth processes.

1.88 eV. This high formation energy gives the concentration of about $2 \times 10^{15} \text{ cm}^{-3}$ where it is too low to be a source of n -type carriers. However, the final $\text{Zn}_i\text{-N}_\text{O}$ concentration is determined after the sample is cool down. The concentration of $\text{Zn}_i\text{-N}_\text{O}$ will be higher due to the kinetic processes that combine mobile Zn_i to N_O . Zn_i in ZnO has been found to have a low migration barrier of 0.6 eV which is occurred via the kick-out (or interstitialcy) mechanism (Janotti and Van de Walle, 2007b). This low migration barrier implies that Zn_i are mobile even below room temperature.

As illustrated in Figure 4.3, during growth, the concentration of Zn_i , N_O , and $\text{Zn}_i\text{-N}_\text{O}$ complex will be 5×10^{16} , 1×10^{17} , and $2 \times 10^{15} \text{ cm}^{-3}$, respectively. During the

cool down, the Zn_i donors which are highly mobile, can bind to N_O acceptors forming Zn_i-N_O complexes. This can be described by the reaction $Zn_i^{2+} + N_O^- \rightarrow (Zn_i-N_O)^+ + 0.95 \text{ eV}$. The detailed balance gives

$$\frac{[Zn_i][N_O]}{[Zn_i-N_O]} = \frac{N_{\text{sites}}}{N_{\text{degeneracy}}} \exp(-E_b / kT), \quad (4.5)$$

where $[Zn_i]$, $[N_O]$, and $[Zn_i-N_O]$ are the concentrations of Zn_i , N_O , and Zn_i-N_O , respectively. The value of N_{sites} , $N_{\text{degeneracy}}$, and E_b are $4.28 \times 10^{22} \text{ cm}^{-3}$, 3, and 0.92 eV, respectively. At the interested growth temperature ($T=950^\circ\text{C}$), we obtained $[Zn_i-N_O]$ of around $2.2 \times 10^{15} \text{ cm}^{-3}$. This gives $[Zn_i-N_O]/[Zn_i] = 0.015$ which means only about 1/100 of Zn_i ions take part in the complex formation. However, during cool down, the formation of the Zn_i-N_O is expected to increase.

To illustrate the situation, we assume that the numbers of defects created during growth are conserved during the cool down processes. However, Zn_i is sufficiently mobile and can bind N_O form Zn_i-N_O complex. The detailed balance equation in Eq. (4.5) can be solved using the condition $[Zn_i^{\text{tot}}] = [Zn_i] + [Zn_i-N_O]$ and $[N_O^{\text{tot}}] = [N_O] + [Zn_i-N_O]$, where $[Zn_i^{\text{tot}}]$ and $[N_O^{\text{tot}}]$ remain constant at the growth values. Decreasing the temperature leads to an increase in the number of Zn_i-N_O complexes and a decrease in the number of Zn_i and N_O . During the growth at the temperature $\sim 950^\circ\text{C}$ (1223 K), the system is in the thermodynamic equilibrium. After the growth, the sample is cooled down. During the cool down, $[Zn_i^{\text{tot}}]$ and $[N_O^{\text{tot}}]$ are assumed to be constant. The $[Zn_i-N_O]/[Zn_i^{\text{tot}}]$ ratio as a function of temperature during cool down is shown in Figure 4.5. It is clear that, at the growth temperature, only a small fraction of Zn_i form complex. However, when temperature is reduced

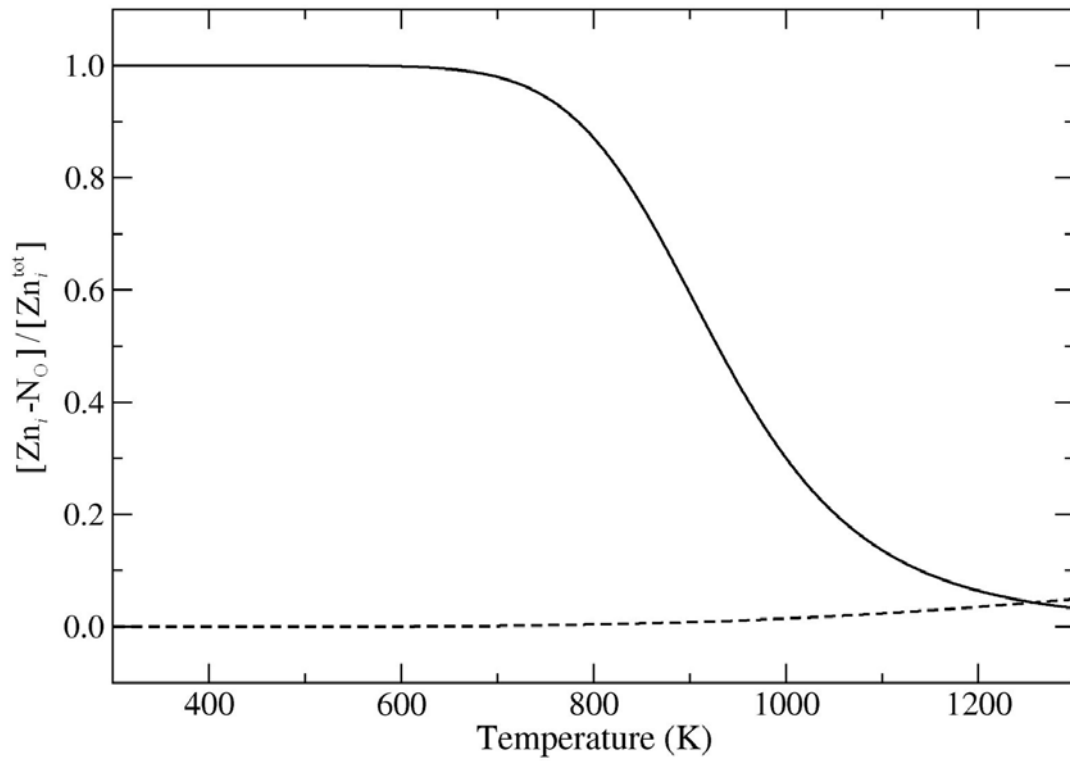


Figure 4.5 Ratio of the concentration of $\text{Zn}_i\text{-N}_\text{O}$ complex to the total concentration of Zn_i as a function of temperature. The dashed line represents thermal equilibrium condition while the solid line represents results in the event that the total concentration of Zn_i and N_O are determined by thermal equilibrium and kept fixed during the cool down to the room temperature.

$[\text{Zn}_i\text{-N}_\text{O}]$ rapidly increased. At a temperature below $\sim 330^\circ\text{C}$ (600K), almost all Zn_i form $\text{Zn}_i\text{-N}_\text{O}$ complexes. On the other hand, if the concentrations of Zn_i , N_O , and $\text{Zn}_i\text{-N}_\text{O}$ complex were determined by thermal equilibrium, the $[\text{Zn}_i\text{-N}_\text{O}]/[\text{Zn}_i^{\text{tot}}]$ ratio would be dramatically small as shown by dashed line in Figure 4.5.

The formation of $\text{Zn}_i\text{-N}_\text{O}$ complex is consistent with optically detected magnetic resonance experiments in epitaxial nitrogen-doped ZnO (Aliev, Bingham,

Wolverson, Davies, Makino, Ko and Yao, 2004). An observed spin-1/2 center is consistent with a Zn_i , possibly in association with a nitrogen atom. The center was not observed in a sample with low nitrogen content. Beside Zn_i , other donors, such as hydrogen interstitial H_i , are also believed to passivate nitrogen (Nickel and Fleischer, 2003; Ohashi, Ishigaki, Okada, Taguchi, Sakaguchi, Hishita, Sekiguchi and Haneda, 2003). However, H_i -N complex is neutral whereas Zn_i -N_O is a shallow donor.

In addition, there are other studies of Zn_i -acceptor complexes. For example, recent work by Wardle *et al.* (Wardle, Goss and Briddon, 2005) based on density functional theory shows that Zn_i -Li_{Zn} complex is bound by 0.7 eV. The complex is a shallow donor.

4.4 Summary

The search for a complex model that is consistent with the 30 meV donor level observed in low temperature photoluminescence on irradiated ZnO has been carried out. Based on experimental measurements and molecular dynamic simulation by our collaborators, Zn_i is suggested to be the best candidate for the donor observed in irradiated ZnO samples. Zn_i can bind with nitrogen forming the Zn_i -N_O complex. Nitrogen is introduced during the annealing processes where N₂ gas is used. A first-principles study based on density functional theory is employed to investigate the Zn_i -N_O complex in ZnO.

The properties of Zn_i , N_O and Zn_i -N_O complex are presented. These include defect geometry, formation energy, and defects concentrations. The calculations show that the Zn_i -N_O complex is bound by 0.95 eV, which is sufficient to stabilize the complex at room temperature. The complex is a shallower donor than isolated Zn_i .

The defect concentration analysis reveals that the isolated Zn_i and N_O prefer to agglomerate into $\text{Zn}_i\text{-N}_\text{O}$ complex during the cool down process. At room temperature, almost all Zn_i bind to N_O forming $\text{Zn}_i\text{-N}_\text{O}$. These results suggested that native defects can contribute as a donor in *n*-type ZnO, especially in the complex forms.

CHAPTER V

MUTUAL PASSIVATION OF ELECTRICALLY ACTIVE AND ISOVALENT IMPURITIES IN DILUTE NITRIDES

5.1 Introduction

Semiconductor alloys involving highly mismatched compounds show remarkable properties and offer unique opportunities for band-structure engineering. $\text{GaAs}_{1-x}\text{N}_x$ is a prototype of highly mismatched alloys where a small fraction of As atoms in GaAs (lattice parameter $a = 5.65 \text{ \AA}$) is replaced by N atoms (GaN lattice parameter $a = 4.50 \text{ \AA}$). The bandgap of GaAs dramatically changes with increasing N concentration. It decreases by as much as 180 meV per atomic percent of N (Weyers, Sato and Ando, 1992; Neugebauer and Van de Walle, 1995; Wei and Zunger, 1996; Shan, Walukiewicz, Ager, Haller, Geisz, Friedman, Olson and Kurtz, 1999). This property is remarkably different than that of conventional alloys (Wooley, 1962); one would expect the bandgap of $\text{GaAs}_{1-x}\text{N}_x$ to increase from its value in GaAs (1.5 eV) towards its value in GaN (3.4 eV) as the N concentration increases. This remarkable behavior have become to interest not only from its fundamental perspective but because of its great capability for enhancement of device applications (Ager III and Walukiewicz, 2002). For instance, $\text{GaAs}_{1-x}\text{N}_x$ is a promising material for high efficiency multi-junction solar cells and long-wavelength emitting diode lasers.

It has been reported that the effects of N on the band-gap reduction in GaAsN can be reduced by adding certain impurities. It has also found that N can passivate certain shallow donor impurities, despite N being isovalent to As in GaAsN. One example is the hydrogen (H) in GaAsN. A few percent of nitrogen can drastically reduce the bandgap of GaAs. However, when H is incorporated, a reversal of the drastic band-gap reduction by N is observed. It is well established that H can compensate both donors and acceptors in GaAs. Surprisingly, H does not have this property when N is present in GaAsN. This represents the mutual passivation between hydrogen and nitrogen in diluted III-V nitride (Baldassarri, Bissiri, Polimeni, Capizzi, Fischer, Reinhardt and Forchel, 2001; Polimeni, Baldassarri, Bissiri, Capizzi, Fischer, Reinhardt and Forchel, 2001). An explanation of this mutual passivation effect has been proposed (Janotti, Zhang, Wei and Van de Walle, 2002b).

Doping is necessary for controlling the electrical properties in any semiconductor, including $\text{GaAs}_{1-x}\text{N}_x$ alloys. While the physics of *p*-type and *n*-type doping in the parent compound GaAs and GaN is well understood, doping in $\text{GaAs}_{1-x}\text{N}_x$ is less much explored. Recently, the interaction between extrinsic dopants and N in $\text{GaAs}_{1-x}\text{N}_x$ has been reported to lead to an entire new phenomena (Yu, Walukiewicz, Wu, Mars, Chamberlin, Scarpulla, Dubon and Geisz, 2002; Hong, Nishikawa and Tu, 2003; Wu, Yu, Walukiewicz, He, Haller, Mars and Chamberlin, 2003; Yu, Walukiewicz, Wu, Shan, Beeman, Scarpulla, Dubon, Ridgway, Mars and Chamberlin, 2003). Yu *et al.* (Yu, *et al.*, 2002) reported that when $\text{GaAs}_{1-x}\text{N}_x$ is doped with Si, the interaction between Si and N leads to a “mutual passivation,” characterized by an increase in the bandgap (reversal of the effects of N) and a decrease in the electron concentration (passivation of Si). These phenomena have

been observed in rapid thermal annealing (RTA) experiments. Si-doped (In)GaAsN alloys annealed at temperature above 800°C for 10 seconds show drastically increased the electrical resistivity, and an increased bandgap up to the value corresponding to the net active N, roughly equal to the difference between total N concentration and the Si concentration (Yu, *et al.*, 2002; Wu, *et al.*, 2003). A peak at ~0.8 eV also simultaneously appeared in the photoluminescence spectra (Yu, *et al.*, 2002; Wu, *et al.*, 2003). Ge-doped GaAs_{1-x}N_x alloy also exhibits the mutual passivation between Ge and N, but S- and Se- doped GaAs_{1-x}N_x alloys do not. It has been postulated that substitutional Si_{Ga} and Ge_{Ga} form strong bonds with N_{As}, increasing their ionization energy and changing the shallow-donor character of Si and Ge in GaAs. On the other hand, the donors, S_{As} and Se_{As} are (at best) second-nearest neighbors of N_{As} and not directly bonded to N_{As}; therefore, they would not suffer from the passivation effect (Yu, *et al.*, 2002; Wu, *et al.*, 2003; Yu, *et al.*, 2003).

Recently, Li *et al.* suggested that Si_{Ga}-N_{As} complexes, formerly proposed by experimentalists are deep donors in GaAs (Li, Carrier, Wei, Li and Xia, 2006). Based on density functional calculations, they predicted that Si_{Ga}-N_{As} would result in a single-particle at 0.23 eV below the GaAs conduction-band minimum in the dilute limit. They report a binding energy of 0.26 eV for the Si_{Ga}-N_{As} pair, and 0.12 eV for the Ge_{Ga}-N_{As} in the neutral charge state. Nevertheless, this proposed model where substitutional donors and N isovalent are on adjacent site encounters some serious problems and inconsistency with experiment. First, the binding energy of 0.26 eV is too small to explain the formation of a high concentration of Si_{Ga}-N_{As} pairs under annealing slightly above 800°C. The Ge_{Ga}-N_{As} binding energy of 0.12 eV is expected to give even lower concentrations of Ge_{Ga}-N_{As} pairs. We estimate that less than 40%

of the Si atoms would combine with N_{As} into $Si_{Ga}-N_{As}$ pairs at the temperatures used in RTA. Second, the calculated binding energies of 0.26 eV and 0.12 eV reported by (Li, *et al.*, 2006) are not correctly defined, as will be explained later. The concentration of complexes would be much smaller if evaluated using the appropriate binding energies. This too high binding energy is conflict to experimental results. Finally, the $Si_{Ga}-N_{As}$ pair cannot explain the appearance of a deep-level photoluminescence peak at ~ 0.8 eV above the valence-band maximum (VBM) as observed in the experiments.

In this chapter, we report a comprehensive investigation of the interaction between extrinsic dopants and N in dilute GaAsN alloys. Based on first-principles calculations we find that isovalent N changes the microscopic behavior of Si and Ge donors in a more dramatic way. Si and Ge combine with N into stable $(Si-N)_{As}$ and $(Ge-N)_{As}$ split interstitial which act as compensating centers in *n*-type GaAsN. The $(Si-N)_{As}$ and $(Ge-N)_{As}$ complexes are deep acceptors with formation energies that are considerably lower than that of $Si_{Ga}-N_{As}$ and $Ge_{Ga}-N_{As}$ in *n*-type GaAsN. The deep acceptor level of $(Si-N)_{As}$ can explain the appearance of the deep-level photoluminescence peak, consistent with experimental observations. The formation of $(Si-N)_{As}$ and $(Ge-N)_{As}$ also explains the blue shift in the bandgap. The formation the split interstitials can also explain the high electrical resistivity observed in Si and Ge-doped GaAsN alloys. Our results for electronic structure and the frequency of the local vibration modes of the $(Si-N)_{As}$ and $(Ge-N)_{As}$ split interstitial provide a guide to for further experiments on the investigation of mutual passivation effects in highly mismatched semiconductor alloys.

5.2 Computational Approach

Our calculations are based on density functional theory (DFT) (Hohenberg and Kohn, 1964; Kohn and Sham, 1965) with projector augmented wave (PAW) method (Blöchl, 1994; Kresse and Joubert, 1999) as implemented in VASP code (Kresse and Furthmüller, 1996b; Kresse and Furthmüller, 1996a) within the local density approximation (LDA) for exchange-correlation potential. We use a plane-wave basis set with an energy cutoff of 400 eV. GaAsN alloys with different N concentration were simulated by supercells containing 64, 128, or 216 atoms, in which one of arsenic (As) atom was replaced by one N atom. This corresponds to N contents of 3.1%, 1.6%, or 0.9%, respectively. Integrations over the Brillouin zone were performed using a $2 \times 2 \times 2$ grid of Monkhorst-Pack special k -points for the 64-atom supercell, and only one k -point shifted from Γ for the 128- and 216-atom supercells. These calculations allow us to analyze variation of the bandgap in alloys with nitrogen concentration. All atoms in the supercell are relaxed by minimizing Hellman-Feynman forces to less than 0.01 eV/Å. All defect calculations are carried out at theoretical lattice constant of 5.61 Å which is slightly smaller than experimental lattice constant of 5.65 Å for GaAs. In order to address the DFT-LDA underestimation of the bandgap, we performed calculations with two different pseudopotentials, one in which the Ga 3*d* electrons are explicitly included as valence states, the other with Ga 3*d* electrons frozen in the core. The two situations produce very similar results for structural properties, but the potential with “*d* in the core” results in a bandgap that is larger by 0.15 eV.

In order to discuss the formation and stability of Si and Ge in the dilute nitride alloys, we also examined the behavior of Si and Ge impurities in GaAs, which are

well established as single donors, sitting on the Ga site. The formation energy of Si_{Ga} in 1+ charge state (Si_{Ga}^+) is defined as

$$E^f(\text{Si}_{\text{Ga}}^+) = E_{\text{tot}}(\text{Si}_{\text{Ga}}^+) - E_{\text{tot}}(\text{GaAs}) - \mu_{\text{Si}} + \mu_{\text{Ga}} + E_F, \quad (5.1)$$

where $E_{\text{tot}}(\text{Si}_{\text{Ga}}^+)$ is the total energy of a GaAs supercell in which Ga is replaced with a Si atom. $E_{\text{tot}}(\text{GaAs})$ is the total energy of defect-free GaAs supercell. μ_{Si} and μ_{Ga} are the chemical potentials of Si and Ga, respectively. For Si, μ_{Si} is simply the total energy per atom of a Si crystal. In the Ga-rich limit, μ_{Ga} is given by total energy per atom of a Ga crystal. In the Ga-poor limit, $\mu_{\text{Ga}} = E_{\text{tot}}(\text{Ga}) + \Delta H_f(\text{GaAs})$ where $\Delta H_f(\text{GaAs})$ is the calculated formation enthalpy of GaAs (-0.7 eV). E_F is the Fermi-level position, which is referenced to the VBM. To study impurities in GaAsN, the supercell with one As replaced by N atom is used as the host supercell. The formation energy of Si_{Ga}^+ in GaAsN is given by

$$E^f(\text{Si}_{\text{Ga}}^+) = E_{\text{tot}}(\text{Si}_{\text{Ga}}^+) - E_{\text{tot}}(\text{GaAsN}) - \mu_{\text{Si}} + \mu_{\text{Ga}} + E_F, \quad (5.2)$$

where $E_{\text{tot}}(\text{Si}_{\text{Ga}}^+)$ is the total energy of a GaAsN supercell with one Si atom, $E_{\text{tot}}(\text{GaAsN})$ is the total energy of GaAsN in the same supercell. As in case of GaAs, μ_{Ga} can vary from $\mu_{\text{Ga}} = E_{\text{tot}}(\text{Ga})$ in the Ga-rich limit to $\mu_{\text{Ga}} = E_{\text{tot}}(\text{Ga}) + \Delta H_f(\text{GaAsN})$ in the Ga-poor limit. For the split-interstitial configuration $(\text{Si-N})_{\text{As}}$, the formation energy in charge state q is given by

$$E^f(\text{Si-N})_{\text{As}}^q = E_{\text{tot}}(\text{Si-N})_{\text{As}}^q - E_{\text{tot}}(\text{GaAsN}) - \mu_{\text{Si}} + qE_F. \quad (5.3)$$

The thermodynamic transition level $\varepsilon(0/-)$ of $(\text{Si-N})_{\text{As}}$ can be obtained from

$$\varepsilon(0/-) = E^f((\text{Si-N})_{\text{As}}^-; E_F = 0) - E^f((\text{Si-N})_{\text{As}}^0; E_F = 0), \quad (5.4)$$

where $E^f((\text{Si-N})_{\text{As}}^q; E_F = 0)$ is the formation energy of $(\text{Si-N})_{\text{As}}$ in charge state q for the Fermi level at the VBM.

The binding energy of $X_{\text{Ga}}\text{-N}_{\text{As}}$ in charge state q is defined as

$$E_b(X_{\text{Ga}}\text{-N}_{\text{As}})^q = E^f(X_{\text{Ga}}^q) + E^f(\text{N}_{\text{As}}) - E^f(X_{\text{Ga}}\text{-N}_{\text{As}})^q, \quad (5.5)$$

where $E^f(\text{N}_{\text{As}})$ is formation energy of N_{As} . $E^f(\text{Si}_{\text{Ga}}^q)$ and $E^f(X_{\text{Ga}}\text{-N}_{\text{As}})^q$ are formation energies of Si_{Ga} and $X_{\text{Ga}}\text{-N}_{\text{As}}$ in charge state q . Therefore, E_b will be positive if the complex is lower in energy than the isolated species Si_{Ga} and N_{As} . Note that in Ref. (Li, *et al.*, 2006), the binding energy defined in Eq. (5.5) is calculated by using the CBM of GaAs as a reference for neutral complex. This leads to an overestimated binding energy for neutral $X_{\text{Ga}}\text{-N}_{\text{As}}$.

5.3 Results and Discussion

We present the results for the electronic and structural properties of Si in GaAs and GaAsN as well as the effects of N substituting on As site in GaAs. We discuss the $\text{Si}_{\text{Ga}}\text{-N}_{\text{As}}$ and point out the problems in explaining the experimental results using this complex. The local atomic geometry of $\text{Si}_{\text{Ga}}\text{-N}_{\text{As}}$ complex is shown in Figure 5.1(a). Instead of $\text{Si}_{\text{Ga}}\text{-N}_{\text{As}}$ pairs, we proposed that Si combines with N to form split-interstitial complex $(\text{Si-N})_{\text{As}}$ in the rapid thermal annealing experiments by (Yu, *et al.*, 2002). The formation energy and electrical behavior of $(\text{Si-N})_{\text{As}}$ are reported. Its local atomic geometry is shown in Figure 5.2(b). An explanation for the experimental observed photoluminescence peak based on the $(\text{Si-N})_{\text{As}}$ is proposed. The local vibrational modes associated with these complexes are also calculated.

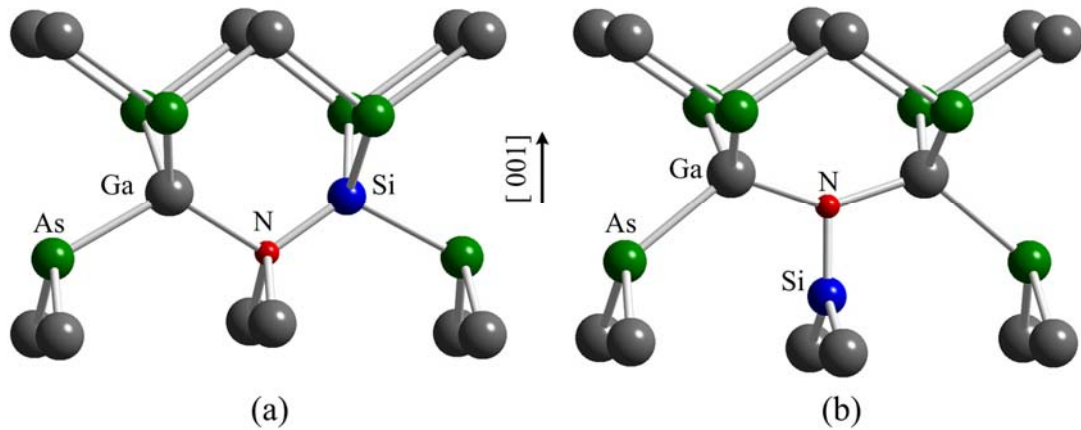


Figure 5.1 Local lattice structure of (a) $(\text{Si}_{\text{Ga}}\text{-N}_{\text{As}})^+$ and (b) $(\text{Si-N})_{\text{As}}^-$. In the $\text{Si}_{\text{Ga}}\text{-N}_{\text{As}}$ configuration, Si_{Ga} is a nearest neighbor of N_{As} . In the $(\text{Si-N})_{\text{As}}$ configuration, Si and N share an As site.

5.3.1 Group-IV donors and isovalent N in GaAs

The elements from the group-IV, such as Si and Ge act as shallow donors when substituting on Ga site, or act as acceptors when substituting on As site. In present study, we focus on the group-IV impurities acting as donors. The extra valence electron of Si and Ge can be thermally transferred to the conduction band of GaAs, rendering the material *n*-type. The calculated bandgap of GaAs is typically underestimated by the DFT within the local density approximation (LDA). This also affects to the $\varepsilon(+/0)$ transition level which is located very near the CBM. If the bandgap is corrected, the donor level will shift up along with the conduction band. Since the impurity level induced by Si_{Ga} is unoccupied in the positive charge state, we expect that its formation energy in positive charge state should be well described by the LDA. Therefore, the correction to the formation energy mainly applies to the neutral charge state. The formation energy as a function of Fermi level of Si_{Ga} is

shown in Figure 5.2. Note that the impurity does not create any level in the bandgap of GaAs, but a perturbation of the conduction band states near the CBM as seen in band structure plots in Figure 5.3. The electron from the Si_{Ga} impurity can be described as in a hydrogenic-like state that can be easily excited to the conduction band.

Incorporation of N into GaAs has been known to dramatically affect its fundamental bandgap. A small amount of N concentration introduces a large reduction of the bandgap. A number of experiments reported that the reduction of GaAs bandgap strongly depends on the N concentration, being as much as 180 meV per atomic percent of N. We studied the effect of N-induced bandgap reduction by calculating the 64-, 128-, and 216-atom supercells of GaAs with an As atom replaced by a N atom. These correspond to the N concentrations of 3.13%, 1.56%, and 0.93%, respectively. The bandgap of $\text{GaAs}_{1-x}\text{N}_x$ as a function of N content is shown in Figure 5.4. The bandgap values were calculated at Γ -point based on LDA. Although, the random fluctuation of N in $\text{GaAs}_{1-x}\text{N}_x$ alloys has not been included in this study, the major effects of N in GaAs are well produced in the calculations. We found that the bandgap of GaAs is decreased by ~ 150 meV per atomic percent of N. This is to compare with the experimental value of 180 meV/mole percent of N (Ager III and Walukiewicz, 2002). Although the absolute DFT bandgap values are severely underestimated, the trend of bandgap reduction is clearly observed.

5.3.2 Former model: $(X)_{\text{Ga}}\text{-N}_{\text{As}}$ complexes

The $X_{\text{Ga}}\text{-N}_{\text{As}}$ model (where $X = \text{Si}$ and Ge) was initially proposed by experimentalists to be the source of observed mutual passivation phenomena as well as a photoluminescence peak at ~ 0.8 eV in Si-doped GaAsN alloys. In the model Si_{Ga}

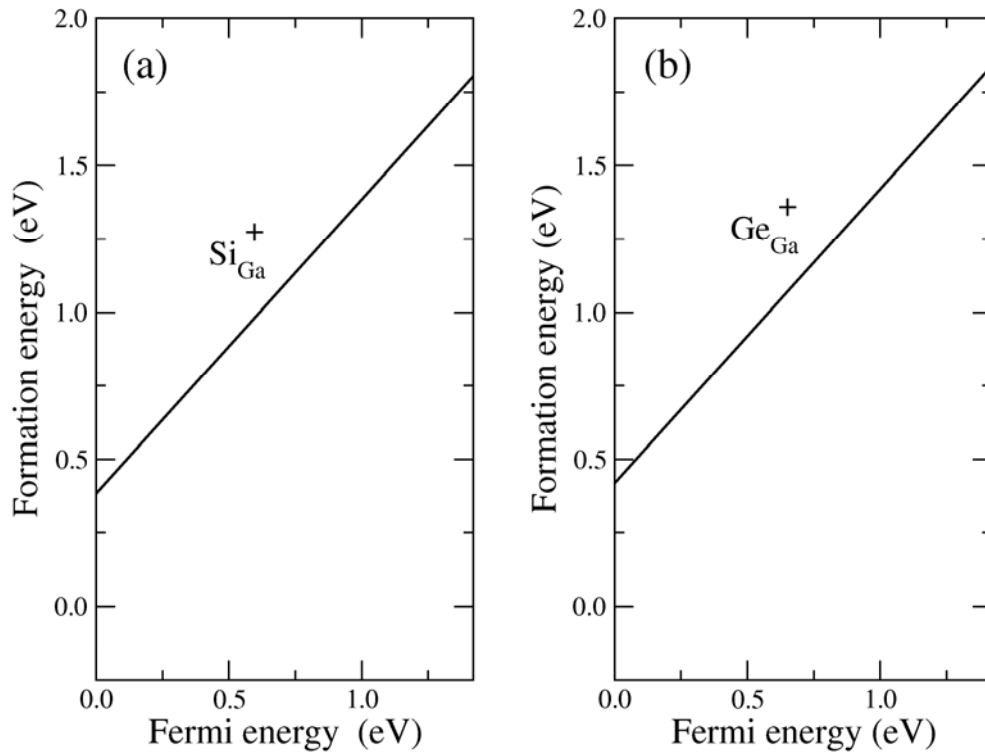


Figure 5.2 Formation energy under Ga-rich conditions as a function of Fermi energy for (a) Si_{Ga} and (b) Ge_{Ga} in GaAs. Both Si_{Ga} and Ge_{Ga} always have 1+ charge state.

(or Ge_{Ga}) forms a strong bond with N_{As} , combining into a $\text{Si}_{\text{Ga}}\text{-N}_{\text{As}}$ complex (or $\text{Ge}_{\text{Ga}}\text{-N}_{\text{As}}$ complex) as shown in Figure 5.1(a). Subsequently, a first-principles study based on DFT suggested that this complex is stable and induces a deep donor level. However, the model lacks a convincing explanation for the mutual passivation effects and contains some. First, N and Si are much smaller than As and Si. The covalent radius of N is 38% smaller than that of As. Similarly, the radius of Si is 12% smaller than Ga. The $\text{Si}_{\text{Ga}}\text{-N}_{\text{As}}$ complex would create high strain if formed.

To investigate a formation of the $X_{\text{Ga}}\text{-N}_{\text{As}}$ complexes, one needs to calculate their binding energy and their electronic properties. From our calculations, if we

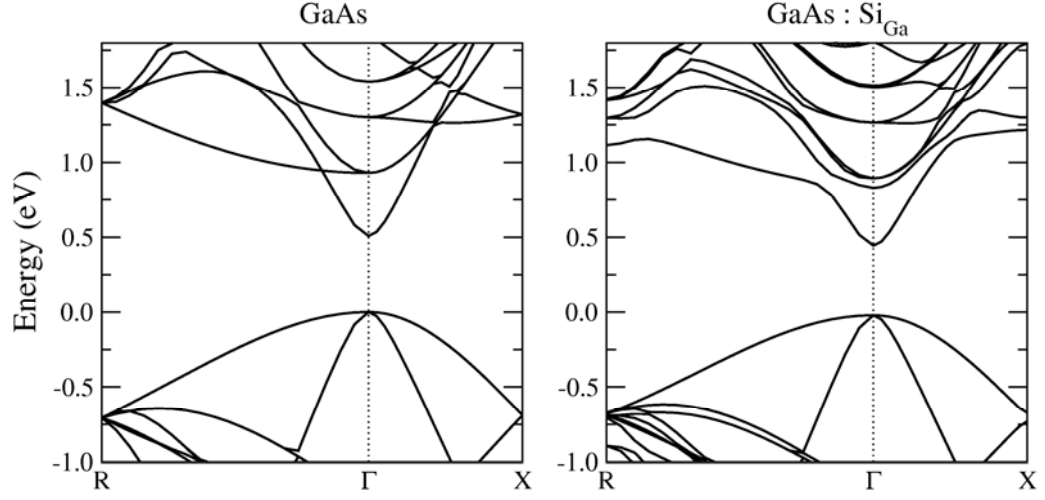


Figure 5.3 Calculated bandstructures of (a) defect-free GaAs (presented in a 64-atom supercell BZ) and (b) GaAs containing Si_{Ga} .

assume both X_{Ga} and $X_{\text{Ga}}\text{-N}_{\text{As}}$ are presented in the positive charge state, then the calculated binding energy is negative. The values are -0.04 and -0.30 eV for $\text{Si}_{\text{Ga}}\text{-N}_{\text{As}}$ and $\text{Ge}_{\text{Ga}}\text{-N}_{\text{As}}$, respectively. Further tests of placing X_{Ga}^+ away from N_{As} in the same supercell also confirm the negative binding energy results, i.e. the energy obtained is lower than the corresponding $(X_{\text{Ga}}\text{-N}_{\text{As}})^+$ complex. Note that Li *et al.* (Li, *et al.*, 2006) earlier reported small binding energies of 0.26 and 0.12 eV for $X = \text{Si}$ and Ge , respectively. However, they assumed that X_{Ga} and $X_{\text{Ga}}\text{-N}_{\text{As}}$ are in the neutral charge state. For shallow donors, X_{Ga} , this implies placing an electron in a shallow level just below the CBM. This leads to an overestimation of X_{Ga} formation energy that Li *et al.* used in their derivation. Although, in defining the binding energy, X_{Ga} should be far from N_{As} , X_{Ga} is still in GaAsN alloy. The CBM of GaAsN is shifted down in comparison to GaAs. In GaAsN, the formation energy of X_{Ga} should be determined by using the GaAsN CBM, which is lower than that of GaAs. If we follow the procedure

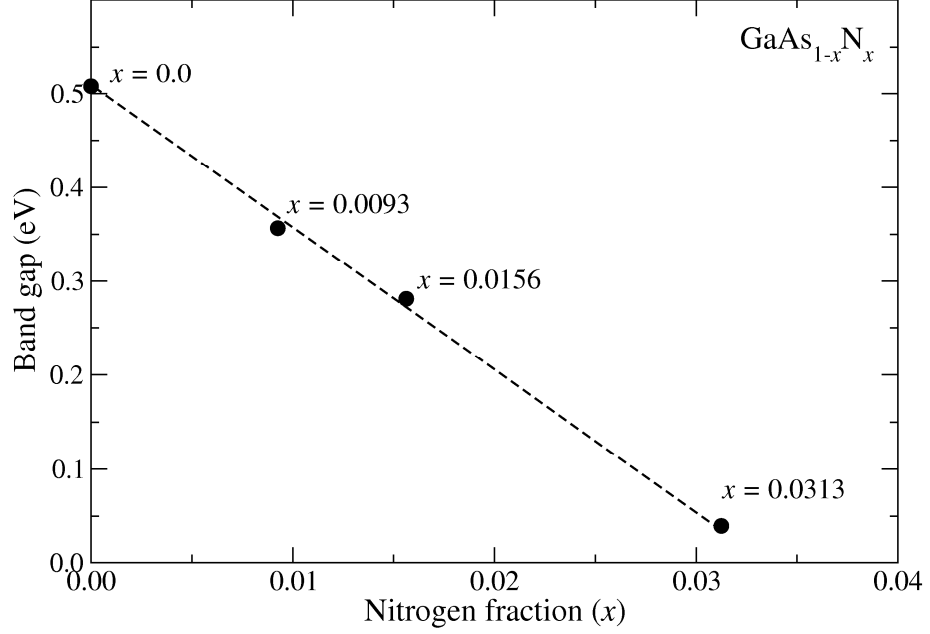


Figure 5.4 Calculated bandgap of $\text{GaAs}_{1-x}\text{N}_x$ alloys as a function of N fraction. The black solid dots represent the calculated bandgap of $\text{GaAs}_{1-x}\text{N}_x$ at mol % N = 0.00, 0.93, 1.56 and 3.13. The calculations were performed by replacing an As atom by a N atom in 216-, 128- and 64-atom supercell respectively. The dashed line serves as a guide to the eye.

of Li *et al.*, we find $X_{\text{Ga}}\text{-N}_{\text{As}}$ binding energies of 0.27 and 0.13 eV when $X = \text{Si}$ and Ge, respectively. This is consistent with what Li *et al.* obtained. However, if we properly calculate the binding energies of $X_{\text{Ga}}\text{-N}_{\text{As}}$ by referencing the formation energy of neutral charge state to the CBM of the GaAsN alloy, we find the binding energy of $\text{Si}_{\text{Ga}}\text{-N}_{\text{As}}$ lowered to 0.11 eV and of $\text{Ge}_{\text{Ga}}\text{-N}_{\text{As}}$ become negative. The binding energies of $X_{\text{Ga}}\text{-N}_{\text{As}}$ complexes are listed in Table 5.1. The values of the binding energies derived using GaAs and GaAsN CBM are shown. These low binding energies, i.e. 0.11 eV for $\text{Si}_{\text{Ga}}\text{-N}_{\text{As}}$ and negative value for $\text{Ge}_{\text{Ga}}\text{-N}_{\text{As}}$ (all binding

energies are negative for the positive charge state calculations) indicate that there is only a very weak driving force for Si_{Ga} and N_{As} to form a $\text{Si}_{\text{Ga}}\text{-N}_{\text{As}}$ complex. There is no driving force for Ge_{Ga} and N_{As} to form a $\text{Ge}_{\text{Ga}}\text{-N}_{\text{As}}$ complex. The assumption in previous work (Yu, *et al.*, 2002; Wu, *et al.*, 2003; Yu, *et al.*, 2003) that X_{Ga} and N_{As} would form a bond that is dramatically stronger than the $\text{Ga}_{\text{Ga}}\text{-N}_{\text{As}}$ bond is unjustified. In addition, we can use the detailed balance to calculate the net concentration of complexes at a specific temperature. If we use the binding energy of 0.27 eV for $\text{Si}_{\text{Ga}}\text{-N}_{\text{As}}$ complex, we found that less than 40% of the Si_{Ga} bind to N_{As} , forming $\text{Si}_{\text{Ga}}\text{-N}_{\text{As}}$ pair, at temperature above 800°C. This number reduces to 12% if we use a correct binding energy of 0.11 eV. In the case of $\text{Ge}_{\text{Ga}}\text{-N}_{\text{As}}$, its binding energy is smaller than that of $\text{Si}_{\text{Ga}}\text{-N}_{\text{As}}$ thus chance of complex formation is even lower.

As shown in Figure 5.4, the LDA bandgap of the 64-atom supercell with one substitutional N atom (3.1% of N concentration) has a very small bandgap, i.e. ~0.03 eV. The bandgap of a larger GaAsN supercell increases when N fraction decreases. To study defects in the GaAsN alloy it is important to verify that the supercell used is sufficiently large. Thus, we investigated the dispersion of Kohn-Sham (KS) states near the band edge of 216-atom GaAsN supercell (0.93% of N concentration). We found that the states are qualitatively similar to the corresponding states of the 64-atom GaAsN supercell. There is no substantial mixing between the states near the bottom of conduction band and the top of valence band states. Therefore, the 64-atom GaAsN supercell is quite adequate. We find that when substitutional group-IV (Si_{Ga} and Ge_{Ga}) pair with N, the extra electron is also loosely bound and can be thermally excited to the conduction band. There is no deep defect-induced level appears in the bandgap of GaAsN therefore the $X_{\text{Ga}}\text{-N}_{\text{As}}$ complexes are shallow donor. Figure 5.5

Table 5.1 Calculated binding energies of $X_{\text{Ga}}\text{-N}_{\text{As}}$ ($X = \text{Si}$ and Ge) in the neutral and positive charge states. The binding energies, derived using GaAs CBM and GaAsN alloy CBM are listed in the columns marked as “ref. GaAs” and “ref. GaAsN”, respectively.

Complex	Charge state	Binding energy (eV)	
		ref. GaAs	ref. GaAsN
$\text{Si}_{\text{Ga}}\text{-N}_{\text{As}}$	1+	-0.16	-0.04
	0	0.27	0.11
$\text{Ge}_{\text{Ga}}\text{-N}_{\text{As}}$	1+	-0.38	-0.30
	0	0.13	-0.04

shows the calculated KS band structures of 64-atom GaAsN supercell ($\text{GaAs}_{0.97}\text{N}_{0.03}$) and the supercell containing $\text{Si}_{\text{Ga}}\text{-N}_{\text{As}}$ complex. Our inspections show that the wavefunctions are not localized. This means that the complexes do not introduce a deep level. Similar results are found for the case of $\text{Ge}_{\text{Ga}}\text{-N}_{\text{As}}$. We conclude that the complexes act as shallow donors. The formation energies of $\text{Si}_{\text{Ga}}\text{-N}_{\text{As}}$ and $\text{Ge}_{\text{Ga}}\text{-N}_{\text{As}}$ are shown in Figure 5.6. If the bandgap is corrected, the formation energies of $\text{Si}_{\text{Ga}}\text{-N}_{\text{As}}$ and $\text{Ge}_{\text{Ga}}\text{-N}_{\text{As}}$ in the neutral charge state are largely affected. Their $\varepsilon(+/0)$ transition levels are shifted up along with the conduction band of GaAsN. $\text{Si}_{\text{Ga}}\text{-N}_{\text{As}}$ and $\text{Ge}_{\text{Ga}}\text{-N}_{\text{As}}$ are in 1+ charge state at any Fermi level, i.e. the $\text{Si}_{\text{Ga}}\text{-N}_{\text{As}}$ and $\text{Ge}_{\text{Ga}}\text{-N}_{\text{As}}$ complexes are shallow donors. Our calculations show no deep level in the GaAsN bandgap for $X_{\text{Ga}}\text{-N}_{\text{As}}$ complexes. These results indicate that the $X_{\text{Ga}}\text{-N}_{\text{As}}$ complexes are unlikely to play an important role in experimental observed mutual passivation effects.

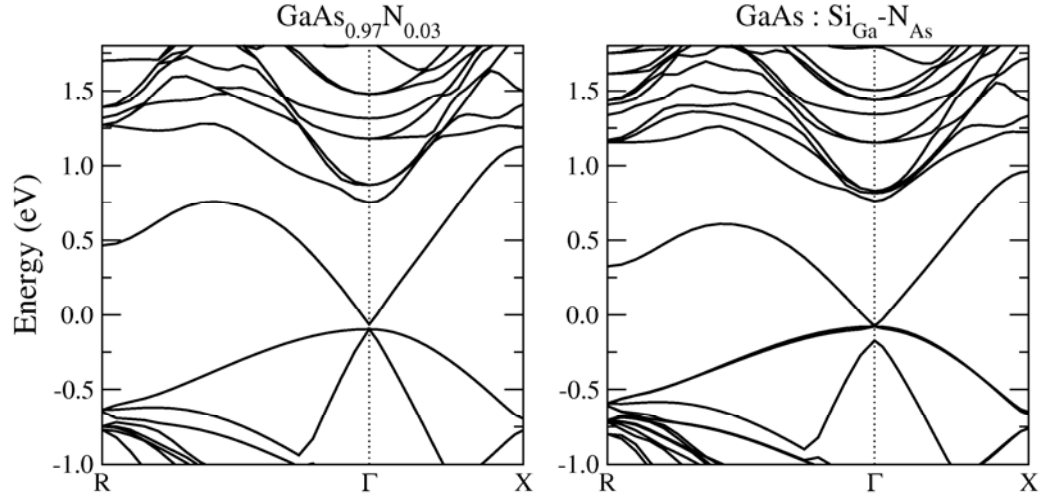


Figure 5.5 Calculated bandstructures of (a) 64-atom GaAsN supercell and (b) the same supercell containing a $\text{Si}_{\text{Ga}}\text{-N}_{\text{As}}$ pair.

5.3.3 Proposed model: Split-interstitial complex

Because the $X_{\text{Ga}}\text{-N}_{\text{As}}$ complex model does not fit the experimental observed mutual passivation in GaAsN and other diluted nitrides, we seek an appropriate model. We propose that the $(X\text{-N})_{\text{As}}$ split-interstitial complex model, where $X = \text{Si}$ and Ge , can explain the mutual passivation effects. In the complex, X and N are both threefold coordinated in a planar geometry. X is bonded to N and two Ga atoms. N is bonded to X and two other Ga atoms. The surrounding Ga atoms are all fourfold coordinated as shown in Figure 5.1 (b). Figure 5.6 shows that the $(\text{Si-N})_{\text{As}}$ and $(\text{Ge-N})_{\text{As}}$ split interstitial can occur in the neutral and negative charge states, with transition levels $\varepsilon(0/-)$ at 0.87 and 0.85 eV above the VBM, respectively. They act as deep acceptors and are stable in the $1-$ charge state for Fermi level above 0.87 and 0.85 eV, respectively.

In the neutral charge state the Si-N bond length of $(\text{Si-N})_{\text{As}}$ complex is 1.65 Å. The N-Ga and Si-Ga bond lengths are 1.89 and 2.33 Å. These Ga atoms are pushed outward from their sites by the distances corresponding to 1.0% and 8.5% of an equilibrium Ga-As bond length. In the case of $(\text{Ge-N})_{\text{As}}$, the Ge-N bond length is 1.80 Å which is longer than Si-N bond. The N-Ga and Ge-Ga bond lengths are 1.87 and 2.35 Å, very close to that of $(\text{Si-N})_{\text{As}}$. These Ga atoms are also pushed outward by the distances corresponding to 0.5% and 11.5% of an equilibrium Ga-As bond length. These relaxations are relatively small compared to the inward displacements of 16% for the Ga surrounding N_{As} . Note that we did not impose any symmetry constraints in the structural relaxations of the $(\text{Si-N})_{\text{As}}$ and $(\text{Ge-N})_{\text{As}}$ configurations. The calculated Si-N, Ge-N bond lengths and the bond lengths between the surrounding Ga atoms and the constituent atoms are tabulated in Table 5.2.

The electronic structures of the $(\text{Si-N})_{\text{As}}$ and $(\text{Ge-N})_{\text{As}}$ split interstitials can be described by the electron counting rule. The absence of an As atom leaves four Ga dangling bonds with a total of three electrons. Si-N pair or Ge-N pair provides nine electrons [four from Si (or Ge) and five from N]. As a result, there are twelve electrons in total. Eight of these electrons are participated in two N-Ga and two Si-N (or Ge-N) bonds. Two electrons are participated in a Si-N (or Ge-N) σ bond, and two electrons are left. The p_z orbitals on the N and Si (or Ge) are mutually perpendicular to each other, so that a formation of π bond is prevented. However, the orbitals are still combined into a doubly occupied bonding state located near the VBM and an empty antibonding state at 0.95 eV [0.89 eV for $(\text{Ge-N})_{\text{As}}$] above the VBM. Because N is more electronegative than either Si (or Ge), the bonding state is localized more on N while the antibonding state is localized more on Si. Figure 5.7 shows the

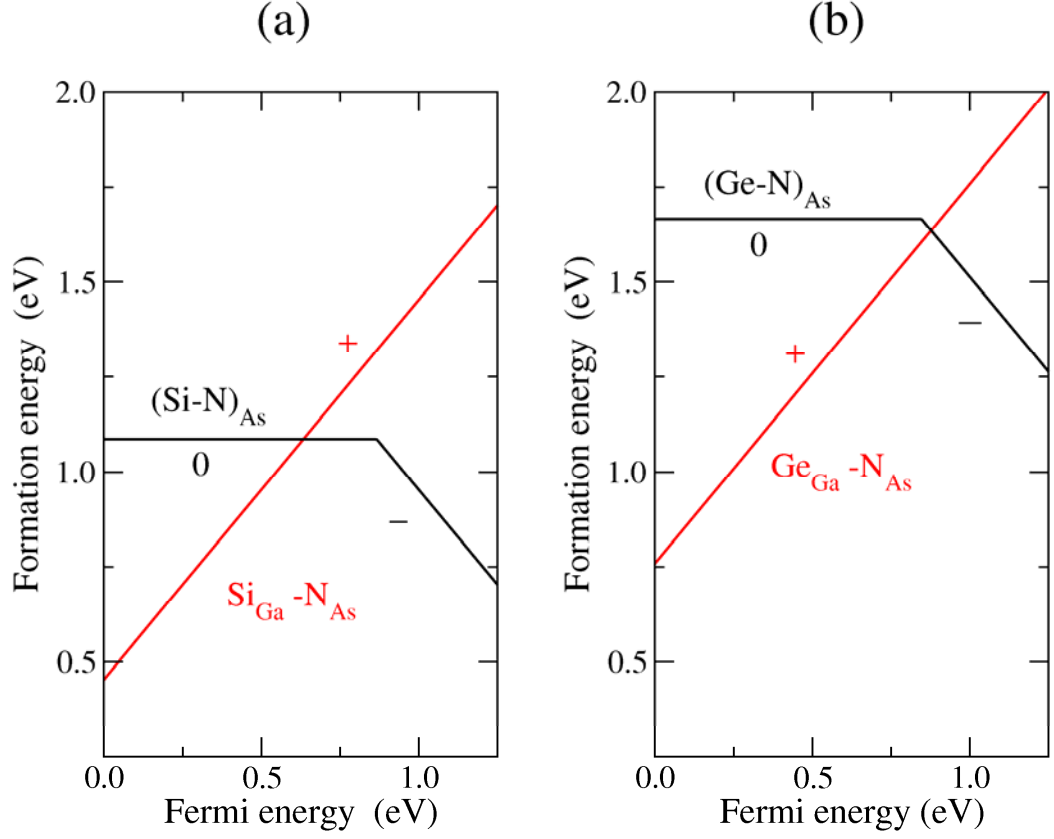


Figure 5.6 Formation energies as a function of Fermi level of (a) $\text{Si}_{\text{Ga}}-\text{N}_{\text{As}}$ and $(\text{Si-N})_{\text{As}}$ and (b) $\text{Ge}_{\text{Ga}}-\text{N}_{\text{As}}$ and $(\text{Ge-N})_{\text{As}}$ in GaAsN under Ga-rich conditions. The plots show the Fermi level in the range 0-1.25 eV which corresponds to the bandgap of GaAsN alloys with the N concentration of ~1%.

projected density of state plots of the split interstitial pairs. The bonding and antibonding states are consisted of p orbitals. From the inspection of the bandgaps, we observe that the $(\text{Si-N})_{\text{As}}$ and $(\text{Ge-N})_{\text{As}}$ split interstitial produce a restoration of the GaAs bandgap. Our band structure calculations (Figure 5.8) reveal that the formation of $(\text{Si-N})_{\text{As}}$ split interstitial introduce a restoration of GaAs bandgap. However, it introduces a deep level, associated with bonding and anti-bonding states. The

Table 5.2 Calculated $(X-N)_{As}$ bond lengths and the bond lengths between the surrounding Ga atoms and $(X-N)_{As}$. The displacements of the surrounding Ga atoms from original sites are given in terms of percentages of equilibrium Ga-As bond length.

X	Charge state	d_{X-N} (Å)	d_{N-Ga} (Å)	d_{X-Ga} (Å)	Ga (next to N) displacement (%)	Ga (next to X) displacement (%)
Si	0	1.66	1.89	2.33	1.0	8.5
	1–	1.68	1.87	2.31	0.8	6.8
Ge	0	1.80	1.87	2.35	0.5	11.5
	1–	1.82	1.85	2.34	0.4	9.8

inspection of the charge density indicates that the next Kohn-Sham state above the antibonding state lies in the conduction band. Therefore, the formation of the $(Si-N)_{As}$ [or $(Ge-N)_{As}$] interstitial complex eliminates the effect of N on the bandgap, but at the expense of forming a deep level.

The charge density plots of the bonding and antibonding state for $(Si-N)_{As}$ are shown in Figure 5.9. We can see that the electron is more localized on N atom. The antibonding state can in principle accept up to two electrons. We find the $\varepsilon(-/2-)$ transition level of $(Si-N)_{As}$ and $(Ge-N)_{As}$ at about 1.25 eV above the VBM, which place them above the CBM of GaAsN alloy. This means that the 2– charge state is never stable.

Figure 5.6 shows that the formation energies of both $(Si-N)_{As}$ and $(Ge-N)_{As}$ are lower than that of the $Si_{Ga}-N_{As}$ and $Ge_{Ga}-N_{As}$ pairs for the Fermi level above 0.6 eV and 0.8 eV, respectively. Even under an extreme Ga-poor conditions the formation

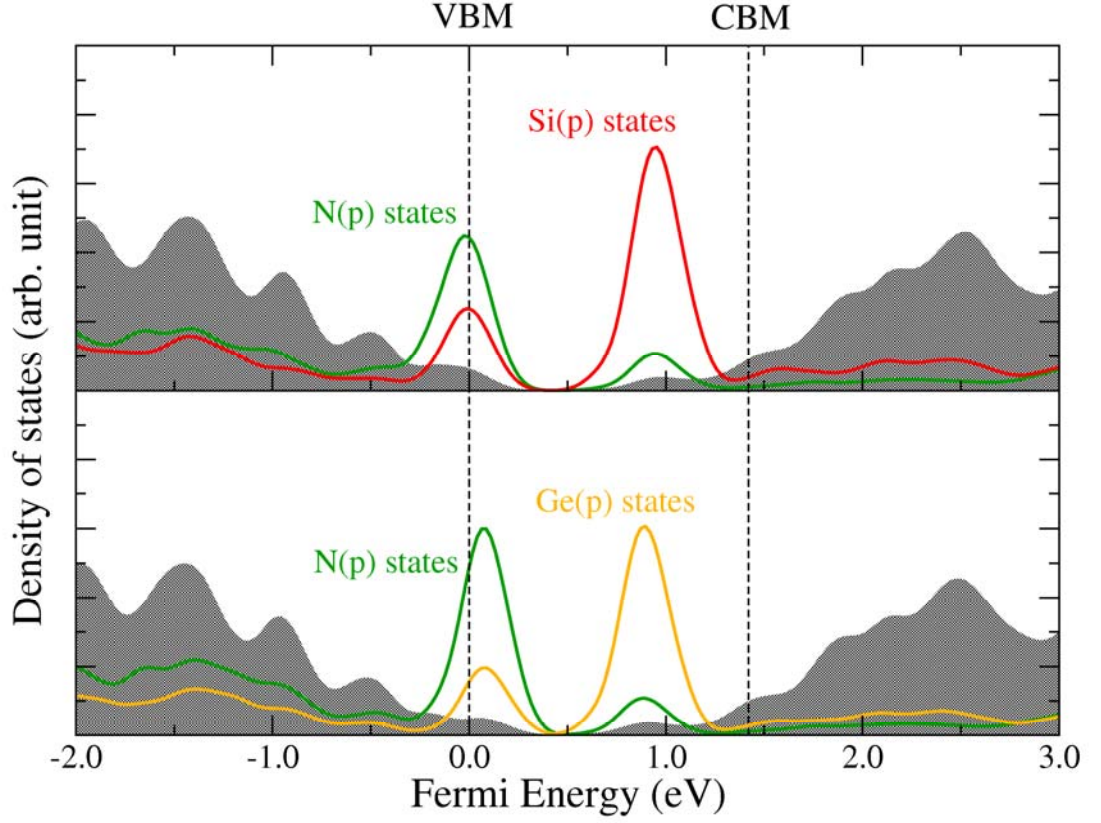


Figure 5.7 Calculated projected density of states of Si (or Ge) and N for p -orbitals (a) $(\text{Si-N})_{\text{As}}$ and (b) $(\text{Ge-N})_{\text{As}}$. The grey shaded area present the summation of projected density of states of host atoms. Density of state plots of p -orbitals scaled up for clarity. Dashed lines indicate the range of GaAs experimental bandgap.

energy of $(\text{Si-N})_{\text{As}}$ is 0.4 eV lower than that of $\text{Si}_{\text{Ga}}^+ - \text{N}_{\text{As}}$ when Fermi-level is near the CBM which is the case in experiments (Wu, *et al.*, 2003). $(\text{Si-N})_{\text{As}}$ and $(\text{Ge-N})_{\text{As}}$ act as compensating acceptors in GaAsN. The charge net electron concentration is the difference between the donor and acceptor defects concentration, i.e., between $[\text{Si}_{\text{Ga}}^+]$ and $[(\text{Si-N})_{\text{As}}^-]$ (or $[\text{Ge}_{\text{Ga}}^+]$ and $[(\text{Ge-N})_{\text{As}}^-]$). In the experiments of Si (or Ge) impurities incorporated in dilute nitrides, the electron concentration is much smaller

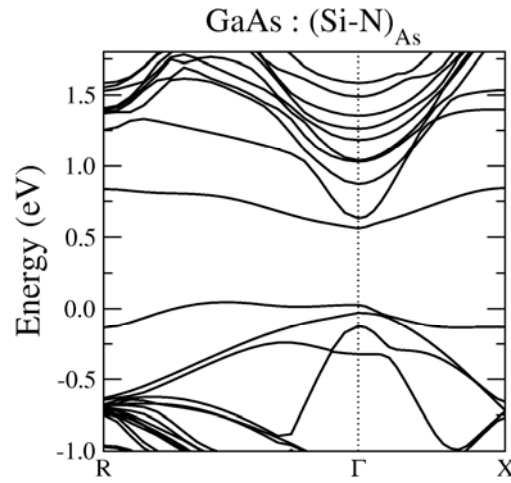


Figure 5.8 Calculated bandstructure of a 64-atom GaAsN supercell containing a $(\text{Si-N})_{\text{As}}$.

than the total of those impurities concentration after annealing above 800°C (or 950°C). Therefore, we conclude that the final concentrations of donors (Si_{Ga} or Ge_{Ge}) and acceptors [$(\text{Si-N})_{\text{As}}$ or $(\text{Ge-N})_{\text{As}}$] should be very close.

The $(\text{Si-N})_{\text{As}}$ split interstitial model also explains the peak at ~0.8 eV appeared in the photoluminescence spectra (Yu, *et al.*, 2002; Yu, *et al.*, 2003). In the photoluminescence experiments, the exciting photons create holes. In the presence of the holes in the valence band, negatively charged $(\text{Si-N})_{\text{As}}$ complex can convert to neutral by emitting photons (during the electron transitions to the VBM) with an energy of 0.83 eV as shown in Figure 5.10(a). Although there is no photoluminescence result for Ge impurity, we expect the peak at ~0.84 eV as shown in Figure 5.10(b). We note that the positions of these peaks are essentially independent of the nitrogen concentration, and also not sensitive to the DFT-LDA

underestimation of the energy gap. This was tested by performing calculations with different pseudopotentials that produce different energy gaps.

The formation mechanism of these split interstitial complex in the Si or Ge doped GaAsN were investigated. It is found that the formation of $(\text{Si-N})_{\text{As}}$ and $(\text{Ge-N})_{\text{As}}$ require annealing at sufficiently high temperatures. Because the mechanism for the formation should be the same for both $(\text{Si-N})_{\text{As}}$ and $(\text{Ge-N})_{\text{As}}$, we will focus on formation of $(\text{Si-N})_{\text{As}}$. Dilute GaAsN alloys are typically grown at relatively low temperatures (below 500°C) to prevent N segregation. Si can be introduced during this low-temperature growth or by ion implantation. In either way, Si_{Ga} donors are not likely to find their lowest-energy configurations during these processes. Subsequent annealing at high temperature (above 800°C) allows Si atoms to diffuse [possibly mediated by Ga vacancies which have low formation energy in *n*-type GaAsN alloys

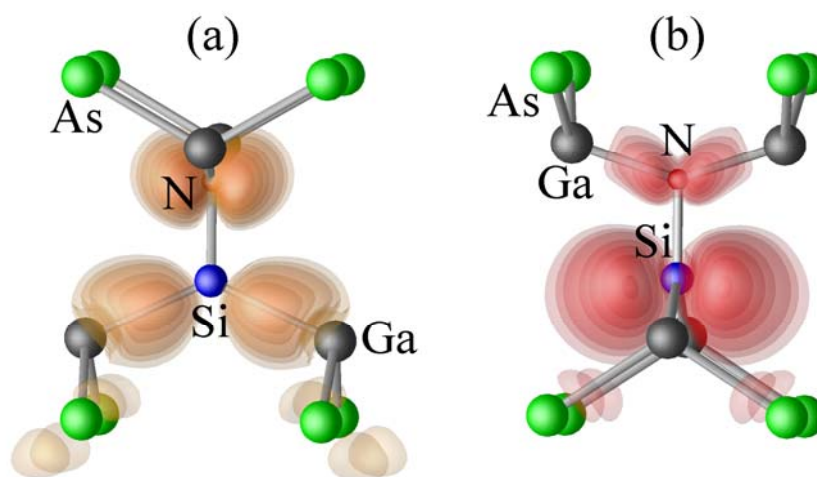


Figure 5.9 Charge density plots of the (a) bonding and (b) antibonding states associated with $(\text{Si-N})_{\text{As}}$. The structure in (b) has been rotated with respect to (a) to improve the visualization.

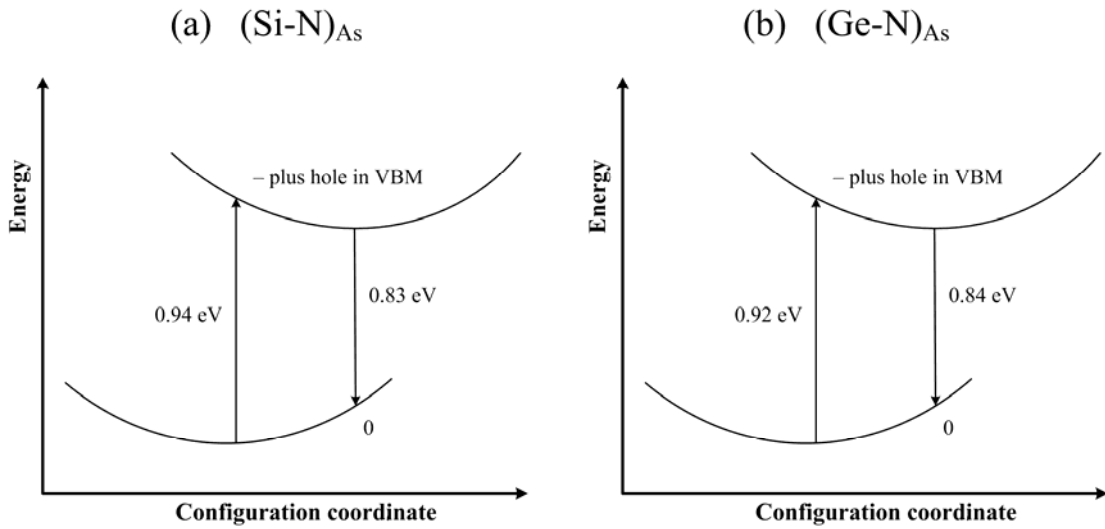


Figure 5.10 Schematic illustrations of the absorption and luminescence energies for (a) $(\text{Si-N})_{\text{As}}$ and (b) $(\text{Ge-N})_{\text{As}}$.

(Janotti, Wei, Zhang, Kurtz and Van de Walle, 2003) and find their equilibrium configurations [$(\text{Si-N})_{\text{As}}$ split-interstitial complex]. N atoms are likely to be immobile because their diffusion has a large barrier (Bösker, Stolwijk, Thordson, Södervall and Andersson, 1998). At 800°C the mean free path of Si is long enough for Si atoms to encounter N atoms (Yu, *et al.*, 2002; Wu, *et al.*, 2003; Yu, *et al.*, 2003). Si_{Ga} can combine with N_{As} and forms $(\text{Si-N})_{\text{As}}$ split interstitial. This process involves an emission of a Ga vacancy. However, Ga vacancies are very mobile and their concentration would rapidly return to the equilibrium concentration.

In addition, the present split-interstitial model can be used to explain why group-VI dopants, e.g. sulfur (S) and selenium (Se) behave differently in dilute nitride alloys. $(\text{S-N})_{\text{As}}$ and $(\text{Se-N})_{\text{As}}$ split interstitials are less stable compared to isolated S_{As} or Se_{As} donors. The reason is that group-VI donors have two more electrons than group-IV donors. These two extra electrons in $(\text{S-N})_{\text{As}}$ and $(\text{Se-N})_{\text{As}}$ occupy the

Table 5.3 Calculated stretch mode vibrational frequencies of (Si-N)_{As} and (Ge-N)_{As} split interstitial in neutral and 1− charge states.

	Charge state	Bond length (Å)	ω (cm ^{−1})
(Si-N) _{As}	0	1.65	935
	1−	1.68	884
(Ge-N) _{As}	0	1.80	731
	1−	1.82	694

antibonding states formed from p_z orbital. This significantly raises the formation energies of these complexes. For example, (Se-N)_{As} is more than 1 eV higher in energy than an isolated Se_{As}. As a result, S- or Se-doped GaAsN does not have the mutual passivation effects.

Finally, we calculated the local vibrational frequencies associated with the (Si-N)_{As} and (Ge-N)_{As} split interstitials. The calculations were performed by displacing each of the split interstitial atoms a small step at a time in the three perpendicular directions. Then, the force constant matrix was constructed and diagonalized in a similar way as the work by Janotti *et al.* (Janotti, Zhang and Wei, 2002a). Because the masses of N and Si are much smaller than that of the surrounding Ga atoms considering only the displacements of Si and N is a good approximation. We obtained the stretch mode frequencies of 935 cm^{−1} and 884 cm^{−1} in the neutral and 1− charge state, respectively (Table 5.3). These frequencies are much higher than the frequency (563 cm^{−1}) associated with the Si_{Ga}-N_{As} pair. The vibrational frequencies of (Ge-N)_{As} are also calculated and found to be lower than that of (Si-N)_{As}. This can be explained by the longer Ge-N bondlength and the larger Ge mass. These predicted vibrational

frequencies can serve as a guide for future experimental identification of the Si-N complex associated with the mutual passivation effects.

5.4 Summary

An interesting phenomenon, called “mutual passivation effect” in Si or Ge doped diluted nitride (GaAsN alloys) has been investigated based on density functional theory first-principles calculations. We have demonstrated the problems of previously proposed model [for e.g., $(\text{Si}_{\text{As}}\text{-N}_{\text{As}})$ and $(\text{Ge}_{\text{As}}\text{-N}_{\text{As}})$]. We illustrated that the corrected binding energies are very small, implying the formation of this complex unlikely. We also find that, even if they are formed, they would act as shallow donors and do not introduce a deep level. They do not give a restoration of GaAs bandgap. Therefore, the previously proposed model cannot explain the observed mutual passivation effects.

The split interstitial complex model has been proposed. We find that Si (or Ge) incorporated in GaAsN alloys are more likely to pair with N, sharing an As site in the form of split interstitial, i.e., $(\text{Si-N})_{\text{As}}$ [or $(\text{Ge-N})_{\text{As}}$]. They are more stable than the previous proposed model in *n*-type GaAsN. The split interstitials are found to introduce deep level. A sign of GaAs bandgap restoration is also found. The deep level can explain the peak (~ 0.8 eV) observed in the photoluminescence spectra of Si doped GaAsN. In addition, the proposed model can reasonably explain why group-VI dopants (e.g., S and Se) do not have the mutual passivation effect. The vibrational frequencies of $(\text{Si-N})_{\text{As}}$ and $(\text{Ge-N})_{\text{As}}$ in the stretch modes are predicted. These frequencies can help experimentalists to identify these complexes.

CHAPTER VI

CARBON-NITROGEN MOLECULES IN GALLIUM

ARSENIDE AND GALLIUM PHOSPHIDE

In this chapter, the computational results of carbon-nitrogen diatomic molecules in the GaAs and GaP are described. This work has been published in Physical Review B (Limpijumnong, *et al.*, 2008).

6.1 Introduction

Small amounts of nitrogen can strongly affect the electronic properties, such as the bandgap and electron effective mass, of GaP and GaAs. This opens up an opportunity to continuously modify the bandgap as well as other properties of these III–V semiconductors for advanced electronic and optoelectronic devices. This prospect has stimulated substantial research on dilute GaAsN and GaPN alloys both experimentally (Shan, *et al.*, 1999; Yu, *et al.*, 2002; Buyanova, Izadifard, Chen, Xin and Tu, 2004; Thinh, Vorona, Buyanova, Chen, Limpijumnong, Zhang, Hong, Tu, Utsumi, Furukawa, Moon, Wakahara and Yonezu, 2004; Ciatto, Boscherini, Bonapasta, Filippone, Polimeni and Capizzi, 2005; Pettinari, Masia, Polimeni, Felici, Frova, Capizzi, Lindsay, O'Reilly, Klar, Stolz, Bais, Piccin, Rubini, Martelli and Franciosi, 2006; Pettinari, Polimeni, Masia, Trotta, Felici, Capizzi, Niebling, Stolz and Klar, 2007) and theoretically (Kent and Zunger, 2001; Kim and Zunger, 2001;

Janotti, *et al.*, 2002b; Bonapasta, Filippone and Giannozzi, 2003; Du, Limpijumnong and Zhang, 2005; Teweldeberhan and Fahy, 2005; Du, Limpijumnong and Zhang, 2006). It is therefore very important that defects and impurities in these alloys are studied in detail. Carbon is a common impurity in various growth techniques (Welser, Setzko, Stevens, Rehder, Lutz, Hill and Zampardi, 2004; Li, Keyes, Asher, Zhang, Wei, Coutts, Limpijumnong and Van de Walle, 2005) and sometimes, it is intentionally used as a *p*-type dopant (Cheong and Chang, 1994; Songprakob, Zallen, Liu and Bacher, 2000; Fernandez, Cerdeira, Meneses, Brasil, Soares, Santos, Noriega, Leite, As, Köhler, Potthast and Pacheco-Salazar, 2003; Tan, Yoon, Huang, Zhang, Sun, Jiang, Feng and Lee, 2003) complex formations between C and N could therefore be an important issue. Recently, Ulrici and Clerjaud (Ulrici and Clerjaud, 2005) observed a sharp local vibration mode at 2087 cm^{-1} (at $T=7\text{ K}$) in GaP and a similar mode in GaAs. They identified it as a CN complex with a triple bond between C and N aligned along the $[100]$ direction.

An experimental work (Ulrici and Clerjaud, 2005) rigorously identified the chemical composition and the dipole direction of the complex; however, the actual location of the CN molecule in the lattice is still unclear. Both CN substituting on anion sites (CN_{As} in GaAs or CN_{P} in GaP) and interstitial CN (CN_{i}) are potentially consistent with experiment and were proposed as possible models in Ref. (Ulrici and Clerjaud, 2005). In other semiconductor compounds such as ZnO, GaN, and ZnSe, small diatomic molecules such as N_2 , O_2 , or CN have been studied both by first-principles calculations and by different experiments and found to prefer substitution on an anion site (Lee, Kim, Jin and Chang, 2001; Li, *et al.*, 2005; Limpijumnong, *et al.*, 2005; Fons, Tampo, Kolobov, Ohkubo, Niki, Tominaga, Carboni, Boscherini and

Friedrich, 2006; Janotti and Van de Walle, 2007b). However, the energy difference between the substitutional and interstitial sites varies from material to material; explicit calculations are therefore required to determine which site is more favorable for a given material.

In this chapter, we use first-principles calculations to calculate the formation energies of $\text{CN}_{\text{As (or P)}}$ and CN_i . We find that, similar to other semiconductor compounds that have been studied before, CN energetically prefers substituting on anion sites of GaAs and GaP over interstitial sites in all thermal equilibrium growth conditions. We also calculate the vibrational frequency of the complex and find reasonable agreement with the measured value. The CN molecule behaves very similarly in GaAs and GaP, and therefore, we will focus our discussion on CN in GaAs. Numerical results will be reported for both GaAs and GaP.

6.2 Computational Method

Our calculations are performed by using density functional theory with the local density approximation (LDA) where it provides a lattice constant of bulk GaP that is slightly in better agreement with that of experiment. On the other hand, generalized gradient approximation (GGA) provides a slightly better lattice constant for GaAs. Test calculations show that the choice of LDA/GGA only slightly affects the numerical value of energy and vibration frequency but does not change the main conclusions. We use ultrasoft pseudopotentials (Vanderbilt, 1990) as implemented in the VASP code (Kresse and Furthmüller, 1996a). The Ga 3*d* electrons are treated as valence electrons. The cutoff energy for the plane-wave basis set is 262 eV. We use a supercell with 64 atoms for the defect studies, and a 2×2×2 shifted Monkhorst–Pack

special k -point grid (Γ point not included) is employed for the Brillouin zone integration. The calculated GaAs lattice constant (5.60 Å, which is within 1% of the experimental value) is used. The electronic deep levels introduced by CN are examined by taking averages over the special k points. All the atoms are relaxed by minimization of the Hellmann–Feynman forces until all the forces are less than 0.05 eV/Å.

The formation energies of CN_i and CN_{As} are defined, following standard formalism (Zhang and Northrup, 1991) as

$$E^f(\text{CN}_i^q) = E_{\text{tot}}(\text{CN}_i^q) - E_{\text{tot}}(\text{bulk}) - \mu_{\text{C}} - \mu_{\text{N}} + qE_F, \quad (6.1)$$

$$E^f(\text{CN}_{\text{As}}^q) = E_{\text{tot}}(\text{CN}_{\text{As}}^q) - E_{\text{tot}}(\text{bulk}) - \mu_{\text{C}} - \mu_{\text{N}} + \mu_{\text{As}} + qE_F, \quad (6.2)$$

where $E_{\text{tot}}(D^q)$ is the total energy of the supercell with defect D in charge state q . $E_{\text{tot}}(\text{bulk})$ is the total energy of the supercell without a defect. μ_{C} , μ_{N} , and μ_{As} are the chemical potentials of a C atom, an N atom, and an As atom, respectively. For convenience, μ_{C} and μ_{As} are referenced to the energy of a C atom in diamond and an As atom in solid As, respectively. μ_{N} is referenced to the energy of an N atom in a free N_2 molecule. Growth conditions for GaAs are close to equilibrium, requiring that $\mu_{\text{Ga}} + \mu_{\text{As}} = \mu_{\text{GaAs}} = -0.69$ eV (calculated GaAs heat of formation), where μ_{Ga} is a chemical potential of a Ga atom, which is referenced to the energy of a Ga atom in bulk Ga. E_F is the electron Fermi level with respect to the valence-band maximum (VBM).

The local vibrational mode frequencies of the molecules are calculated by using the so-called frozen phonon approach (Ashkenazi, 1982) in which we followed a practical methodology described in Ref. (Limpijumnong, Northrup and Van de

Walle, 2003). Because C and N atoms have similar masses, we equally displaced C and N to calculate the potential energy of stretching and compressing bonds. The mass of the oscillator is taken as the reduced mass:

$$\mu = \frac{m_C m_N}{m_C + m_N} \quad (6.3)$$

where m_C and m_N are the masses of C and N atoms. We find that the (harmonic) stretching vibrational frequencies of the oscillator agree very well with a full dynamic matrix calculation with the matrix constructed by displacing each and every atom in the supercell one at a time in all three principal axes directions. A test calculation (on $\text{CN}_{\text{As}}^{2+}$) shows that the agreement between the full dynamic and reduced-mass results is better than 5 cm^{-1} . An important benefit of the reduced-mass calculation (besides a significant reduction in computational effort) is that it allows us to calculate the anharmonic part of the vibration, which we found to be on the order of 20 cm^{-1} . The potential energy is evaluated at seven values of displacements, with a maximum amplitude of up to 10% of the C-N equilibrium bond distance. To test the accuracy of the approach, we calculated the stretch frequency of a C-N mode in the HCN molecule and obtained the value of 2057 cm^{-1} , which is slightly smaller than the experimental value of 2089 cm^{-1} (Kim and King, 1979). The calculated equilibrium C-N bond distance is fortuitously equal to the experimental value of 1.156 \AA . The small underestimation in vibrational frequency, which is by 32 cm^{-1} , is expected to be systematic. Therefore, we have added the value of $\omega_{ER}=32 \text{ cm}^{-1}$ to all of our calculated frequencies as a systematic correction.

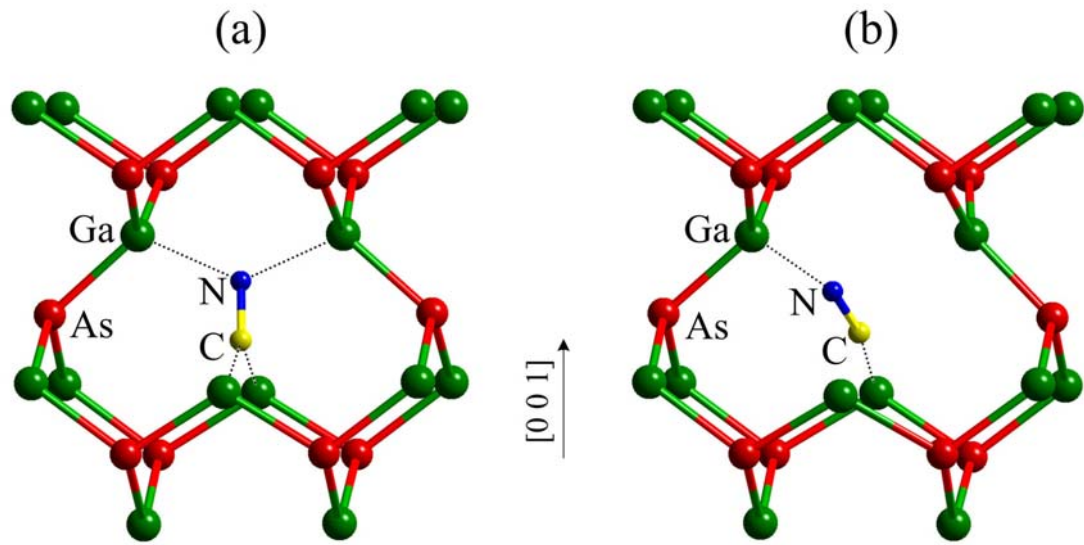


Figure 6.1 Local atomic geometry of a CN molecule substituting on an As site in GaAs: (a) symmetric configuration, CN_{As} , and (b) asymmetric configuration, CN_{As} (asym). Both are shown for the 2+ charge state.

6.3 Results and Discussion

We investigated two forms of CN molecules in GaAs: at the substitutional As site and at the interstitial site. If initially the CN molecule is symmetrically placed at the As site in the form of a split-interstitial configuration with its principal axis aligned along the [100] direction, due to the symmetry, the orientation of the molecule will remain unchanged even when relaxation is allowed. The resulting symmetric configuration, $\text{CN}_{\text{As}}(\text{sym})$, is shown in Figure 6.1(a). However, this orientation is not the lowest energy one for all charge states. Breaking the symmetry causes the molecule (in some charge states) to spontaneously rotate, without any barrier, into an

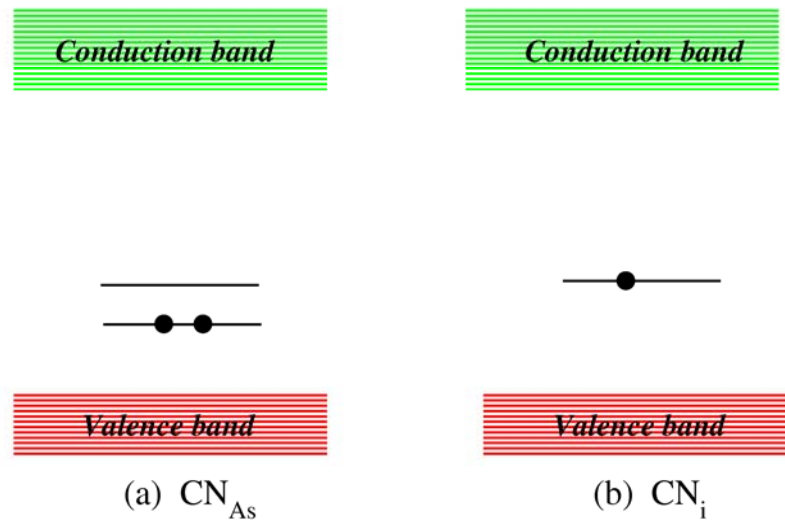


Figure 6.2 Schematic illustrations of the $pp\pi^*$ single-particle energy levels of the CN molecule in the GaAs bandgap. (a) Substituting on an As site (CN_{As}) and (b) CN on an interstitial site (CN_i). The solid dots show the electron occupation for the neutral charge state.

asymmetric configuration [Figure 6.1(b), CN_{As} (asym) in the 2+ charge state]. For an interstitial CN, there are two possible sites for the zinc-blende crystal: the tetrahedral interstitial sites surrounded by either Ga [$T_d(\text{Ga})$] or As atoms $T_d(\text{As})$. The calculations show that CN_i energetically prefers the $T_d(\text{Ga})$ site over the $T_d(\text{As})$ site. The $T_d(\text{Ga})$ site is surrounded by four Ga atoms in a tetrahedral configuration similar to the local structure surrounding a substitutional As lattice site. Again, if the molecule is initially placed in a high-symmetry orientation, $\text{CN}_i(\text{sym})$, the orientation remains fixed by symmetry but breaking the symmetry can lead to rotation of the molecule into a lower-energy asymmetric configuration, $\text{CN}_i(\text{asym})$.

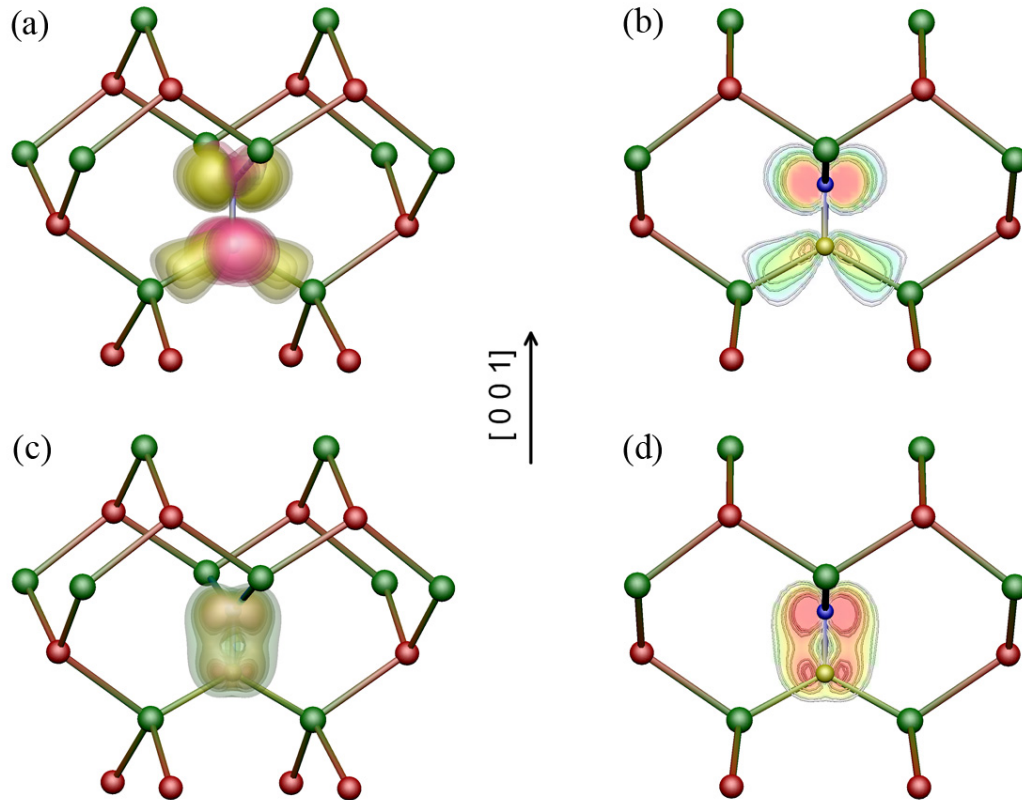


Figure 6.3 (a) Charge density of the $pp\pi^*$ states of CN_{As} that are located in the GaAs bandgap. (b) Contour plot of one of the states in (a) in a (001) plane cutting through the CN molecule. (c) Charge density of one of the $pp\pi$ states of CN_{As} that resides below the valence-band maximum. (d) The corresponding contour plot of (c)

6.3.1 Substitutional CN molecules (CN_{As})

The substitutional molecule CN_{As} introduces a deep donor level (at approximately 0.25 eV) in the GaAs bandgap, as shown in Figure 6.2. The charge density (Figure 6.3) of these levels resembles the $pp\pi^*$ molecular orbital of the CN molecule (Limpijumnong, *et al.*, 2005). The molecular orbital theory tells us that the CN molecule has the following molecular orbitals, which are in order of increasing

energy: $ss\sigma$, $ss\sigma^*$, $pp\pi$ (doublet), $pp\sigma$, $pp\pi^*$ (doublet), and $pp\sigma^*$. In the neutral charge state, the CN molecule on an As site has 12 valence electrons: 9 from the CN itself and 3 more contributed from the surrounding Ga atoms. These 12 electrons occupy the CN molecular orbitals up to the lower $pp\pi^*$ level and leave the higher $pp\pi^*$ level empty. Because the lower $pp\pi^*$ level is located deep inside the GaAs bandgap, CN_{As} can donate up to two electrons and become $\text{CN}_{\text{As}}^{2+}$ when the Fermi level of the system falls below the 0.25 eV donor level. The bonding between the C and N atoms in $\text{CN}_{\text{As}}^{2+}$ is a triple bond ($\text{C} \equiv \text{N}$), with a bond distance of 1.17–1.20 Å (depending on the orientation), which is in good agreement with the known triple-bond length between C and N in HCN of 1.156 Å (Herzberg, 1966). In the 2+ charge state, the $pp\pi^*$ level is unoccupied; hence, the $\text{CN}_{\text{As}}^{2+}$ has little interaction with the surrounding neighbor. The molecule can therefore rotate quite freely, and it indeed moves away from the symmetric configuration to a new orientation that has a lower energy. Our calculated energy profile for the molecule rotating from the [001] to the (near) [110] direction, which is based on the nudged elastic band (NEB) method (Jónsson, *et al.*, 1998) is shown in Figure 6.4. We can see that starting from the symmetric [001] orientation, the molecule can rotate without any barrier to a new orientation in which the molecule's principal axis is nearly parallel with the [110] direction, lowering its energy by 0.27 eV in the process. By investigating the charge density (not shown), we found that the asymmetric configuration allows better interactions between the bonding pp states of CN and two of the surrounding Ga atoms, resulting in a lower formation energy.

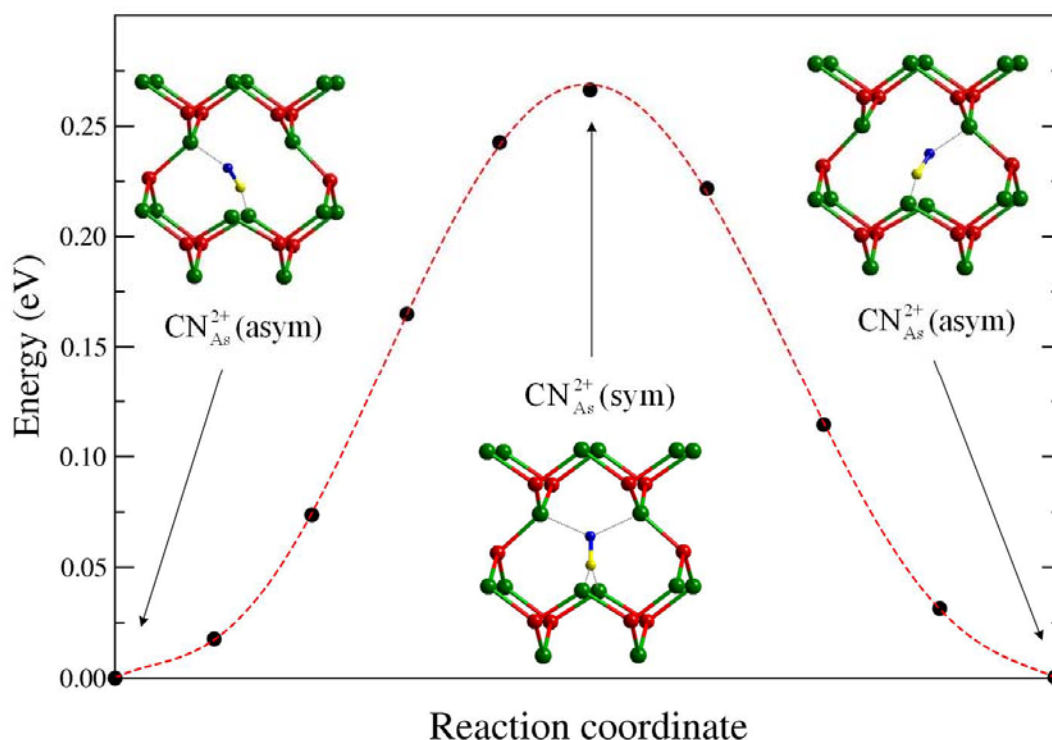


Figure 6.4 Calculated energy of $\text{CN}_{\text{As}}^{2+}$ as the CN molecule rotates from asymmetric to symmetric and back to an equivalent asymmetric configuration. The symmetric configuration is the saddle point along this path.

Starting from $\text{CN}_{\text{As}}^{2+}$, when the Fermi level is raised, the defect levels characteristic of $pp\pi^*$ molecular orbitals become occupied with electrons, and the charge state of CN_{As} increases from 2+ to 1+, 0, 1−, and 2−. Because these defect states correspond to antibonding orbitals of the free molecule, occupying them leads to an increase in the CN bond length (of approximately 0.05 Å per electron added), as shown in Table 6.1. In addition, the charge density plots [Figure 6.3(a) and 6.3(b)] reveal that the $pp\pi^*$ states hybridize with the dangling-bond states of the surrounding Ga atoms in the directions in which the density lobes are pointing. For instance, the

lower two lobes in Figure 6.3(b) clearly show the bond formation between the C atom and two Ga atoms, whereas the upper two lobes still maintain the molecular $pp\pi^*$ features. Because of the possibility of bond formation with the neighboring Ga atoms, $\text{CN}_{\text{As}}^{1+}$, CN_{As}^0 , and $\text{CN}_{\text{As}}^{1-}$ all favor the symmetric configuration (CN_{As} in the 1+ and 0 charge states is stable in the symmetric configuration. Test calculations for 1+ showed that a dimer initially tilted by as much as 15° away from the symmetric direction, i.e., the [001] direction, spontaneously rotated back after relaxations. The asymmetric configurations are only metastable. The (higher-energy) metastable asymmetric configuration for each charge state is found by initially aligning the CN molecule along the [110] direction and allowing relaxation of its neighbors before letting the molecule itself relax. The metastable asymmetric configurations are higher in energy than the symmetric ones by 0.1 and 0.5 eV for the 1+ and neutral charge states, respectively. The dimer qualitatively behaves the same in GaP except that none of the metastable asymmetric configurations exists.

$\text{CN}_{\text{As}}^{2-}$, on the other hand, favors an asymmetric configuration (with a different orientation from that of $\text{CN}_{\text{As}}^{2+}$). Because the $pp\pi^*$ states are fully occupied, the molecule tries to optimize the Coulombic interaction between these $pp\pi^*$ states and its four Ga neighbors. Since the charge distribution for the CN molecule is not symmetric (the N atom is more electronegative than the C atom), the asymmetric configuration allows the N side of the molecule to bind with three Ga atoms instead of two, making the configuration more stable.

Table 6.1 Calculated bond lengths $d_{\text{C-N}}$, stretching frequencies ω , and formation energies E^f (for the Fermi level at the VBM) of CN molecules in GaAs in the symmetric (asymmetric in parentheses) configurations. For each charge state, the lower energy configuration is shown in boldface.

Charge state (q)	$d_{\text{C-N}}$ (Å)	ω (cm ⁻¹)	E^f (eV)	
			Ga-rich	As-rich
CN on the As site (CN _{As})				
2+	1.20	1779	2.42	3.11
	(1.17)	(2052)	(2.15)	(2.84)
1+	1.25	1481	2.42	3.11
	(1.22)	(1734)	(2.46)	(3.15)
0	1.30	1328	2.58	3.27
	(1.25)	(1345)	(3.08)	(3.77)
1-	1.35	1173	3.13	3.82
	(1.31)	(1182)	(3.34)	(4.03)
2-	1.38	1095	4.03	4.72
	(1.40)	(1097)	(3.82)	(4.51)
CN on the interstitial site (CN _i)				
1+	1.20	1897	4.41	4.41
	(1.19)	(1934)	(3.85)	(3.85)
0	(1.25)	(1519)	(4.37)	(4.37)

Table 6.2 Calculated bond lengths $d_{\text{C-N}}$, stretching frequencies ω , and formation energies E^f (for the Fermi level at the VBM) of CN molecules in GaP in the symmetric (asymmetric in parentheses) configurations. For each charge state the lower energy configuration is shown in boldface.

Charge state (q)	$d_{\text{C-N}}$ (Å)	ω (cm ⁻¹)	E^f (eV)	
			Ga-rich	P-rich
CN on the P site (CN _P)				
2+	1.20	1734	2.25	3.13
	(1.18)	(2028)	(2.12)	(3.00)
1+	1.25	1517	2.40	3.28
0	1.31	1352	2.75	3.63
1-	1.36	1197	3.58	4.46
	(1.33)	(1283)	(3.74)	(4.62)
2-	1.39	1113	4.77	5.65
	(1.41)	(1105)	(4.50)	(5.38)
CN on the interstitial site (CN _i)				
1+	1.21	1875	4.43	4.43
	(1.19)	(1933)	(3.96)	(3.96)
0	(1.26)	(1511)	(4.82)	(4.82)

The formation energies of CN_{As} are shown in Table 6.1 (Table 6.2 for CN in GaP) and plots as a function of Fermi level are shown in Figure 6.5 for two growth conditions: Ga rich ($\mu_{\text{Ga}} = 0$) and As rich ($\mu_{\text{As}} = 0$). As can be seen from Eq. (6.1) and (6.2), the slope of the plot indicates the charge state of the CN molecule. In our

plots, only the lowest energy charge state (at a given Fermi energy) is shown. For example, CN_{As} (asym) is stable in the 2+ charge state when the E_F of the system is located between 0.0 and 0.25 eV; therefore, the line has a slope of 2. For $0.25 \text{ eV} < E_F < 0.70 \text{ eV}$, the symmetric configuration becomes more stable and the neutral and 1- (for a narrow range near $E_F = 0.70 \text{ eV}$) charge states are the lowest in energy. At higher E_F , the asymmetric configuration with the 2- charge state, i.e., $\text{CN}_{\text{As}}^{2-}$ (asym), becomes the most stable (although the calculated LDA bandgap for GaAs is only 0.6 eV at the Γ point, our calculations are performed at special k -points wherein the lowest conduction band occurs at 1.08 eV above the VBM. Any defect levels that lie below 1.08 eV are therefore accounted for and can be properly occupied). Therefore, the stable configurations in order of increasing E_F are as follows: $\text{CN}_{\text{As}}^{2+}$ (asym), CN_{As}^0 (sym), $\text{CN}_{\text{As}}^{1-}$ (sym), and $\text{CN}_{\text{As}}^{2-}$ (asym). $\text{CN}_{\text{As}}^{1+}$ is never stable. Because CN is substituting on the As site to form CN_{As} , its formation energy is lower in the Ga-rich condition than that in the As-rich condition. The plots also show that the formation energy of CN_{As} is always lower than that of CN_i for both the Ga- and As-rich conditions throughout the entire Fermi-energy range, with an energy difference of at least 1 eV. This implies that CN_{As} is far easier to form than CN_i .

The trends in bonding discussed above are reflected in our calculated values of vibrational frequencies, which show that the frequency is highest for $\text{CN}_{\text{As}}^{2+}$ (2052 cm^{-1} for an asymmetric configuration and 1779 cm^{-1} for a hypothetical symmetric configuration). This is because in the 2+ charge state, the bonding states of the molecule are all occupied and the antibonding states ($pp\pi^*$) are all empty. As electrons are added into the antibonding states of CN_{As} , the C-N bond is weakened

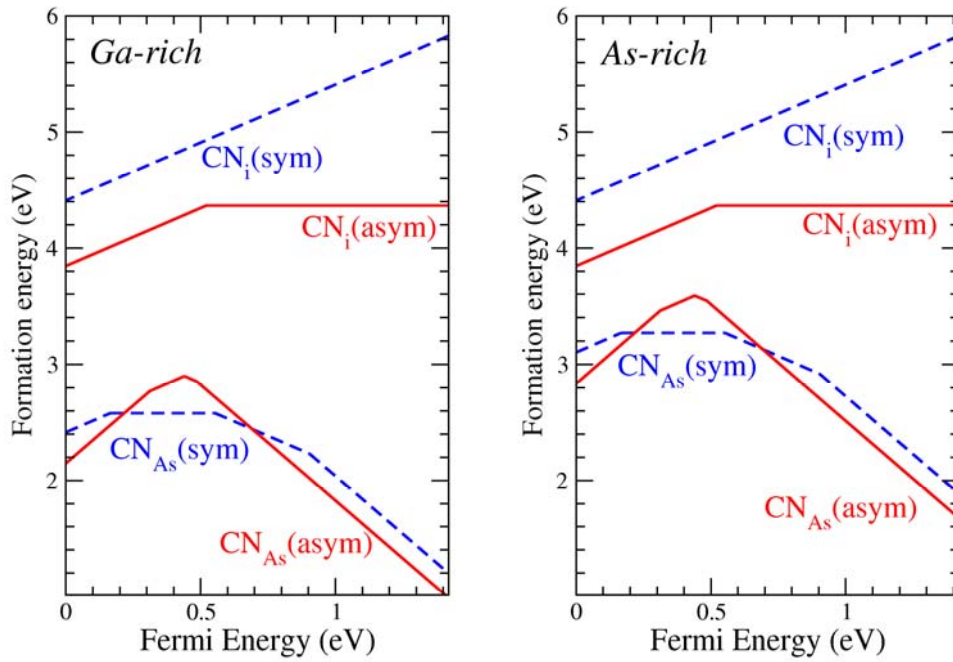


Figure 6.5 Formation energies of CN molecules in GaAs as a function of the Fermi energy. The solid lines and dashed lines represent the asymmetric and symmetric configurations, respectively.

and the frequency is reduced to 1481, 1328, 1173, and 1097 cm^{-1} for $\text{CN}_{\text{As}}^{1+}$, CN_{As}^0 , $\text{CN}_{\text{As}}^{1-}$, and $\text{CN}_{\text{As}}^{2-}$, respectively.

6.3.2 Interstitial CN molecules (CN_i)

The CN molecule has a total of nine electrons filling its molecular orbitals in the following order: $ss\sigma$, $ss\sigma^*$, $pp\pi$ (doublet) and with the last electron occupying $pp\sigma$. This leaves the $pp\sigma$ bonding state half-occupied and able to accept one more electron. Due to the strong bonding nature in the CN molecule, this $pp\sigma$ state has a low energy. When the molecule is placed in GaAs, the $pp\sigma$ state lies below the VBM and always

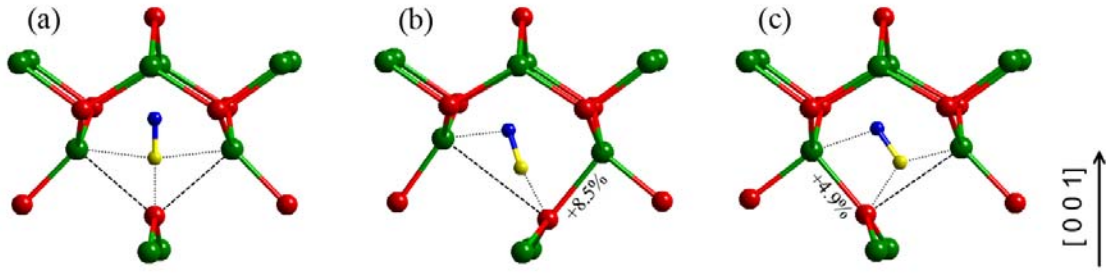


Figure 6.6 Local atomic geometry of interstitial CN molecules in GaAs: (a) CN_i^+ (sym), (b) CN_i^+ (asym), and (c) CN_i^0 (asym)

becomes fully occupied. At the same time, the insertion of CN at an interstitial site also creates strain in nearby Ga-As bonds, leading to Ga-As bond extension (or breaking). The broken Ga-As bonds are shown in dotted lines in Figure 6.6. CN_i is stable in two charge states: 1+ and neutral. We initially used symmetric configurations in our calculations [Figure 6.6(a)], but this configuration can spontaneously relax into asymmetric configurations with lower energies [Figure 6.6(b) and 6.6(c)] if symmetry breaking is allowed. The energy change as the CN_i rotates from the symmetric configuration into the asymmetric one (for 1+ charge state) calculated by using the NEB method is shown in Figure 6.7. Figure 6.7 shows that the asymmetric configuration is favored over the symmetric one by ~ 0.6 eV. We can clearly see in the asymmetric configuration [Figure 6.6(c)] that only one of the Ga-As bonds is now broken (another bond is extended from a typical Ga-As bond). One of the two electrons released from the broken bond goes to the $pp\sigma$ state of the CN molecule, whereas another one is removed, resulting in the 1+ charge state. As an additional electron is added (increasing the charge state of the defect from 1+ to neutral), the additional electron goes to the $pp\pi^*$ level, which is located at

approximately 0.5 eV above the VBM (see Figure 6.2). This leads to the +/0 transition level of CN_i at 0.5 eV above the VBM. The occupation of the $pp\pi^*$ level leads to the increase in the CN bond to 1.25 Å and is reflected in an enhanced binding between the molecule and its neighbors [Figure 6.6(c)] compared to the 1+ charge state [Figure 6.6(b)]. Because the electron density of the $pp\pi^*$ state has four lobes pointing outward, which is similar to Figure 6.3(b), when this state is occupied, the molecule can gain energy by turning the lobes to form bonds with the neighboring atoms.

Vibrational frequencies for the stretching modes of CN_i in GaAs and GaP are shown in Tables 6.1 and 6.2. The frequency is higher for the CN_i in the 1+ charge state, which has all the bonding states occupied and the antibonding states empty. The frequency of 1934 cm^{-1} (1897 cm^{-1} for a hypothetical symmetric configuration) is comparable to that of $\text{CN}_{\text{As}}^{2+}(\text{asym})$, which has a similar electron occupation on the molecule. For the neutral charge state CN_i , with an electron occupying the $pp\pi^*$ state, the C-N bond length increases to 1.25 Å and the vibrational frequency decreases to 1519 cm^{-1} .

6.3.3 General trends of the bond length and the vibrational frequency

Our results show that the C-N bond distance becomes larger (and the vibrational frequency becomes lower) as more electrons are added into the $pp\pi^*$ states. Our investigations of the various configurations of CN molecules in GaAs and GaP allow us to quantitatively study the relationship between the electron occupation (of the CN molecule) and the bond length as well as the vibrational frequency. To do

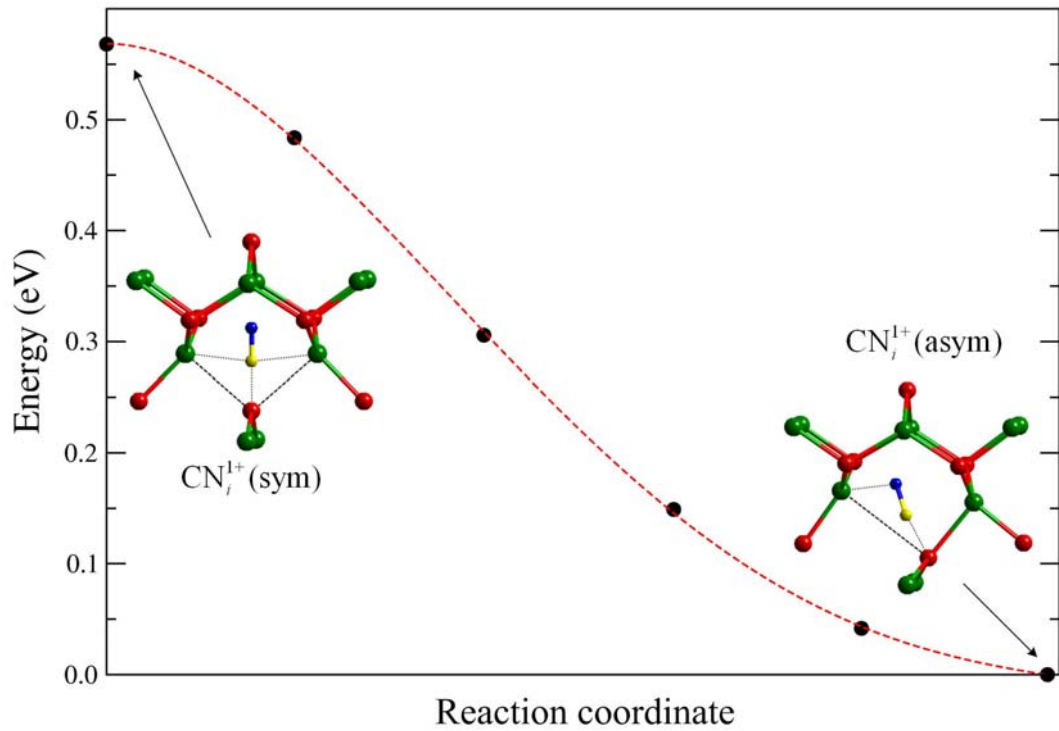


Figure 6.7 Calculated energy of CN_i^{1+} as the CN molecule rotates from a symmetric to an asymmetric configuration. The rotation occurs without any barrier and lowers the energy by almost 0.6 eV.

this, we define Δq as the additional charge being added to the CN molecule relative to the neutral free CN molecule. A free CN molecule has nine electrons, which occupy the molecular states up to half of the $pp\sigma$ state. Since this state is located below the VBM of GaAs, it is always fully occupied. This means that at least one electron from the host has to be added to the molecule $q = -1$ and the electron occupation of the molecule becomes the same as that of a free (triple-bonded) CN^- ion. For the CN molecule in GaAs, this occupation corresponds to the lowest charge state, i.e., $\text{CN}_{\text{As}}^{2+}$ and CN_i^{1+} . As the Fermi energy is raised, electrons are inserted into the antibonding

states ($pp\pi^*$ states) of the CN molecule, thus weakening the C-N bond. When two electrons are inserted into the antibonding state (i.e., CN_{As}^0), making $q = -3$, the C-N bond is reduced to a double bond instead of a triple bond. When four electrons are inserted into the antibonding states (i.e., $\text{CN}_{\text{As}}^{2-}$), making $q = -5$, the C-N bond is reduced to a single bond. Our calculations thus show that CN_{As} can have its bond strength varied from a triple bond down to a single bond depending on the electron occupation. CN_i , on the other hand, can only exhibit the bond strength of a triple bond ($\text{CN}_{\text{As}}^{1+}$) or a triple bond with one electron in the antibonding state (CN_{As}^0) (which can be considered as halfway between a double bond and a triple bond).

A plot of the C-N bond distance as a function of Δq is shown in Figure 6.8(b). The bond distance, especially of the symmetric configurations, clearly show a linear trend with Δq . The deviations from the linear trend in the case of some of the asymmetric configurations can be attributed to the interaction with neighboring host atoms. A linear fit between the bond distance and Δq for all data points yields

$$d_{\text{C-N}} = -0.0496\Delta q + 1.143, \quad (6.4)$$

where $d_{\text{C-N}}$ is the bond distance between C and N in Å. The bond length increases by approximately 0.05 Å for every electron inserted. The vibrational frequency decreases as the bond is extended. The relationship between the frequency and q is shown in Figure 6.8(a). Again, a linear trend is seen. A linear fit yields

$$\omega = 207\Delta q + 2057, \quad (6.5)$$

where ω is the vibration frequency in cm^{-1} , i.e., the frequency is redshifted by approximately 200 cm^{-1} for every electron that is inserted. Deviations from the fit (on the order of 100 cm^{-1}) occur because the actual frequency also depends on other

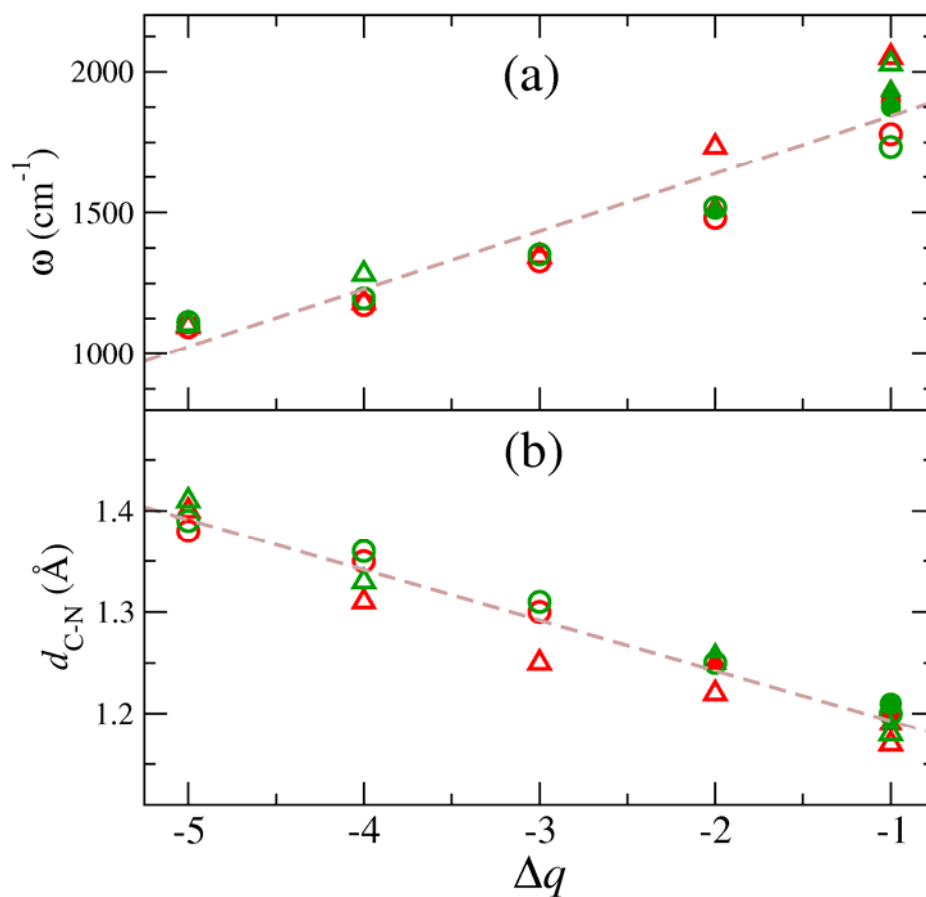


Figure 6.8 (a) Calculated vibration frequencies and (b) C-N bond distances for various configurations of a CN molecule in GaAs and GaP as a function of charge Δq inserted into the molecule, which are measured relative to a neutral free CN molecule with nine electrons. The solid symbols are for interstitial CN and the open symbols are for substitutional CN. The colors code the host materials (red for GaAs and green for GaP), whereas the symbols are used to distinguish the symmetric (circle) from asymmetric (triangle) configurations. The CN molecules is characterized as triply, doubly, or singly bonded for $\Delta q = -1, -3$, and -5 , respectively. The dashed lines are linear fits to all of the data points.

factors such as the detailed local geometry. Still, the linear fit in Eq. (6.4) nicely highlights the general trend, even if it does not provide a completely accurate prediction of the frequency.

6.3.4 Discussion and comparison with experiment

Ulrici and Clerjaud (Ulrici and Clerjaud, 2005) performed a polarized infrared absorption spectroscopy on C-doped dilute-nitride GaAs and GaP. They observed a sharp local vibrational mode at 2087.1 cm^{-1} (at $T=7 \text{ K}$) in GaP and a similar mode 2088.5 cm^{-1} in GaAs. They identified it as a CN complex with a triple bond (between C and N) aligned along three equivalent $\langle 100 \rangle$ directions. Their C and N assignments were based on their observation of additional weak peaks at 2031 and 2048 cm^{-1} , which exhibit an intensity ratio and frequency shift that match the natural abundance and predicted frequency shift for C^{13} and N^{15} isotopes. The orientation of the molecule was confirmed by polarized IR absorption under different types of uniaxial stress.

An inspection of Tables 6.1 and 6.2 shows that the measured frequency of 2087 cm^{-1} is most consistent with our calculated frequencies for triply bonded CN molecules with $\Delta q = -1$. A more detailed identification runs into some complications, however. There are four configurations with triple bonds covered in our study: $\text{CN}_{\text{As}}^{2+}(\text{asym})$, $\text{CN}_{\text{As}}^{2+}(\text{sym})$, $\text{CN}_i^{1+}(\text{asym})$, $\text{CN}_{\text{As}}^{2+}(\text{sym})$. (1) $\text{CN}_{\text{As}}^{2+}(\text{asym})$ provides the best matching frequency to the experiment (lower by 36 cm^{-1} , which is well within the computational error bar). However, the molecule does not align along $\langle 100 \rangle$ but, instead, prefers to align in a direction close to $\langle 110 \rangle$. (2) $\text{CN}_{\text{As}}^{2+}(\text{sym})$ has the correct orientation; however, its frequency is too low (by 309 cm^{-1}), and, even more

importantly, it is not energetically stable and spontaneously rotates to $\text{CN}_{\text{As}}^{2+}(\text{asym})$, lowering the energy by 0.27 eV. Therefore, we can rule out $\text{CN}_{\text{As}}^{2+}(\text{sym})$. (3) $\text{CN}_i^{1+}(\text{asym})$ is a possible candidate. Its calculated vibrational frequency is not too far from the observed value (lower by 154 cm^{-1}). However, its orientation also deviated from $\langle 100 \rangle$ by 16° . In addition, the interstitial configurations are energetically unfavorable compared to those of $\text{CN}_{\text{As}}^{2+}(\text{asym})$. (4) $\text{CN}_i^{1+}(\text{sym})$ is an unlikely candidate because it is not energetically stable. It can spontaneously rotate to the asymmetric configuration and gain 0.6 eV. In addition, its vibrational frequency is even lower than that of the asymmetric configuration, widening the disagreement with experiment to 191 cm^{-1} .

Our first-principles calculations of vibrational frequencies for CN molecules in various configurations in GaAs and GaP therefore generally support Ulrici and Clerjaud's (Ulrici and Clerjaud, 2005) assignment of the 2087 cm^{-1} mode to a triply bonded CN molecule. However, our calculations also show that the triply bonded CN molecule (in either the substitutional or interstitial configurations) does not symmetrically align in a tetrahedral site surrounded by four Ga atoms. As a result, neither CN_{As} nor CN_i have the C-N axis aligned in the $\langle 100 \rangle$ direction, as proposed by Ulrici and Clerjaud (Ulrici and Clerjaud, 2005). However, given a rather low rotation barrier of only 0.27 eV (Figure 6.4), it is possible that $\text{CN}_{\text{As}}^{2+}(\text{asym})$ is constantly rotating, resulting in an average orientation in the $\langle 100 \rangle$ direction observed in the experiment.

6.4 Conclusions

We have presented first-principles results for CN molecules in GaAs and GaP. The study covered two possible lattice locations: (1) CN molecules substituting for anions $\text{CN}_{\text{As(or P)}}$ and (2) interstitial CN molecules at the T_d site surrounded by four Ga atoms (CN_i). All possible charge states and various orientations were considered. The calculated formation energies show that the molecule favors substituting for the anion site over the interstitial configuration for all equilibrium growth conditions with a margin of at least 1 eV. The calculations predict the CN molecule to produce a level with a strong $pp\pi^*$ molecular orbital characteristic at approximately 0.5–0.8 eV above the VBM. In p -type conditions, where the Fermi level is located below this $pp\pi^*$ level, the molecules are triply bonded and form donor defect centers (double donor $\text{CN}_{\text{As}}^{2+}$ and single donor CN_i^{1+}). The calculations with full relaxation show that triply bonded $\text{CN}_{\text{As}}^{2+}$ and CN_i^{1+} do not symmetrically orient in the Ga tetrahedron but, instead, are tilted in order to gain better interactions with neighboring Ga atoms. The calculated vibration frequencies of the triply bonded $\text{CN}_{\text{As}}^{2+}$ and CN_i^{1+} are in reasonable agreement with the measurement by Ulrici and Clerjaud supporting their identification that the bonding is triple bond type. Although neither CN_{As} nor CN_i have the C-N bond oriented along the 100 directions, as proposed by Ulrici and Clerjaud (Ulrici and Clerjaud, 2005) the low rotation barrier of $\text{CN}_{\text{As}}^{2+}$ makes it possible that the molecule might be constantly rotating, leading to an average orientation in the $\langle 100 \rangle$ direction. At higher Fermi levels, the CN_i^{1+} can accept an electron and becomes CN_i^0 , whereas $\text{CN}_{\text{As}}^{2+}$ can accept one, two, three, or four

electrons (depending on the Fermi level) and becomes $\text{CN}_{\text{As}}^{1+}$, CN_{As}^0 (metastable), $\text{CN}_{\text{As}}^{1-}$, or $\text{CN}_{\text{As}}^{2-}$, respectively. We found that the C-N bond length and vibrational frequency linearly change (to a good approximation) with the number of electrons added into the antibonding states of the molecule.

CHAPTER VII

SUMMARY AND POTENTIAL FUTURE RESEARCH

In this thesis, a number of defect complexes in semiconductors have been studied by first-principles calculations based on density functional theory. In this chapter, the defect complexes described in previous three chapters are briefly summarized. Moreover, some potential future research are discussed.

7.1 Brief Summary of Studied Defect Complexes

7.1.1 $\text{Zn}_i\text{-N}_\text{O}$ complex in ZnO

An electron-irradiated experiment indicates that the observed 30 meV donor peak in ZnO corresponds to Zn_i . Because the ZnO sample was annealed in N_2 , the $\text{Zn}_i\text{-N}_\text{O}$ complex is a potential candidate for the donor center. The calculations show that the $\text{Zn}_i\text{-N}_\text{O}$ complex is indeed a shallow donor. The high binding energy between Zn_i and N_O of 0.95 eV is sufficient to stabilize the complex at room temperature.

7.1.2 Silicon-nitrogen complex in dilute nitrides

In Si doped dilute nitrides (for e.g., $\text{GaAs}_{1-x}\text{N}_x$), it is found that Si restores the bandgap back to the bandgap value without nitrogen. At the same time, nitrogen passivates the carriers that would be created by Si. These effects are called “mutual passivation”. To explain the mutual passivation effect, a model of the complex is proposed. The complexes between group-IV and N in the form of split-interstitial, i.e.,

(Si-N)_{As}, and (Ge-N)_{As} have been calculated and found to be the most likely model. This model overcomes several problems in the pre-existing model (Si_{Ga}-N_{As} complex). In the new model, the gap restoration and reduction of electron carriers were explained through the deep level introduced by the split-interstitials. It also can explain the photoluminescence peak ~0.8 eV appeared after annealing.

7.1.3 Carbon-nitrogen complexes in GaAs and GaP

Previous experimental work observed an infrared absorption spectroscopy peak associated with carbon and nitrogen impurity in GaAs and GaP. The work suggested that the infrared absorption spectroscopy peak should come from CN complex. In this thesis, several forms of CN molecules in GaAs and GaP are calculated. The calculations show that the molecule prefers to substitute for an anion site over being an interstitial. Under *p*-type conditions, the molecule acts as a double donor (CN_{As}²⁺). The calculated vibration frequency of the triply bonded CN_{As}²⁺ is in a reasonable agreement with the measurement. This makes CN_{As} the most likely candidate to explain the observation.

7.2 Potential Future Research

Although there are quite a number of defect complexes that have been investigated theoretically, there are still a lot more of them waiting to be discovered and investigated. For instance, complexes formed between nitrogen vacancy and nitrogen interstitial in GaN (N-Frenkel pair). Frenkel defects are long believed to exist because of their neutral nature. However, so little is known theoretically about them. Complexes in oxide and nitride alloys (such as Mg_xZn_{1-x}O and Al_xGa_{1-x}N) are also of

fundamental interests. In the past, only simple defects can be studied computationally due to limited computational resources. Because computers are much faster and the codes are much more advanced, realistic problems such as defects in alloys can be studied. These studies would help in better understanding of alloys that are currently used or potentially will be used.

In addition to tetrahedral binary semiconductors, the other oxide and nitride based compounds, such as Zn_3N_2 , TiO_2 , SnO_2 and In_2O_3 that have more complicated crystal structures are currently of interest. This is because of their promising properties for many applications. To utilize them, information on defects in these materials should be available. However, currently the theoretical studies of defects in these materials are limited to native point defects and some dopants. Complexes between dopants and common impurities that are highly possible to form are largely unexplored.

In the future, we are planning to study defect complexes in nitride and oxide alloys as well as III-VI and II-V semiconductors. In addition, we would like to apply advance calculation techniques, such as hybrid functional, to reconfirm existing results of defects in semiconductors and related materials.

REFERENCES

REFERENCES

- Abramowitz, M. and Stegun, I. A. (1965). **Handbook of mathematical functions**. New York: Dover Publications.
- Ager III, J. W. and Walukiewicz, W. (2002). Current status of research and development of III-N-V semiconductor alloys. **Semicond. Sci. Technol.** 17: 741.
- Aliev, G. N., Bingham, S. J., Wolverson, D., Davies, J. J., Makino, H., Ko, H. J. and Yao, T. (2004). Optically detected magnetic resonance of epitaxial nitrogen-doped ZnO. **Phys. Rev. B** 70: 115206.
- Anisimov, V. I. and Gunnarsson, O. (1991). Density-functional calculation of effective Coulomb interactions in metals. **Phys. Rev. B** 43: 7570.
- Ashcroft, N. W. and Mermin, N. D. (1976). **Solid state physics**. Philadelphia: Saunders Company.
- Ashkenazi, J. (1982). New approach to the calculation of ground-state properties in solids. **Phys. Rev. B** 26: 1512.
- Baldassarri, G., Bissiri, M., Polimeni, A., Capizzi, M., Fischer, M., Reinhardt, M. and Forchel, A. (2001). Hydrogen-induced band gap tuning of (InGa)(AsN)/GaAs single quantum wells. **Appl. Phys. Lett.** 78: 3472.
- Baldereschi, A. (1973). Mean-value point in the Brillouin zone. **Phys. Rev. B** 7: 5212.
- Becke, A. (1988). Density-functional exchange-energy approximation with correct asymptotic behavior. **Phys. Rev. A** 38: 3098.
- Blöchl, P. E. (1994). Projector augmented-wave method. **Phys. Rev. B** 50: 17953.

- Bonapasta, A. A., Filippone, F. and Giannozzi, P. (2003). Nitrogen passivation by atomic hydrogen in $\text{GaAs}_y\text{N}_{1-y}$ and $\text{In}_x\text{Ga}_{1-x}\text{As}_y\text{N}_{1-y}$ alloys. **Phys. Rev. B** 68: 115202.
- Born, M. and Oppenheimer, R. (1927). Zur Quantentheorie der Molekeln. **Ann. Phys.** 389: 457.
- Böscher, G., Stolwijk, N. A., Thordson, J. V., Södervall, U. and Andersson, T. G. (1998). Diffusion of nitrogen from a buried doping layer in gallium arsenide revealing the prominent role of As interstitials. **Phys. Rev. Lett.** 81: 3443.
- Buyanova, I. A., Izadifard, M., Chen, W. M., Xin, H. P. and Tu, C. W. (2004). Experimental evidence for N-induced strong coupling of host conduction band states in $\text{GaN}_x\text{P}_{1-x}$: Insight into the dominant mechanism for giant band-gap bowing. **Phys. Rev. B** 69: 201303.
- Ceperley, D. and Alder, B. (1980). Ground state of the electron gas by a stochastic method. **Phys. Rev. Lett.** 45: 566.
- Chadi, D. J. and Cohen, M. L. (1973). Special points in the Brillouin zone. **Phys. Rev. B** 8: 5747.
- Chadi, D. J. and Zhang, S. B. (1990). Vacancy complexes in GaAs: Effects on impurity compensation. **Phys. Rev. B** 41: 5444.
- Chand, N., Henderson, T., Klem, J., Masselink, W. T., Fischer, R., Chang, Y.-C. and Morkoç, H. (1984). Comprehensive analysis of Si-doped $\text{Al}_x\text{Ga}_{1-x}\text{As}$ ($x=0$ to 1): Theory and experiments. **Phys. Rev. B** 30: 4481.
- Chen, Z. Q., Betsuyaku, K. and Kawasuso, A. (2008). Vacancy defects in electron-irradiated ZnO studied by Doppler broadening of annihilation radiation. **Phys. Rev. B** 77: 113204.

- Cheong, B.-H. and Chang, K. J. (1994). Compensation and diffusion mechanisms of carbon dopants in GaAs. **Phys. Rev. B** 49: 17436.
- Ciatto, G., Boscherini, F., Bonapasta, A. A., Filippone, F., Polimeni, A. and Capizzi, M. (2005). Nitrogen-hydrogen complex in $\text{GaAs}_x\text{N}_{1-x}$ revealed by x-ray absorption spectroscopy. **Phys. Rev. B** 71: 201301.
- Coşkun, C., Look, D. C., Farlow, G. C. and Sizelove, J. R. (2004). Radiation hardness of ZnO at low temperatures. **Semicond. Sci. Technol.** 19: 752.
- Cox, S. F. J., Davis, E. A., Cottrell, S. P., King, P. J. C., Lord, J. S., Gil, J. M., Alberto, H. V., Vilão, R. C., Piroto Duarte, J., Ayres de Campos, N., Weidinger, A., Lichti, R. L. and Irvine, S. J. C. (2001). Experimental confirmation of the predicted shallow donor hydrogen state in zinc oxide. **Phys. Rev. Lett.** 86: 2601.
- Dean, J. A. (1992). **Lange's handbook of chemistry (14th ed.)**. New York: McGraw-Hill.
- Dederichs, P. H. and Pollmann, J. (1972). Elastic displacement field of point defects in anisotropic cubic crystals. **Z. Physik** 255: 315.
- Dirac, P. (1930). Note on exchange phenomena in the Thomas atom. **Proceedings Cambridge** 26: 376.
- Du, M.-H., Limpijumnong, S. and Zhang, S. B. (2005). Hydrogen pairs and local vibrational frequencies in H-irradiated $\text{GaAs}_{1-y}\text{N}_y$. **Phys. Rev. B** 72: 073202.
- Du, M.-H., Limpijumnong, S. and Zhang, S. B. (2006). Hydrogen-mediated nitrogen clustering in dilute III-V nitrides. **Phys. Rev. Lett.** 97: 075503.

- Fermi, E. (1928). A statistical method for the determination of some atomic properties and the application of this method to the theory of the periodic system of elements. **Z. Physik** 48: 32.
- Fernandez, J. R. L., Cerdeira, F., Meneses, E. A., Brasil, M. J. S. P., Soares, J. A. N. T., Santos, A. M., Noriega, O. C., Leite, J. R., As, D. J., Köhler, U., Potthast, S. and Pacheco-Salazar, D. G. (2003). Optical and x-ray diffraction studies on the incorporation of carbon as a dopant in cubic GaN. **Phys. Rev. B** 68: 155204.
- Feynman, R. P. (1939). Forces in molecules. **Phys. Rev.** 56: 340.
- Fons, P., Tampo, H., Kolobov, A. V., Ohkubo, M., Niki, S., Tominaga, J., Carboni, R., Boscherini, F. and Friedrich, S. (2006). Direct observation of nitrogen location in molecular beam epitaxy grown nitrogen-doped ZnO. **Phys. Rev. Lett.** 96: 045504.
- Fons, P., Tampo, H., Kolobov, A. V., Ohkubo, M., Niki, S., Tominaga, J., Carboni, R. and Friedrich, S. (2007). Direct observation of nitrogen location in molecular beam epitaxy grown nitrogen-doped ZnO. **AIP Conf. Proc.** 882: 381.
- Gorelkinskii, Y. V. and Watkins, G. D. (2004). Defects produced in ZnO by 2.5-MeV electron irradiation at 4.2 K: Study by optical detection of electron paramagnetic resonance. **Phys. Rev. B** 69: 115212.
- Greco, D. and Dederichs, P. H. (1971). The asymptotic behaviour of the displacement field of point defects in isotropic' crystals. **Phys. Lett. A** 36: 135
- Hamann, D. R., Schlüter, M. and Chiang, C. (1979). Norm-conserving pseudopotentials. **Phys. Rev. Lett.** 43: 1494.

- Hartree, D. R. (1928) The wave mechanics of an atom with a non-Coulomb central field. Part I. Theory and methods **Proc. Camb. Phil. Soc.** 24: 89.
- Hellmann, H. (1937). Einführung in die Quantenchemie. Leipzig: Deuticke.
- Herring, C. (1940). A new method for calculating wave functions in crystals. **Phys. Rev.** 57: 1169.
- Herzberg, G. (1966). **Molecular spectra and molecular structure: Electronic spectra and electronic structure of polyatomic molecules.** New York: Van Nostrand.
- Hofmann, D. M., Hofstaetter, A., Leiter, F., Zhou, H., Henecker, F., Meyer, B. K., Orlinskii, S. B., Schmidt, J. and Baranov, P. G. (2002). Hydrogen: A relevant shallow donor in zinc oxide. **Phys. Rev. Lett.** 88: 045504.
- Hohenberg, P. and Kohn, W. (1964). Inhomogeneous electron gas. **Phys. Rev.** 136: 864.
- Hong, Y. G., Nishikawa, A. and Tu, C. W. (2003). Effect of nitrogen on the optical and transport properties of $\text{Ga}_{0.48}\text{In}_{0.52}\text{N}_y\text{P}_{1-y}$ grown on GaAs (001) substrates. **Appl. Phys. Lett.** 83: 5446.
- Hubbard, J. (1965). Electron correlations in narrow energy bands. IV. The atomic representation. **Proc. Roy. Soc. A** 285: 542.
- Ip, K., Overberg, M. E., Heo, Y. W., Norton, D. P., Pearton, S. J., Stutz, C. E., Luo, B., Ren, F., Look, D. C. and Zavada, J. M. (2003). Hydrogen incorporation and diffusivity in plasma-exposed bulk ZnO. **Appl. Phys. Lett.** 82: 385.
- Janotti, A., Reunchan, P., Limpijumnong, S. and Van de Walle, C. G. (2008). Mutual passivation of electrically active and isovalent impurities in dilute nitrides. **Phys. Rev. Lett.** 100: 045505.

- Janotti, A., Segev, D. and Van de Walle, C. G. (2006). Effects of cation d states on the structural and electronic properties of III-nitride and II-oxide wide-band-gap semiconductors. **Phys. Rev. B** 74: 045202.
- Janotti, A. and Van de Walle, C. G. (2005). Oxygen vacancies in ZnO. **Appl. Phys. Lett.** 87: 122102.
- Janotti, A. and Van de Walle, C. G. (2007a). Hydrogen multicentre bonds. **Nat Mater** 6: 44.
- Janotti, A. and Van de Walle, C. G. (2007b). Native point defects in ZnO. **Phys. Rev. B** 76: 165202.
- Janotti, A., Wei, S.-H., Zhang, S. B., Kurtz, S. and Van de Walle, C. G. (2003). Interactions between nitrogen, hydrogen, and gallium vacancies in $\text{GaAs}_{1-x}\text{N}_x$ alloys. **Phys. Rev. B** 67: 161201.
- Janotti, A., Zhang, S. B. and Wei, S.-H. (2002a). Hydrogen vibration modes in GaP:N: the pivotal role of nitrogen in stabilizing the H_2^* complex. **Phys. Rev. Lett.** 88: 125506.
- Janotti, A., Zhang, S. B., Wei, S.-H. and Van de Walle, C. G. (2002b). Effects of hydrogen on the electronic properties of dilute GaAsN alloys. **Phys. Rev. Lett.** 89: 086403.
- Jónsson, H., Mills, G. and Jacobsen, K. W. (1998). **Classical and quantum dynamics in condensed phase simulations**. Singapore: World Scientific.
- Kent, P. R. C. and Zunger, A. (2001). Theory of electronic structure evolution in GaAsN and GaPN alloys. **Phys. Rev. B** 64: 115208.
- Kim, K. and King, W. T. (1979). Integrated intensities in hydrogen cyanide. **J. Chem. Phys.** 71: 1967.

- Kim, K. and Zunger, A. (2001). Spatial correlations in GaInAsN alloys and their effects on band-Gap enhancement and electron localization. **Phys. Rev. Lett.** 86: 2609.
- Kim, Y.-S. and Park, C. H. (2009). Rich variety of defects in ZnO via an attractive interaction between O vacancies and Zn interstitials: origin of *n*-type doping. **Phys. Rev. Lett.** 102: 086403.
- Kohan, A. F., Ceder, G., Morgan, D. and Van de Walle, C. G. (2000). First-principles study of native point defects in ZnO. **Phys. Rev. B** 61: 15019.
- Kohn, W. and Sham, L. (1965). Self-consistent equations including exchange and correlation effects. **Phys. Rev.** 140: A1133.
- Kresse, G. and Furthmüller, J. (1996a). Efficiency of *ab-initio* total energy calculations for metals and semiconductors using a plane-wave basis set. **Comput. Mater. Sci.** 6: 15.
- Kresse, G. and Furthmüller, J. (1996b). Efficient iterative schemes for *ab initio* total-energy calculations using a plane-wave basis set. **Phys. Rev. B** 54: 11169.
- Kresse, G. and Joubert, D. (1999). From ultrasoft pseudopotentials to the projector augmented-wave method. **Phys. Rev. B** 59: 1758.
- Kröger, F. A. (1964). **The chemistry of imperfect crystals**. Amsterdam: North-Holland.
- Langreth, D. C. and Mehl, M. J. (1983). Beyond the local-density approximation in calculations of ground-state electronic properties. **Phys. Rev. B** 28: 1809.
- Lee, C., Yang, W. and Parr, R. G. (1988). Development of the Colle-Salvetti correlation-energy formula into a functional of the electron density. **Phys. Rev. B** 37: 785.

- Lee, E.-C., Kim, Y. S., Jin, Y. G. and Chang, K. J. (2001). Compensation mechanism for N acceptors in ZnO. **Phys. Rev. B** 64: 085120.
- Li, J., Carrier, P., Wei, S. H., Li, S. S. and Xia, J. B. (2006). Mutual passivation of donors and isovalent nitrogen in GaAs. **Phys. Rev. Lett.** 96: 035505.
- Li, X., Keyes, B., Asher, S., Zhang, S. B., Wei, S. H., Coutts, T. J., Limpijumnong, S. and Van de Walle, C. G. (2005). Hydrogen passivation effect in nitrogen-doped ZnO thin films. **Appl. Phys. Lett.** 86: 122107.
- Liechtenstein, A. I., Anisimov, V. I. and Zaanen, J. (1995). Density-functional theory and strong interactions: Orbital ordering in Mott-Hubbard insulators. **Phys. Rev. B** 52: R5467.
- Limpijumnong, S., Li, X. N., Wei, S. H. and Zhang, S. B. (2005). Substitutional diatomic molecules NO, NC, CO, N₂, and O₂: Their vibrational frequencies and effects on *p* doping of ZnO. **Appl. Phys. Lett.** 86: 211910.
- Limpijumnong, S., Northrup, J. E. and Van de Walle, C. G. (2003). Identification of hydrogen configurations in *p*-type GaN through first-principles calculations of vibrational frequencies. **Phys. Rev. B** 68: 075206.
- Limpijumnong, S., Reunchan, P., Janotti, A. and Van de Walle, C. G. (2008). Carbon-nitrogen molecules in GaAs and GaP. **Phys. Rev. B** 77: 195209.
- Limpijumnong, S., Zhang, S. B., Wei, S. H. and Park, C. H. (2004). Doping by large-size-mismatched impurities: the microscopic origin of arsenic- or antimony-doped *p*-type zinc oxide. **Phys. Rev. Lett.** 92: 155504.
- Linde, M., Uftring, S. J., Watkins, G. D., Härle, V. and Scholz, F. (1997). Optical detection of magnetic resonance in electron-irradiated GaN. **Phys. Rev. B** 55: R10177.

- Look, D. C. (2001). Recent advances in ZnO materials and devices. **Mat. Sci. Eng. B** 80: 383.
- Look, D. C., Farlow, G. C., Reunchan, P., Limpijumnong, S., Zhang, S. B. and Nordlund, K. (2005). Evidence for native-defect donors in *n*-type ZnO. **Phys. Rev. Lett.** 95: 225502.
- Look, D. C., Hemsky, J. W. and Sizelove, J. R. (1999a). Residual native shallow donor in ZnO. **Phys. Rev. Lett.** 82: 2552.
- Look, D. C., Renlund, G. M., Burgener II, R. H. and Sizelove, J. R. (2004). As-doped *p*-type ZnO produced by an evaporation/sputtering process. **Appl. Phys. Lett.** 85: 5269.
- Look, D. C., Reynolds, D. C., Hemsky, J. W., Jones, R. L. and Sizelove, J. R. (1999b). Production and annealing of electron irradiation damage in ZnO. **Appl. Phys. Lett.** 75: 811.
- Look, D. C., Reynolds, D. C., Hemsky, J. W., Sizelove, J. R., Jones, R. L. and Molnar, R. J. (1997). Defect donor and acceptor in GaN. **Phys. Rev. Lett.** 79: 2273.
- Look, D. C., Reynolds, D. C., Litton, C. W., Jones, R. L., Eason, D. B. and Cantwell, G. (2002). Characterization of homoepitaxial *p*-type ZnO grown by molecular beam epitaxy. **Appl. Phys. Lett.** 81: 1830.
- Look, D. C., Reynolds, D. C., Sizelove, J. R., Jones, R. L., Litton, C. W., Cantwell, G. and Harsch, W. C. (1998). Electrical properties of bulk ZnO. **Solid State Commun.** 105: 399.
- Madelung, O. (1996). **Semiconductors-basic data**. Berlin: Springer.

- Makov, G. and Payne, M. C. (1995). Periodic boundary conditions in *ab initio* calculations. **Phys. Rev. B** 51: 4014.
- Miehlich, B., Savin, A., Stoll, H. and Preuss, H. (1989). Results obtained with the correlation energy density functionals of Becke and Lee, Yang and Parr. **Chem. Phys. Lett.** 157: 200.
- Monkhorst, H. J. and Pack, J. D. (1976). Special points for Brillouin-zone integrations. **Phys. Rev. B** 13: 5188.
- Morkoc, H., Strite, S., Gao, G., Lin, M., Sverdlov, B. and Burns, M. (1994). Large-band-gap SiC, III-V nitride, and II-VI ZnSe-based semiconductor device technologies. **J. Appl. Phys.** 76: 1363.
- Neugebauer, J. and Van de Walle, C. G. (1995). Electronic structure and phase stability of GaAs_{1-x}N_x alloys. **Phys. Rev. B** 51: 10568.
- Neugebauer, J. and Van de Walle, C. G. (1996). Gallium vacancies and the yellow luminescence in GaN. **Appl. Phys. Lett.** 69: 503.
- Nickel, N. H. and Fleischer, K. (2003). Hydrogen local vibrational modes in zinc oxide. **Phys. Rev. Lett.** 90: 197402.
- Oba, F., Nishitani, S., Isotani, S., Adachi, H. and Tanaka, I. (2001). Energetics of native defects in ZnO. **J. Appl. Phys.** 90: 824.
- Ogino, T. and Aoki, M. (1980). Mechanism of yellow luminescence in GaN. **Jpn. J. Appl. Phys.** 19: 2395.
- Ohashi, N., Ishigaki, T., Okada, N., Taguchi, H., Sakaguchi, I., Hishita, S., Sekiguchi, T. and Haneda, H. (2003). Passivation of active recombination centers in ZnO by hydrogen doping. **J. Appl. Phys.** 93: 6386.

- Pearnton, S., Norton, D., Ip, K., Heo, Y. and Steiner, T. (2005). Recent progress in processing and properties of ZnO. **Pro. Mat. Sci.** 50: 293.
- Perdew, J. P. (1991). **Electronic structure of solids '91**. Berlin: Akademie Verlag.
- Perdew, J. P., Burke, K. and Ernzerhof, M. (1996). Generalized gradient approximation made simple. **Phys. Rev. Lett.** 77: 3865.
- Perdew, J. P. and Zunger, A. (1981). Self-interaction correction to density-functional approximations for many-electron systems. **Phys. Rev. B** 23: 5048.
- Perkins, C. L., Lee, S.-H., Li, X., Asher, S. E. and Coutts, T. J. (2005). Identification of nitrogen chemical states in N-doped ZnO via x-ray photoelectron spectroscopy. **J. Appl. Phys.** 97: 034907.
- Pettinari, G., Masia, F., Polimeni, A., Felici, M., Frova, A., Capizzi, M., Lindsay, A., O'Reilly, E. P., Klar, P. J., Stolz, W., Bais, G., Piccin, M., Rubini, S., Martelli, F. and Franciosi, A. (2006). Influence of nitrogen-cluster states on the gyromagnetic factor of electrons in $\text{GaAs}_{1-x}\text{N}_x$. **Phys. Rev. B** 74: 245202.
- Pettinari, G., Polimeni, A., Masia, F., Trotta, R., Felici, M., Capizzi, M., Niebling, T., Stolz, W. and Klar, P. J. (2007). Electron mass in dilute nitrides and its anomalous dependence on hydrostatic pressure. **Phys. Rev. Lett.** 98: 146402.
- Phillips, J. C. and Kleinman, L. (1959). New method for calculating wave functions in crystals and molecules. **Phys. Rev.** 116: 287.
- Polimeni, A., Baldassarri, G., Bissiri, H. M., Capizzi, M., Fischer, M., Reinhardt, M. and Forchel, A. (2001). Effect of hydrogen on the electronic properties of $\text{In}_x\text{Ga}_{1-x}\text{As}_{1-y}\text{N}_y/\text{GaAs}$ quantum wells. **Phys. Rev. B** 63: 201304.
- Segev, D. and Wei, S.-H. (2003). Design of shallow donor levels in diamond by isovalent-donor coupling. **Phys. Rev. Lett.** 91: 126406.

- Shan, W., Walukiewicz, W., Ager, J. W., Haller, E. E., Geisz, J. F., Friedman, D. J., Olson, J. M. and Kurtz, S. R. (1999). Band anticrossing in GaInNAs alloys. **Phys. Rev. Lett.** 82: 1221.
- Shimomura, K., Nishiyama, K. and Kadono, R. (2002). Electronic structure of the muonium center as a shallow donor in ZnO. **Phys. Rev. Lett.** 89: 255505.
- Singh, D. J. and Nordstrom, L. (2006). **Planewaves, pseudopotentials, and the LAPW method.** New York: Springer.
- Skowronski, M. (1992). Complexes of oxygen and native defects in GaAs. **Phys. Rev. B** 46: 9476.
- Songprakob, W., Zallen, R., Liu, W. K. and Bacher, K. L. (2000). Infrared studies of hole-plasmon excitations in heavily-doped *p*-type MBE-grown GaAs:C. **Phys. Rev. B** 62: 4501.
- Strzhemechny, Y. M., Mosbacker, H. L., Look, D. C., Reynolds, D. C., Litton, C. W., Garces, N. Y., Giles, N. C., Halliburton, L. E., Niki, S. and Brillson, L. J. (2004). Remote hydrogen plasma doping of single crystal ZnO. **Appl. Phys. Lett.** 84: 2545.
- Tan, K. H., Yoon, S. F., Huang, Q. F., Zhang, R., Sun, Z. Z., Jiang, J., Feng, W. and Lee, L. H. (2003). Dicarbon defects in carbon-doped GaAs. **Phys. Rev. B** 67: 035208.
- Tarsa, E. J., Heying, B., Wu, X. H., Fini, P., DenBaars, S. P. and Speck, J. S. (1997). Homoepitaxial growth of GaN under Ga-stable and N-stable conditions by plasma-assisted molecular beam epitaxy. **J. Appl. Phys.** 82: 5472.

- Teweldeberhan, A. M. and Fahy, S. (2005). Calculated pressure dependence of the localized vibrational mode of nitrogen in $\text{GaN}_x\text{As}_{1-x}$. **Phys. Rev. B** 72: 195203.
- Thinh, N. Q., Vorona, I. P., Buyanova, I. A., Chen, W. M., Limpijumnong, S., Zhang, S. B., Hong, Y. G., Tu, C. W., Utsumi, A., Furukawa, Y., Moon, S., Wakahara, A. and Yonezu, H. (2004). Identification of Ga-interstitial defects in $\text{GaN}_y\text{P}_{1-y}$ and $\text{Al}_x\text{Ga}_{1-x}\text{N}_y\text{P}_{1-y}$. **Phys. Rev. B** 70: 121201.
- Thomas, L. H. (1927) The calculation of atomic fields **Proc. Camb. Phil. Soc.** 23: 542.
- Troxell, J. R. and Watkins, G. D. (1980). Interstitial boron in silicon: A negative- U system. **Phys. Rev. B** 22: 921.
- Ulrici, W. and Clerjaud, B. (2005). A carbon-nitrogen complex in gallium phosphide. **Phys. Rev. B** 72: 045203.
- Van de Walle, C. G. (2000). Hydrogen as a cause of doping in zinc oxide. **Phys. Rev. Lett.** 85: 1012.
- Van de Walle, C. G., Limpijumnong, S. and Neugebauer, J. (2001). First-principles studies of beryllium doping of GaN. **Phys. Rev. B** 63: 245205.
- Van de Walle, C. G. and Neugebauer, J. (2004). First-principles calculations for defects and impurities: Applications to III-nitrides. **J. Appl. Phys.** 95: 3851.
- Vanderbilt, D. (1990). Soft self-consistent pseudopotentials in a generalized eigenvalue formalism. **Phys. Rev. B** 41: 7892.
- Wagner, P. and Helbig, R. (1974). Hall effect and anisotropy of the mobility of the electrons in zinc oxide. **J. Phys. Chem. Solids** 35: 327.

- Wahl, U., Rita, E., Correia, J. G., Marques, A. C., Alves, E. and Soares, J. C. (2005). Direct evidence for As as a Zn-site impurity in ZnO. **Phys. Rev. Lett.** 95: 215503.
- Wardle, M. G., Goss, J. P. and Briddon, P. R. (2005). Theory of Li in ZnO: A limitation for Li-based *p*-type doping. **Phys. Rev. B** 71: 155205.
- Wei, S. H. and Zunger, A. (1996). Giant and composition-dependent optical bowing coefficient in GaAsN alloys. **Phys. Rev. Lett.** 76: 664.
- Welser, R. E., Setzko, R. S., Stevens, K. S., Rehder, E. M., Lutz, C. R., Hill, D. S. and Zampardi, P. J. (2004). Minority carrier properties of carbon-doped GaInAsN bipolar transistors. **J. Phys. Condens. Matter** 16: 3373.
- Weyers, M., Sato, M. and Ando, H. (1992). Red shift of photoluminescence and absorption in dilute GaAsN alloy layers. **Jpn. J. Appl. Phys.** 31: L853.
- Wigner, P. E. (1938). Effects of the electron interaction on the energy levels of electrons in metals. **Trans. Faraday Soc.** 34: 678.
- Wooley, J. C. (1962). **Compound semiconductors**. New York: Reinhold.
- Wu, J., Yu, K. M., Walukiewicz, W., He, G., Haller, E. E., Mars, D. E. and Chamberlin, D. R. (2003). Mutual passivation effects in Si-doped diluted $\text{In}_y\text{Ga}_{1-y}\text{As}_{1-x}\text{N}_x$ alloys. **Phys. Rev. B** 68: 195202.
- Yu, K. M., Walukiewicz, W., Wu, J., Mars, D. E., Chamberlin, D. R., Scarpulla, M. A., Dubon, O. D. and Geisz, J. F. (2002). Mutual passivation of electrically active and isovalent impurities. **Nat. Mater.** 1: 185.
- Yu, K. M., Walukiewicz, W., Wu, J., Shan, W., Beeman, J. W., Scarpulla, M. A., Dubon, O. D., Ridgway, M. C., Mars, D. E. and Chamberlin, D. R. (2003).

Mutual passivation of group IV donors and nitrogen in diluted $\text{GaN}_x\text{As}_{1-x}$ alloys. **Appl. Phys. Lett.** 83: 2844.

Zhang, S. B. and Northrup, J. E. (1991). Chemical potential dependence of defect formation energies in GaAs: Application to Ga self-diffusion. **Phys. Rev. Lett.** 67: 2339.

Zhang, S. B., Wei, S. H. and Zunger, A. (2001). Intrinsic *n*-type versus *p*-type doping asymmetry and the defect physics of ZnO. **Phys. Rev. B** 63: 075205.

APPENDIX

APPENDIX

PUBLICATIONS AND PRESENTATIONS

1. List of publications

Look, D. C., Farlow, G. C., Reunchan, P., Limpijumnong, S., Zhang, S. B. and Nordlund, K. (2005). Evidence for native-defect donors in *n*-type ZnO. **Phys. Rev. Lett.** 95: 225502.

Janotti, A., Reunchan, P., Limpijumnong, S. and Van de Walle, C. G. (2008). Mutual passivation of electrically active and isovalent impurities in dilute nitrides. **Phys. Rev. Lett.** 100: 045505.

Limpijumnong, S., Reunchan, P., Janotti, A. and Van de Walle, C. G. (2008). Carbon-nitrogen molecules in GaAs and GaP. **Phys. Rev. B** 77: 195209.

2. List of presentations (oral)

Reunchan, P. and Limpijumnong, S. (June 2006). Carbon-nitrogen molecules in GaAs: the first-principles study. In **The First National Symposium on Physics Graduate Research**. Chaiya Phum: Suranaree University of Technology.

Reunchan, P., Janotti, A., Limpijumnong, S. and Van de Walle, C. G. (March 2008). Mutual passivation of electrically active and isovalent impurities in GaAsN alloys. In **Siam Physics Congress 2008**. Nakhon Ratchasima: Thai Physics Society.

Reunchan, P., Limpijumnong, S., Janotti, A. and Van de Walle, C. G. (April 2008). A carbon-nitrogen molecule in GaAs: a first principles study. In **RGJ-Ph.D. Congress IX**. Chon Buri: The Thailand Research Fund.

Reunchan, P., Limpijumnong, S., Janotti, A. and Van de Walle, C. G. (October 2008). Carbon-nitrogen molecule in gallium arsenide. In **34th Congress on Science and Technology of Thailand**. Bangkok: The Science Society of Thailand.

Reunchan, P. and Limpijumnong, S. (June 2009). Diatomic molecules in dilute nitrides: a first-principles study. In **Junior Research Group seminar 2009**. Pohang, South Korea: Asia Pacific Center for Theoretical Physics.

Reunchan, P. and Limpijumnong, S. (June 2009). First principles study of gallium-Frenkel pairs in gallium nitride. In **International Conference on Materials for Advanced Technologies 2009**. Singapore: Materials Research Society Singapore.

3. List of presentations (poster)

Reunchan, P. and Limpijumnong, S., Janotti, A. and Van de Walle, C. G. (March 2009). Vacancy defects in indium oxide. In **Siam Physics Congress 2009**. Petcha Buri: Thai Physics Society.

Evidence for Native-Defect Donors in *n*-Type ZnOD. C. Look,^{1,2} G. C. Farlow,¹ Pakpoom Reunchan,³ Sukit Limpijumnong,^{3,4} S. B. Zhang,⁴ and K. Nordlund⁵¹Semiconductor Research Center, Wright State University, Dayton, Ohio 45435, USA²Materials and Manufacturing Directorate, Air Force Research Laboratory, Wright-Patterson Air Force Base, Ohio 45433, USA³School of Physics, Suranaree University of Technology and National Synchrotron Research Center, Nakhon Ratchasima, Thailand⁴National Renewal Energy Laboratory, Golden, Colorado 80401, USA⁵Accelerator Laboratory, University of Helsinki, FIN-00014, Helsinki, Finland

(Received 5 August 2005; published 21 November 2005)

Recent theory has found that native defects such as the O vacancy V_O and Zn interstitial Zn_i have high formation energies in *n*-type ZnO and, thus, are not important donors, especially in comparison to impurities such as H. In contrast, we use both theory and experiment to show that, under N ambient, the complex Zn_i-N_O is a stronger candidate than H or any other known impurity for a 30 meV donor commonly found in bulk ZnO grown from the vapor phase. Since the Zn vacancy is also the dominant acceptor in such material, we must conclude that native defects are important donors and acceptors in ZnO.

DOI: 10.1103/PhysRevLett.95.225502

PACS numbers: 61.72.Ji, 71.55.Gs, 72.20.Fr, 78.55.Et

Semiconducting ZnO has generated great interest in the past decade because of advances in bulk and epitaxial growth that have opened the door for new photonic and electronic applications, such as UV light emitting diodes and transparent transistors [1,2]. Previous research had established that ZnO was always *n*-type and that the dominant donors were usually shallow with activation energies of between 30 and 60 meV [3,4]. Because it was also known that the crystal growth was typically Zn-rich, the dominant donor was almost always identified as either the O vacancy V_O or the Zn interstitial Zn_i [5,6]. This model was strongly challenged in the year 2000 when Kohan *et al.* showed theoretically that both V_O and Zn_i have high formation energies in *n*-type ZnO and that, furthermore, both are deep, not shallow, donors [7]. More recent theory has concluded that Zn_i is actually a shallow donor, rather than deep [8,9], as has also been suggested by electron-irradiation experiments [6]; however, its high formation energy would still limit its participation in the conductivity of *n*-type material. Also in the year 2000, the defect-donor model was further challenged by Van de Walle's theoretical result that H is always a donor in ZnO, that it is easily ionized, and that it has a low enough formation energy to be abundant; thus, Van de Walle suggested that it was likely to be a dominant background donor in ZnO materials that were exposed to H during growth [10]. This proposal has been amenable to testing, because H-containing, high-quality, bulk ZnO, grown by a seeded chemical vapor transport (SCVT) technology, has been commercially available for the past few years. For the most part, these tests have confirmed that a shallow donor due to H exists in SCVT ZnO and can contribute significantly to the conductivity [11–16]. This fact, coupled with the theoretical evidence of high formation energies for the native donors [7], has led to a prevailing opinion that native donors do not play a significant role in the conductivity of as-grown ZnO. In contrast, we will offer evidence here that native donors

can contribute significantly to conduction in ZnO but as complexes, rather than isolated elements.

The main sample used in this study was a $5\text{ mm} \times 5\text{ mm} \times 0.42\text{ mm}$ piece cut from a wafer grown by the SCVT technique at ZN Technology, Inc. [17]. Material of this type is of very high quality, with peak electron mobility $>2000\text{ cm}^2/\text{Vs}$, 300 K carrier concentration in the 10^{16} cm^{-3} range, and photoluminescence (PL) linewidths under 0.5 meV, as shown in Figs. 1 and 2 [4]. The sample was first annealed at 715°C , in order to release most of the H [14,15], then was irradiated with high-energy electrons to create point defects, and finally was annealed again at temperatures from $200\text{--}500^\circ\text{C}$, in order to investigate the annihilation of the point defects. As seen in Fig. 1, several sharp PL lines appear in the region $3.357\text{--}3.365\text{ eV}$, and these spectral features are usually assigned to transitions of excitons bound to neutral donors (D^0X transitions), in which the donor remains in its ground state ($n=1$) during the transition. Some of these lines have been tentatively identified; for example, the lines at 3.35964 eV (I_8 or I_{8a} in

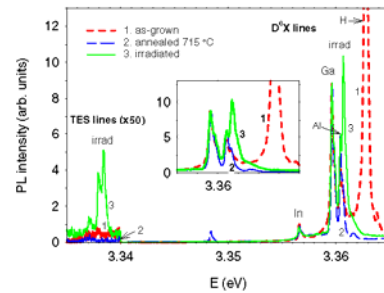


FIG. 1 (color online). 4-K photoluminescence spectra for ZnO sample. The inset shows the D^0X lines in greater detail.

the literature) and 3.36042 eV (I_6 or I_{6a}) have been assigned to Ga_{Zn} and Al_{Gn} , respectively. (See Ref. [18] for an excellent review of PL in ZnO.) All of the spectra presented in this work are normalized to the I_8 line, because it is relatively isolated and also not expected to change significantly as a result of annealing or irradiation treatments. However, the most dominant PL line in this particular sample before annealing is the D^0X line at 3.36270 eV (I_4), now almost universally assigned to interstitial H [16,18]. This identification results at least partially from annealing experiments, because I_4 disappears for anneals above 600 °C, in good correlation with the effusion of H from the sample [14–16,19]. Our sample behaves in the same way, as evidenced by the strong reduction of I_4 after an anneal of 715 °C (curve 2 in Fig. 1). Not shown in Fig. 1 is a two-electron satellite (TES) replica of I_4 , appearing at 3.32961 eV. A TES transition is one in which the donor is left in an excited $n = 2$ state after the collapse of the exciton. If the donor associated with I_4 follows a hydrogenic model, then the ground-state ($n = 1$) energy of this donor should be given by $4/3(3.36270 - 3.32961) = 44.1$ meV. Other TES transitions, also not shown, are seen near 3.32 eV and may be associated with I_6 and I_8 [18]. If so, then the hydrogenic model would predict - ground-state energies of 53–55 meV for these donors, presumably associated with Ga_{Zn} and Al_{Zn} . Thus, the donors identified from PL are H, at 44 meV, and Ga_{Zn} and Al_{Zn} , at about 55 meV.

To create point defects, we have used the Van de Graaff electron accelerator at Wright State University. The sample was irradiated on the Zn face (0001) with 1 MeV electrons three separate times, making a total fluence of $3 \times 10^{17} \text{ cm}^{-2}$. The PL spectrum after the third irradiation is presented as curve 3 in Fig. 1. A new sharp defect line at 3.36070 eV, which we will designate as I_D , is generated by the irradiation. Concomitantly, a triplet feature, comprised of energies 3.33711, 3.33793, and 3.33840 eV, is also generated. These we will designate $I_{D,\text{TES}1}$, $I_{D,\text{TES}2}$, and $I_{D,\text{TES}3}$. This triplet has an intensity about 100 times less than that of I_D , and this reduction is about the same as that observed for the TES line of H compared with its parent line, I_4 . Thus, the defect triplet at 3.338 eV clearly is related to I_D , and, if the hydrogenic model holds, the associated energy is $4/3(3.3607 - 3.3379) \approx 30.4$ meV. This value is less than that predicted from an empirical version of Haynes' rule presented in Ref. [18]. However, that version was developed for simple, isolated impurities, Al, Ga, In, and H, and there is no reason to expect that it should hold for a defect-related complex. Both I_D and its TES triplet are greatly reduced for anneals greater than 500 °C (not shown), evidently due to defect recombination. It is important to note at this point that the as-grown sample, represented by curve 1 in Fig. 1, has two small lines at the energies of $I_{D,\text{TES}1}$ and $I_{D,\text{TES}2}$, respectively, and possibly also a line in the I_D region, although obscured by I_6 . This is our first indication that the as-grown sample contains defect-related donors.

We next discuss the temperature-dependent mobility μ and carrier concentration n , shown in Fig. 2. To avoid clutter, we show curves representing only four stages in the evolution of this sample: (1) as-grown; (2) annealed at 715 °C for 1/2 hour in flowing N_2 gas; (3) irradiated with 1 MeV electrons, in three equal stages up to a total fluence of $3 \times 10^{17} \text{ cm}^{-2}$; and (4) annealed at 400 °C, following previous anneals beginning at 200 °C. It should be noted that a final anneal at 500 °C (not shown) eliminated almost all of the irradiation damage and basically returned the μ and n curves to those of stage 2. [Note that a return to the μ and n curves of stage 1 (as-grown) is of course impossible, because the H content was lost in stage 2, the first 715 °C anneal.]

The mobility data (inset in Fig. 2) were fitted to an accurate charge-carrier scattering theory, described elsewhere [20], and the only fitting parameter was the acceptor concentration N_A . The carrier concentration data of Fig. 2 were then fitted to the charge-balance equation:

$$n + N_A = \sum_i \frac{N_{Di}}{1 + n/\phi_{Di}}, \quad (1)$$

where the subscript i denotes a particular donor and where ϕ_{Di} is a function of T and E_{Di} , the donor energy [cf. Eq. (8) of Ref. [20]]. The fitting parameters in Eq. (1) are the donor concentrations (N_{Di} 's), donor energies (E_{Di} 's), and acceptor concentration N_A . Excellent fits to the n vs $1/T$ data in Fig. 2 were obtained by also including a degenerate surface layer in the analysis [20,21].

The PL results discussed above determined the energies of three different donors, calculated from their respective TES lines: 55 meV, possibly associated with Ga_{Zn} and/or Al_{Zn} ; 44 meV, associated with H; and 30 meV, produced by irradiation and thus associated with a defect. Indeed, the 30 and 44 meV energies turn out to be good fitting parameters for two of the three donors required to fit our Hall-effect data, but the third donor is best fitted with about 75 meV, rather than 55 meV. The carrier concentration fits are

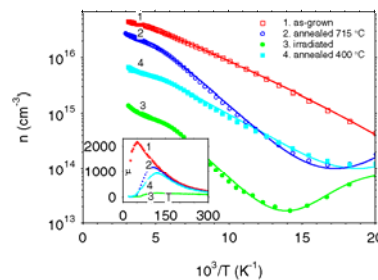


FIG. 2 (color online). Temperature-dependent carrier concentration for ZnO sample. The solid lines are theoretical fits. The inset shows the experimental mobility curves after the same four treatments.

shown as solid lines in Fig. 2, and the fitting parameters are given in Table I. Two major conclusions are evident from the results: (1) the 44 meV H level essentially disappears during the 715 °C anneal, in agreement with the PL data; and (2) a 30 meV level is produced by irradiation but also exists in the as-grown sample and the sample annealed at 715 °C. It should be emphasized that the choice of 30 meV as a Hall fitting parameter is not dependent on the fact that the PL analysis also found a donor at 30 meV. Indeed, a donor of this energy has been found previously by a number of groups to give good fits to ZnO Hall-effect data [3,4,6]. To help identify this 30 meV donor, we appeal to theory.

First of all, we calculate the expected 1 MeV-electron-bombardment production rates of Zn and O Frenkel pairs from molecular dynamics simulations [22]. The threshold energies were calculated by giving a randomly chosen O or Zn atom a recoil energy in a random direction in an experimentally controlled angular window of 15 degrees around the desired (0001) direction. The interatomic interaction model for the ZnO system will be published elsewhere [23], but the potential development principles are described in Ref. [24]. To account for the experimental situation with a beam acceptance angle, the threshold was determined as the average over the direction-specific thresholds obtained within the 15° angular window.

For Zn-face (0001) irradiation at 300 K, the threshold for O displacement is 44 eV, and that for Zn displacement, 34 eV. We then apply the McKinley-Feshbach relativistic cross-section formula [25] to give effective production rates of 0.18 cm⁻¹ for O displacement and 0.30 cm⁻¹ for Zn displacement. Thus, we would expect that our fluence of 3×10^{17} cm⁻² would produce O_i and V_O concentrations of about 5×10^{16} cm⁻³ and Zn_i and V_{Zn} concentrations of about 9×10^{16} cm⁻³. Either of these numbers is consistent with the observed 30 meV donor concentration of about 2×10^{17} cm⁻³ in the irradiated sample (see Table I), because the value 2×10^{17} cm⁻³ is actually an upper limit. That is, the mobility after such a heavy irradiation is almost certainly reduced by electrical inhomogeneity, and, thus, it is artificially low, leading to artificially high donor and acceptor concentrations. However, the concentration of Zn_i should still be about twice that of V_O , and, moreover, there is abundant evidence that V_O is a deep, not shallow, donor [7–9,26]. Thus, Zn_i is a much better candidate for the irradiation donor than V_O . However, there also is evidence that isolated Zn_i is mobile

at room temperature, so that it likely has to form a complex to be stable [27,28].

A search for potential complexing partners for Zn_i immediately suggests N, which easily substitutes for O in the ZnO lattice and which indeed has a concentration of about 10^{17} cm⁻³ in ZnO material of the type we are using [29]. Thus, we have examined the formation energy, binding energy, and (0/+) transition energy of the complex Zn_i-N_O using first principles calculations. We applied density functional theory (DFT) within the local density approximation (LDA) and used Vanderbilt-type ultrasoft pseudopotentials, as implemented in the VASP code [30]. To obtain defect formation energies, defined elsewhere [31,32], a supercell approach was used, with a ZnO supercell size of 96 atoms. The main result of the calculation is that the binding energy of the Zn_i-N_O complex is about 0.9 eV; thus, the complex should be stable at room temperature. The formation energies of the N_O , Zn_i , and Zn_i-N_O species in ZnO depend on the Fermi energy and the partial pressures of the elements or, in other words, the chemical potentials of the elements, during growth. The secondary-ion mass-spectroscopy measurements [29] found a N concentration $[N]$ of about 1×10^{17} cm⁻³. Based on our calculated formation energies of N_O , Zn_i , and Zn_i-N_O , together with the measured N concentration ($[N] = [N_O] + [Zn_i-N_O]$), we estimate a N chemical potential of 0.92 eV below the N_2 precipitation limit (assuming Zn-rich and charge-neutral growth conditions and a growth temperature of 950 °C). The calculated formation energy [33] shows that, during growth, N_O^- acts as the dominant acceptor and Zn_i^{2+} as the dominant donor, with the Fermi energy pinned at about 1.0 eV above the valence band where the two defects have approximately the same energy, about 1.4 eV. The corresponding defect concentrations are on the order of 10^{17} cm⁻³. The concentration of the Zn_i-N_O complex is about 2 orders of magnitude lower, as determined from the reaction $N_O + Zn_i \rightarrow Zn_i-N_O + 0.9$ eV and the associated detailed-balance relationship $[N_O][Zn_i]/N_{site}[Zn_i-N_O] = \exp(-E_b/kT)$. Here we use $N_{site}(ZnO) = 4.28 \times 10^{22}$ cm⁻³ and $E_b = 0.9$ eV. At $T = 950$ °C, we get $[Zn_i-N_O]/[Zn_i] = 0.012$, which means that only about 1/100 of the Zn_i ions take part in formation of the complex. However, during cool-down, it is expected that the formation of the complex will accelerate, assuming a sufficiently low Zn_i diffusion barrier. As the temperature cools to about 500 °C, the quantity $[Zn_i-N_O]/[Zn_i]$ approaches unity, which means that about half of the Zn_i are already bound in the com-

TABLE I. Fitting parameters for mobility and carrier concentration data.

	E_{D1} (meV)	N_{D1} (10^{16} cm ⁻³)	E_{D2} (meV)	N_{D2} (10^{16} cm ⁻³)	E_{D3} (meV)	N_{D3} (10^{16} cm ⁻³)	N_A (10^{16} cm ⁻³)
As-grown	30	0.45	44	3.0	75	2.0	0.13
715 °C	30	0.74			75	3.2	0.7
Irradiated	30	~20			75	0.13	~20
400 °C	30	1.35			75	0.4	1.2

Manuscript Published in Physical Review Letters

PRL **95**, 225502 (2005)

PHYSICAL REVIEW LETTERS

week ending
25 NOVEMBER 2005

plexes. At room temperature, $[Zn_i-N_O]/[Zn_i] \approx 10^3$, so that nearly 100% of the Zn_i are in complexes. With other impurities (such as H_i) in the sample, the above balance conditions would vary somewhat, but the main conclusions should remain the same.

The electronic transition energy of Zn_i-N_O is somewhat uncertain, due to the well-known LDA gap error. However, our calculations show that the donor level of Zn_i-N_O is shallower than that of isolated Zn_i , which itself is argued to be a shallow donor [8,9]. In addition, a wave function analysis of Zn_i shows delocalization, which is characteristic of a shallow level. In short, although the $(0/+)$ transition energy of Zn_i-N_O cannot be accurately calculated, it is entirely consistent with the observed value of 30 meV. Further details of these calculations will be published elsewhere.

It is also interesting to compare the 0.9 eV binding energy with the activation energy for irradiation-defect annealing in ZnO, measured previously as 1.7 eV [34]. The difference between these two energies, 0.8 eV, should be the motional energy for Zn_i and is a reasonable value for an interstitial.

Other evidence for a Zn_i-N_O complex comes from optically detected magnetic resonance experiments in epitaxial N-doped ZnO [35]. An observed spin-1/2 center was consistent with a Zn interstitial, possibly in association with an N atom, since it was not observed in a sample with lower N content. Besides Zn_i , other donors, such as H, are also believed to associate with N [14,36]. However, H-N would be neutral, whereas Zn_i-N has a shallow-donor level.

Finally, other Zn_i -acceptor complexes that behave as shallow donors are also predicted to be stable. For example, very recently Wardle *et al.* [37] have used DFT to show that Zn_i-Li_{Zn} is bound by 0.7 eV and has a shallow-donor transition. This result further strengthens and generalizes our assertion that Zn_i -related shallow donors can exist and be important in as-grown ZnO.

In summary, we have carried out extensive low-temperature photoluminescence and temperature-dependent Hall-effect measurements on irradiated ZnO and have identified a defect-related donor at about 30 meV, which also exists in as-grown ZnO. We have further carried out molecular dynamics simulations, to show that the expected production rate of Zn_i is consistent with the concentrations of the 30 meV donor after irradiation, and density functional calculations to show that the Zn_i-N_O defect complex is a shallow donor with a sufficient binding energy to explain the annealing data. Thus, the conclusion is that native-defect-related donors can exist in *n*-type ZnO and contribute to its conductance.

D. C. L. and G. C. F. were supported by U.S. Air Force (F33615-00-C-5402), ARO (W911NF05C0024), SVTA, Inc., and Structured Materials Industries, Inc. (41471-010605-01). P. R. and S. L. were supported by AFOSR/AOARD (FA5209-05-P-0309) and TRF (BRG4880015 and PHD0203/2546). Work at NREL was supported by DOE/BES and EERE (DE-AC36-99GO10337).

- [1] D. C. Look, Mater. Sci. Eng. B **80**, 383 (2001).
- [2] S. J. Pearton *et al.*, Prog. Mater. Sci. **50**, 293 (2005).
- [3] P. Wagner and R. Helbig, J. Phys. Chem. Solids **35**, 327 (1974).
- [4] D. C. Look *et al.*, Solid State Commun. **105**, 399 (1998).
- [5] F. A. Kröger, *The Chemistry of Imperfect Crystals* (North-Holland, Amsterdam, 1964).
- [6] D. C. Look, J. W. Hemsky, and J. R. Sizelove, Phys. Rev. Lett. **82**, 2552 (1999).
- [7] A. F. Kohan *et al.*, Phys. Rev. B **61**, 15019 (2000).
- [8] F. Oba *et al.*, J. Appl. Phys. **90**, 824 (2001).
- [9] S. B. Zhang, S.-H. Wei, and A. Zunger, Phys. Rev. B **63**, 075205 (2001).
- [10] C. G. Van de Walle, Phys. Rev. Lett. **85**, 1012 (2000).
- [11] S. F. J. Cox *et al.*, Phys. Rev. Lett. **86**, 2601 (2001).
- [12] D. M. Hofmann *et al.*, Phys. Rev. Lett. **88**, 045504 (2002).
- [13] K. Shimomura, K. Nishiyama, and R. Kadono, Phys. Rev. Lett. **89**, 255505 (2002).
- [14] N. H. Nickel and K. Fleischer, Phys. Rev. Lett. **90**, 197402 (2003).
- [15] K. Ip *et al.*, Appl. Phys. Lett. **82**, 385 (2003).
- [16] Y. M. Strzhemechny *et al.*, Appl. Phys. Lett. **84**, 2545 (2004).
- [17] ZN Technology, 910 Columbia Street, Brea, CA 92821, USA.
- [18] B. K. Meyer *et al.*, Phys. Status Solidi B **241**, 231 (2004).
- [19] D. C. Look *et al.*, Phys. Status Solidi A **195**, 171 (2003).
- [20] D. C. Look, Semicond. Sci. Technol. **20**, S55 (2005).
- [21] D. C. Look and R. J. Molnar, Appl. Phys. Lett. **70**, 3377 (1997).
- [22] J. Nord, K. Nordlund, and J. Keinonen, Phys. Rev. B **68**, 184104 (2003).
- [23] P. Erhart, K. Albe, N. Juslin, and K. Nordlund (to be published).
- [24] J. Nord *et al.*, J. Phys. Condens. Matter **15**, 5649 (2003).
- [25] F. Agullo-Lopez, C. R. A. Catlow, and P. D. Townsend, *Point Defects in Materials* (Academic, New York, 1988).
- [26] P. Kasai, Phys. Rev. **130**, 989 (1963).
- [27] Yu. V. Gorelinskii and G. D. Watkins, Phys. Rev. B **69**, 115212 (2004).
- [28] C. Coşkun *et al.*, Semicond. Sci. Technol. **19**, 752 (2004).
- [29] D. C. Look *et al.*, Appl. Phys. Lett. **81**, 1830 (2002).
- [30] G. Kresse and J. Furthmüller, Comput. Mater. Sci. **6**, 15 (1996).
- [31] S. B. Zhang and J. E. Northrup, Phys. Rev. Lett. **67**, 2339 (1991).
- [32] S. Limpitjumnong *et al.*, Phys. Rev. Lett. **92**, 155504 (2004).
- [33] See EPAPS Document No. E-PRLTAO-030548 for the calculated defect formation energy. This document can be reached via a direct link in the online article's HTML reference section or via the EPAPS homepage (<http://www.aip.org/pubservs/epaps.html>).
- [34] D. C. Look *et al.*, Appl. Phys. Lett. **75**, 811 (1999).
- [35] G. N. Aliev *et al.*, Phys. Rev. B **70**, 115206 (2004).
- [36] N. Ohashi *et al.*, J. Appl. Phys. **93**, 6386 (2003).
- [37] M. G. Wardle, J. P. Goss, and P. R. Briddon, Phys. Rev. B **71**, 155205 (2005).

Mutual Passivation of Electrically Active and Isovalent Impurities in Dilute Nitrides

A. Janotti,¹ P. Reunchan,^{1,2} S. Limpijumnong,^{1,2} and C. G. Van de Walle¹¹Materials Department, University of California, Santa Barbara, California 93106-5050, USA²School of Physics, Suranaree University of Technology and National Synchrotron Research Center, Nakhon Ratchasima, Thailand
(Received 24 July 2007; published 30 January 2008)

Using first-principles calculations we investigate the mutual passivation of shallow donor Si and isovalent N in dilute GaAsN alloys. Instead of the recently proposed pairing of Si and N on adjacent substitutional sites ($\text{Si}_{\text{Ga}}\text{-N}_{\text{As}}$) [K. M. Yu *et al.*, Nat. Mater. **1**, 185 (2002); J. Li *et al.*, Phys. Rev. Lett. **96**, 035505 (2006)] we find that N changes the behavior of Si in dilute nitride alloys in a more dramatic way. N and Si combine into a deep-acceptor split interstitial, where Si and N share an As site [(Si-N)_{As}], with a significantly lower formation energy than that of the $\text{Si}_{\text{Ga}}\text{-N}_{\text{As}}$ pair in *n*-type GaAs and dilute GaAsN alloys. The formation of (Si-N)_{As} explains the GaAs band-gap recovery and the appearance of a photoluminescence peak at ~ 0.8 eV. This model can also be extended to Ge-doped GaAsN alloys, and correctly predicts the absence of mutual passivation in the case of column-VI dopants.

DOI: 10.1103/PhysRevLett.100.045505

PACS numbers: 61.72.-y, 71.55.Eq

Alloys of highly mismatched semiconductors offer unique opportunities for band-structure engineering. For example, when a small fraction of As atoms in GaAs is replaced by N to form GaAsN alloys, the band gap changes rapidly with increasing N concentration, decreasing by as much as 180 meV per atomic percent of N [1–4]. This behavior is markedly different from that of conventional alloys [5]: one would expect the band gap of $\text{GaAs}_{1-x}\text{N}_x$ to increase from its value in GaAs (1.5 eV) towards its value in GaN (3.4 eV) as the N content increases. This unusual behavior is of interest not only from a fundamental perspective, but also because of its significant potential in device applications [6].

As for any semiconductor, doping is essential for controlling the electrical conductivity in $\text{GaAs}_{1-x}\text{N}_x$ alloys. While the physics of *n*-type and *p*-type doping in the parent compounds GaAs and GaN is well established, doping in $\text{GaAs}_{1-x}\text{N}_x$ is much less explored. Recent reports indicate that the interaction between extrinsic dopants and N in $\text{GaAs}_{1-x}\text{N}_x$ alloys can lead to entirely new phenomena [7–10]. Yu *et al.* [7] reported that when $\text{GaAs}_{1-x}\text{N}_x$ is doped with Si, the interaction between Si and N leads to a “mutual passivation,” characterized by an increase in the band gap and an elimination of the electrical activity of the Si donor. It was observed that rapid thermal annealing of Si-doped dilute (In)GaAsN alloys at temperatures above 800 °C leads to a drastic increase in the electrical resistivity, accompanied by an increase in the band gap up to a value corresponding to the net “active” N, roughly equal to the total N concentration minus the Si concentration [7–9]. Simultaneously, a peak at ~ 0.8 eV appeared in the photoluminescence spectra [7,8]. Similar effects were observed for Ge-doped, but not for S- or Se-doped $\text{GaAs}_{1-x}\text{N}_x$ [9]. It was postulated that substitutional Si_{Ga} and Ge_{Ga} form strong bonds with N_{As} and lead to deep donor levels, eliminating the shallow-donor character of Si and Ge in $\text{GaAs}_{1-x}\text{N}_x$ alloys. On the other hand, S_{As} and Se_{As} are (at best) second-nearest neighbors of N_{As} and not

directly bonded to N_{As} ; therefore they would not suffer from the passivation effect [7–9].

First-principles calculations by Li *et al.* suggested that the $\text{Si}_{\text{Ga}}\text{-N}_{\text{As}}$ complex [Fig. 1(a)] indeed induces a deep donor level in the band gap [11]; it was predicted that in the impurity limit this state would be located at 0.23 eV below the GaAs conduction-band minimum (CMB) [11]. Li *et al.* also reported a binding energy of 0.26 eV for the $\text{Si}_{\text{Ga}}\text{-N}_{\text{As}}$ pair in the neutral charge state [11]. However, this proposed model exhibits some serious problems and discrepancies with experiment. First, a binding energy of 0.26 eV is too small to explain the formation of a high concentration of $\text{Si}_{\text{Ga}}\text{-N}_{\text{As}}$ pairs at temperatures above 800 °C. At these temperatures, we estimate that less than 40% of the Si atoms would be bonded to N_{As} in $\text{Si}_{\text{Ga}}\text{-N}_{\text{As}}$ pairs. Second, as will be shown later, their binding energy of 0.26 eV is overestimated. With a corrected binding energy, the number of complexes formed would be much smaller, in contrast to the experimental results [7–9]. Finally, the $\text{Si}_{\text{Ga}}\text{-N}_{\text{As}}$ pair does not explain the appearance of a deep-level luminescence at ~ 0.8 eV above the valence-band maximum (VBM) as observed in the experiments of Yu *et al.* [7,9].

In this Letter we show that isovalent N changes the microscopic behavior of Si donors in dilute GaAsN alloys

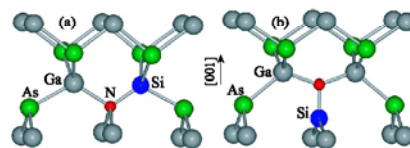


FIG. 1 (color online). Local structure of (a) $(\text{Si}_{\text{Ga}}\text{-N}_{\text{As}})^+$ and (b) $(\text{Si-N})_{\text{As}}$. In the $\text{Si}_{\text{Ga}}\text{-N}_{\text{As}}$ configuration, Si_{Ga} is a nearest neighbor of N_{As} ; in the $(\text{Si-N})_{\text{As}}$ configuration, Si and N share an As site.

in a more dramatic way. Based on first-principles density-functional calculations we find that Si combines with N into stable $(\text{Si-N})_{\text{As}}$ split interstitials that act as compensating centers in *n*-type GaAsN. The $(\text{Si-N})_{\text{As}}$ split interstitial is a *deep acceptor* with a formation energy that is significantly lower than that of $\text{Si}_{\text{Ga}}\text{-N}_{\text{As}}$ in *n*-type GaAsN. The calculated acceptor level is located at 0.89 eV above the valence-band maximum. This explains the appearance of the photoluminescence peak that accompanies the mutual passivation effect. The formation of $(\text{Si-N})_{\text{As}}$ split interstitials also leads to a blueshift in the band gap by reducing the nitrogen concentration that effectively participates in the band-gap reduction in GaAsN alloys. The formation of $(\text{Si-N})_{\text{As}}$ split interstitials in annealed Si-doped $\text{GaAs}_{1-x}\text{N}_x$ therefore leads to highly resistive alloys with a band gap governed by the net active N, in full agreement with experimental results. Our results for the electronic structure and the frequency of the local vibrational mode of the Si-N split interstitial provide a guide for further experiments on mutual passivation effects in highly mismatched semiconductor alloys.

Our calculations are based on density-functional theory (DFT) within the local density approximation (LDA) and pseudopotentials as implemented in the VASP code [12–15]. We use a plane-wave basis set with a cutoff of 400 eV. GaAsN alloys with different N concentrations were simulated by supercells containing 64, 128, or 216 atoms, in which one As was replaced by one N; this corresponds to a N content of 3.1%, 1.6%, or 0.9%, respectively. Integrations over the Brillouin zone were performed using a $2 \times 2 \times 2$ grid of Monkhorst-Pack special *k* points for the 64-atom supercell, and $1 \times 1 \times 1$ grids for 128- and 216-atom supercells. These calculations allow us to analyze trends with band gap in alloys with different nitrogen concentrations. In order to address the DFT-LDA underestimation of the band gap, we performed calculations with two different pseudopotentials: one in which the Ga 3*d* electrons are explicitly included as valence states, the other with Ga 3*d* electrons frozen in the core. The two situations produce very similar results for structure and energetics, but the “*d* in the core” potential results in a band gap that is larger by 0.15 eV.

The behavior of Si in GaAs is well established. Si predominantly occupies Ga sites and is a hydrogenic shallow donor; i.e., its extra valence electron is loosely bound and can be thermally excited to the GaAs conduction band. In GaAsN, the formation energy of Si_{Ga}^+ is given by

$$E^f(\text{Si}_{\text{Ga}}^+) = E_{\text{tot}}(\text{Si}_{\text{Ga}}^+) - E_{\text{tot}}(\text{GaAsN}) - \mu_{\text{Si}} + \mu_{\text{Ga}} + E_F, \quad (1)$$

where $E_{\text{tot}}(\text{Si}_{\text{Ga}}^+)$ is the total energy of a GaAsN supercell with one Ga replaced by one Si atom, $E_{\text{tot}}(\text{GaAsN})$ is the total energy of GaAsN in the same supercell, and μ_{Si} and μ_{Ga} are the Si and Ga chemical potentials. For Si, μ_{Si} is simply the total energy per atom in a Si crystal, $E_{\text{tot}}(\text{Si})$. μ_{Ga} , on the other hand, can vary from $\mu_{\text{Ga}} = E_{\text{tot}}(\text{Ga})$ (the

total energy per atom in a Ga crystal) under Ga-rich conditions to $\mu_{\text{Ga}} = E_{\text{tot}}(\text{Ga}) + \Delta H_f(\text{GaAsN})$ (Ga-poor conditions), where $\Delta H_f(\text{GaAsN})$ is the calculated formation enthalpy of the GaAsN alloys [16]. E_F is the Fermi-level position, which is commonly referenced to the valence-band maximum. Our calculated formation energy is shown in Fig. 2.

The binding energy of $\text{Si}_{\text{Ga}}\text{-N}_{\text{As}}$ with respect to the isolated species Si_{Ga} and N_{As} is defined as

$$E_b = E^f(\text{Si}_{\text{Ga}}) + E^f(\text{N}_{\text{As}}) - E^f(\text{Si}_{\text{Ga}}\text{-N}_{\text{As}}), \quad (2)$$

resulting in a positive E_b if the complex is lower in energy than the isolated species. If we assume both Si_{Ga} and $\text{Si}_{\text{Ga}}\text{-N}_{\text{As}}$ to be in the *positive* charge state, then the calculated binding energy is actually negative: the configuration where Si_{Ga}^+ is far away from N_{As} has an energy that is lower than that of $\text{Si}_{\text{Ga}}\text{-N}_{\text{As}}^+$ by 0.04 eV. This value differs from the result of Li *et al.* [11], who found a binding energy of 0.26 eV. Li *et al.* [11] assumed that Si_{Ga} and $\text{Si}_{\text{Ga}}\text{-N}_{\text{As}}$ would be in the *neutral* charge state; for the shallow donor Si_{Ga} this implies placing an electron in a shallow level close to the conduction-band minimum (CBM). Li *et al.* [11] used the value of the GaAs CBM in their derivation. While it is true that for purposes of defining the binding energy Si_{Ga} should be far from the N_{As} , it should be clear that in an alloy such as GaAsN the CBM is shifted down throughout the material. Therefore the formation energy of Si_{Ga}^0 should be determined using the GaAsN CBM, which is considerably lower than that of GaAs. If we strictly follow the procedure of Li *et al.*, we find $E_b = 0.27$ eV, virtually identical to their value; however, if we properly reference the formation energy of the neutral charge state to the CBM of the GaAsN alloy, the calculated binding energy is lowered to 0.11 eV. This low value (along with the negative value we obtained for the binding energy of

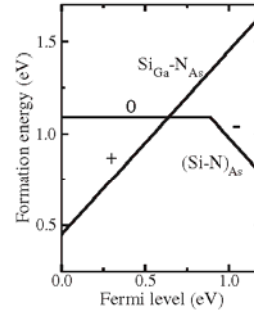


FIG. 2. Formation energy as a function of Fermi-level position for $\text{Si}_{\text{Ga}}\text{-N}_{\text{As}}$ and $(\text{Si-N})_{\text{As}}$ in GaAsN, under Ga-rich conditions. The Fermi level varies from 0 to 1.25 eV, which corresponds to the band gap of GaAsN alloys with a N concentration of about 1% [7].

the positive charge state) indicates that there is only a very weak driving force for Si_{Ga} and N_{As} to form $\text{Si}_{\text{Ga}}\text{-N}_{\text{As}}$ pairs. The assumption in previous work [7–9] that Si_{Ga} and N_{As} would form a bond that is significantly stronger than the $\text{Ga}_{\text{Ga}}\text{-N}_{\text{As}}$ bond is clearly unjustified.

A much more likely bonding configuration is found in our proposed $(\text{Si-N})_{\text{As}}$ split-interstitial complex. The formation energy of $(\text{Si-N})_{\text{As}}$ in charge state q is given by

$$E'[(\text{Si-N})_{\text{As}}^q] = E_{\text{tot}}[(\text{Si-N})_{\text{As}}^q] - E_{\text{tot}}(\text{GaAsN}) - \mu_{\text{Si}} + qE_F. \quad (3)$$

Figure 2 shows that the split interstitial can occur in the neutral and negative charge states, with a transition level $\epsilon(0/-)$ at 0.89 eV above the VBM. $(\text{Si-N})_{\text{As}}$ thus acts as a deep acceptor and is stable in the negative charge state for $E_F > 0.89$ eV.

In the $(\text{Si-N})_{\text{As}}$ configuration, Si and N are both threefold coordinated in planar geometries: Si is bonded to N and two Ga atoms, and N is bonded to Si and two other Ga atoms; the surrounding Ga atoms are all fourfold coordinated as shown in Fig. 1(b). In the neutral charge state the Si-N bond length is 1.65 Å. The N-Ga and Si-Ga bond lengths are 1.89 and 2.33 Å, and these Ga atoms are displaced outward from their nominal lattice sites by distances corresponding to 1.0% and 8.5% of the equilibrium Ga-As bond length. This is a small perturbation when compared to inward displacements of 16% for the Ga atoms surrounding an isolated N in GaAsN alloys, or 12% for the three Ga atoms surrounding the N in the $\text{Si}_{\text{Ga}}\text{-N}_{\text{As}}$ pair. Note that we did not impose any symmetry constraints in the relaxation of the Si-N configurations.

The electronic structure of the $(\text{Si-N})_{\text{As}}$ split interstitial can be understood based on electron counting: the removal of an As atom leaves four Ga dangling bonds with a total of three electrons. The $(\text{Si-N})_{\text{As}}$ pair contributes nine valence electrons, leading to a combined total of 12 electrons. Eight of these are accommodated in two N-Ga and two Si-Ga bonds. Two electrons are accommodated in a Si-N σ bond, and we are left with two electrons. The p_z orbitals on N and Si are oriented in mutually perpendicular directions, preventing the formation of a π bond. However, they still combine into a doubly occupied bonding state located near the VBM, and an empty antibonding state at 0.95 eV above the VBM. Since N is more electronegative than Si, the bonding state has more nitrogen character and the antibonding state more Si character, as shown in Fig. 3. Moreover, we observe that the band gap of GaAs is restored upon formation of the $(\text{Si-N})_{\text{As}}$ split interstitial. In our supercell, the next available Kohn-Sham state above the antibonding state is in the GaAs conduction band. Therefore the formation of the $(\text{Si-N})_{\text{As}}$ complex removes the effect of N on the band gap, but at the expense of forming a deep level.

The antibonding state at 0.95 eV (averaged over the special k points) above the VBM can in principle accept up to two electrons, corresponding to negative ($-$) and

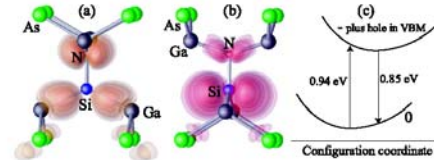


FIG. 3 (color online). Charge density isosurfaces of the (a) bonding and (b) antibonding states associated with $(\text{Si-N})_{\text{As}}$. The structure in (b) has been rotated with respect to (a) to better visualize the localization of the states. (c) Calculated configuration coordinate diagram for $(\text{Si-N})_{\text{As}}$ indicating energies at which absorption and luminescence occur.

doubly negative ($2-$) charge states of $(\text{Si-N})_{\text{As}}$. We find the $\epsilon(-/2-)$ transition level at 1.25 eV above the VBM, which places it above the CBM of the GaAsN alloy. In the $-$ and $2-$ charge states we observe a small increase in the Si-N bond length (1.68 Å) compared to the value in the neutral configuration (1.65 Å). The Ga atoms are displaced outward from their nominal lattice sites by 0.8% and 6.8% of the equilibrium Ga-As bond length.

Figure 2 also shows that the formation energy of $(\text{Si-N})_{\text{As}}$ is lower than that of the $\text{Si}_{\text{Ga}}\text{-N}_{\text{As}}$ pair for Fermi-level positions above 0.6 eV. Even under extreme Ga-poor conditions the formation energy of $(\text{Si-N})_{\text{As}}$ remains lower than that of $\text{Si}_{\text{Ga}}^+\text{-N}_{\text{As}}$ when E_F is near the CBM (as is the case in the experiments [8]). In this case the formation energy of negatively charged $(\text{Si-N})_{\text{As}}$ is 0.4 eV lower than that of positively charged $\text{Si}_{\text{Ga}}\text{-N}_{\text{As}}$. $(\text{Si-N})_{\text{As}}$ acts as a compensating acceptor in GaAsN, and charge neutrality requires that the net electron concentration is the difference between the Si_{Ga} and $(\text{Si-N})_{\text{As}}$ concentrations. Since the electron concentration is much smaller than the total Si concentration after annealing at 800 °C or above [8], we conclude that the final concentrations of Si_{Ga} and $(\text{Si-N})_{\text{As}}$ must be very close.

The formation of $(\text{Si-N})_{\text{As}}$ split interstitials can also explain the peak at ~ 0.8 eV in the photoluminescence spectra [7,9]. The exciting photons create electron-hole pairs. In the presence of holes in the valence band, negatively charged $(\text{Si-N})_{\text{As}}$ complexes can convert to neutral by emitting a photon at 0.85 eV, as shown in Fig. 3(c). We note that the position of this peak is essentially independent of the nitrogen concentration, and also not sensitive to the DFT-LDA underestimation of the gap, as checked by performing calculations with different pseudopotentials that produce different gaps.

Now we consider why the formation of $(\text{Si-N})_{\text{As}}$ in Si-doped GaAsN requires annealing at temperatures above 800 °C. Dilute GaAsN alloys are typically grown at relatively low temperatures ($T < 500$ °C) to prevent N segregation. Si can be introduced during this low-temperature growth or by ion implantation; either way, the resulting Si_{Ga} donors are unable to find their lowest-energy configu-

ration [in $(\text{Si-N})_{\text{As}}$ complexes] during this nonequilibrium incorporation process. Annealing at temperatures above 800 °C allows Si atoms to diffuse (mediated by Ga vacancies [17]) and find their equilibrium configuration, while the N atoms are locked into the lattice since their diffusion requires much higher temperatures [18]. At 800 °C the mean free path of Si is long enough for Si atoms to encounter N atoms [7–9]. Si_{Ga} then combines with N_{As} into stable $(\text{Si-N})_{\text{As}}$ split interstitials. This process involves the emission of a Ga vacancy, but since Ga vacancies are mobile at these temperatures their concentration will rapidly return to the equilibrium concentration.

Germanium is also an important candidate for n -type doping in dilute GaAsN alloys. We find that Ge also combines with N into stable $(\text{Ge-N})_{\text{As}}$ split interstitials that have lower formation energy than $\text{Ge}_{\text{Ga}}\text{-N}_{\text{As}}$ pairs. The formation of $(\text{Ge-N})_{\text{As}}$ also explains the mutual passivation between Ge and N in Ge-doped GaAsN alloys as observed by Wu *et al.* [8]. A detailed discussion of the results for Ge-doped GaAsN will be published elsewhere. Our results indicate that the formation of $(\text{Si-N})_{\text{As}}$ or $(\text{Ge-N})_{\text{As}}$ split interstitials is also likely to occur in other III–V based dilute nitride alloys, such as InGaAsN, GaPN, and InGaPN alloys.

In addition, our model nicely explains why column-VI dopants (such as S and Se) behave differently. In this case, $(\text{S-N})_{\text{As}}$ and $(\text{Se-N})_{\text{As}}$ split interstitials are less stable than the isolated S_{As} or Se_{As} donor configurations. The reason is that the column-VI donors have two more electrons than column-IV donors, and hence the antibonding state formed from p_z orbitals is occupied by two electrons in the $(\text{S-N})_{\text{As}}$ or $(\text{Se-N})_{\text{As}}$ split interstitial. This causes the formation energies of these complexes to be significantly higher [e.g., $(\text{Se-N})_{\text{As}}$ is more than 1 eV higher in energy than isolated Se_{As}], rendering them unstable with respect to the isolated species. Therefore S- or Se-doped GaAsN does not suffer from the mutual passivation effect.

Finally, we also calculated the local vibrational mode associated with the $(\text{Si-N})_{\text{As}}$ split interstitial. The calculations were performed by displacing the Si and N atoms in the three Cartesian directions and diagonalizing the force-constant matrix as described in Ref. [19]. Since the masses of N and Si are much smaller than the mass of the Ga atoms, we find that considering the displacements of Si and N alone is a good approximation. The calculated frequency of the Si-N stretch mode of $(\text{Si-N})_{\text{As}}$ is 935 cm^{-1} in the neutral charge state and 884 cm^{-1} in the negative charge state. These frequencies are much higher than the Si-N stretch frequency of 563 cm^{-1} associated with the $\text{Si}_{\text{Ga}}^+\text{-N}_{\text{As}}$ pair. These predicted vibrational frequencies can therefore serve as a guide for experimental identifica-

tion of the Si-N complex associated with the mutual passivation effect.

This work was supported in part by the MRSEC Program of the National Science Foundation under Grant No. DMR05-20415, by the NSF IMI Program under Grant No. DMR 04-09848, and by the UCSB Solid State Lighting and Display Center. It also made use of the CNSI Computing Facility under NSF Grant No. CHE-0321368. S.L. and P.R. thank the Thailand Research Fund (Grants No. BRG4880015 and No. PHD/0203/2546) and the California NanoSystems Institute for its hospitality.

- [1] M. Weyers *et al.*, Jpn. J. Appl. Phys., Part 2 **31**, L853 (1992).
- [2] J. Neugebauer and C. G. Van de Walle, Phys. Rev. B **51**, 10 568 (1995).
- [3] S.-H. Wei and A. Zunger, Phys. Rev. Lett. **76**, 664 (1996).
- [4] W. Shan *et al.*, Phys. Rev. Lett. **82**, 1221 (1999).
- [5] J. C. Woolley, in *Compound Semiconductors*, edited by R. K. Willardson and H. L. Goering (Reinhold, New York, 1962), p. 3.
- [6] Special issue on III-N-V Semiconductor Alloys, edited by J. W. Ager III and W. Walukiewicz [Semicond. Sci. Technol. **17**, 8 (2002)].
- [7] K. M. Yu, W. Walukiewicz, J. Wu, D. E. Mars, D. R. Chamberlin, M. A. Scarpula, O. D. Dubon, and J. F. Geisz, Nat. Mater. **1**, 185 (2002).
- [8] J. Wu, K. M. Yu, W. Walukiewicz, G. He, E. E. Haller, D. E. Mars, and D. R. Chamberlin, Phys. Rev. B **68**, 195202 (2003).
- [9] K. M. Yu, W. Walukiewicz, J. Wu, W. Shan, J. W. Beeman, M. A. Scarpula, O. D. Dubon, M. C. Ridgway, D. E. Mars, and D. R. Chamberlin, Appl. Phys. Lett. **83**, 2844 (2003).
- [10] Y. G. Hong, A. Nishikawa, and C. W. Tu, Appl. Phys. Lett. **83**, 5446 (2003).
- [11] J. Li, P. Carrier, and S.-H. Wei, S.-S. Li, and J.-B. Xia, Phys. Rev. Lett. **96**, 035505 (2006).
- [12] P. Hohenberg and W. Kohn, Phys. Rev. **136**, B864 (1964); W. Kohn and L. J. Sham, Phys. Rev. **140**, A1133 (1965).
- [13] P. E. Blöchl, Phys. Rev. B **50**, 17 953 (1994); G. Kresse and J. Joubert, Phys. Rev. B **59**, 1758 (1999).
- [14] D. Vanderbilt, Phys. Rev. B **32**, 8412 (1985).
- [15] G. Kresse and J. Furthmüller, Phys. Rev. B **54**, 11 169 (1996); G. Kresse and J. Furthmüller, Comput. Mater. Sci. **6**, 15 (1996).
- [16] C. G. Van de Walle and J. Neugebauer, J. Appl. Phys. **95**, 3851 (2004).
- [17] A. Janotti, S.-H. Wei, S. B. Zhang, and S. Kurtz, and C. G. Van de Walle, Phys. Rev. B **67**, 161201 (2003).
- [18] G. Bosker, N. A. Stolwijk, J. Thordson, U. Sodervall, and T. G. Andersson, Phys. Rev. Lett. **81**, 3443 (1998).
- [19] A. Janotti, S. B. Zhang, and S.-H. Wei, Phys. Rev. Lett. **88**, 125506 (2002).

PHYSICAL REVIEW B 77, 195209 (2008)

Carbon-nitrogen molecules in GaAs and GaP

Sukit Limpijumnong,^{1,2} Pakpoom Reunchan,^{1,2} Anderson Janotti,¹ and Chris G. Van de Walle¹¹Materials Department, University of California, Santa Barbara, California 93106, USA²School of Physics, Suranaree University of Technology and National Synchrotron Research Center, Nakhon Ratchasima 30000, Thailand
(Received 6 February 2008; published 21 May 2008)

A carbon-nitrogen molecule in GaAs and GaP is investigated by using first-principles density functional pseudopotential calculations. The formation energy calculations show that the molecule favors substituting for an anion site (As or P) over being an interstitial under all equilibrium growth conditions. Under *p*-type conditions, the molecule exhibits the characteristic triple bonding and acts as a donor. When the Fermi level is higher (*n* type), the molecule acts as an acceptor by accepting electrons into its antibonding states and exhibits double or single bonding. The bond length and vibrational frequencies for each configuration are calculated and compared to those in recent experiments. Trends in the changes in bond length and vibrational frequencies with respect to the number of electrons in the antibonding states are discussed.

DOI: 10.1103/PhysRevB.77.195209

PACS number(s): 61.72.-y, 71.55.Eq

I. INTRODUCTION

Small amounts of nitrogen can strongly affect the electronic properties, such as the band gap and electron effective mass, of GaP and GaAs. This opens up an opportunity to continuously modify the band gap (as well as other properties) of these III-V semiconductors for advanced electronic and optoelectronic devices. This prospect has stimulated substantial research on dilute GaAsN and GaPN alloys both experimentally¹⁻⁷ and theoretically.⁸⁻¹⁴ It is therefore very important that defects and impurities in these alloys are studied in detail. Carbon is a common impurity in various growth techniques^{15,16} and sometimes, it is intentionally used as a *p*-type dopant.¹⁷⁻²⁰ complex formations between C and N could therefore be an important issue. Recently, Ulrici and Clerjaud²¹ observed a sharp local vibration mode at 2087 cm⁻¹ (at *T*=7 K) in GaP and a similar mode in GaAs. They identified it as a CN complex with a triple bond (between C and N) aligned along the [100] direction.

An experimental work²¹ rigorously identified the chemical composition and the dipole direction of the complex; however, the actual location of the CN molecule in the lattice is still unclear. Both CN substituting on anion sites (CN_{As} in GaAs or CN_P in GaP) and interstitial CN (CN_i) are potentially consistent with experiment and were proposed as possible models in Ref. 21. In other semiconductor compounds (such as ZnO, GaN, and ZnSe), small diatomic molecules such as N₂, O₂, or CN have been studied both by first-principles calculations and by different experiments and found to prefer substitution on an anion site.^{15,22-25} However, the energy difference between the substitutional and interstitial sites varies from material to material; explicit calculations are therefore required to determine which site is more favorable for a given material.

In this paper, we use first-principles calculations to calculate the formation energies of CN_{As(or P)}} and CN_i. We find that, similar to other semiconductor compounds that have been studied before, CN energetically prefers substituting on anion sites of GaAs and GaP over interstitial sites in all thermal equilibrium growth conditions. We also calculate the vibrational frequency of the complex and find reasonable

agreement with the measured value. The CN molecule behaves very similarly in GaAs and GaP, and therefore, we will focus our discussion on CN in GaAs. Numerical results will be reported for both GaAs and GaP.

II. COMPUTATIONAL METHOD

Our calculations are performed by using density functional theory with the local density approximation (LDA).²⁶ We use ultrasoft pseudopotentials,²⁷ as implemented in the VASP code.²⁸ The Ga 3*d* electrons are treated as valence electrons. The cutoff energy for the plane-wave basis set is 262 eV. We use a supercell with 64 atoms for the defect studies, and a 2×2×2 shifted Monkhorst-Pack special *k*-point grid (Γ point not included) is employed for the Brillouin zone integration. The calculated GaAs lattice constant (5.60 Å, which is within 1% of the experimental value) is used. The electronic deep levels introduced by CN are examined by taking averages over the special *k* points. All the atoms are relaxed by minimization of the Hellmann-Feynman forces until all the forces are less than 0.05 eV/Å.

The formation energies of CN_i and CN_{As} are defined, following Refs. 22 and 29, as

$$E_f(\text{CN}_i^q) = E_{\text{tot}}(\text{CN}_i^q) - E_{\text{tot}}(\text{bulk}) - \mu_{\text{C}} - \mu_{\text{N}} + qE_F,$$

$$E_f(\text{CN}_{\text{As}}^q) = E_{\text{tot}}(\text{CN}_{\text{As}}^q) - E_{\text{tot}}(\text{bulk}) - \mu_{\text{C}} - \mu_{\text{N}} + \mu_{\text{As}} + qE_F, \quad (1)$$

where $E_{\text{tot}}(D^q)$ is the total energy of the supercell with defect *D* in charge state *q*. $E_{\text{tot}}(\text{bulk})$ is the total energy of the supercell without a defect. μ_{C} , μ_{N} , and μ_{As} are the chemical potentials of a C atom, an N atom, and an As atom, respectively. For convenience, μ_{C} and μ_{As} are referenced to the energy of a C atom in diamond and an As atom in solid As, respectively. μ_{N} is referenced to the energy of an N atom in a free N₂ molecule. Growth conditions for GaAs are close to equilibrium, requiring that $\mu_{\text{Ga}} + \mu_{\text{As}} = \mu_{\text{GaAs}} = -0.69$ eV (calculated GaAs heat of formation), where μ_{Ga} is a chemical potential of a Ga atom, which is referenced to the energy of a Ga atom in bulk Ga. E_F is the electron Fermi level with

LIMPIJUMNONG *et al.*

PHYSICAL REVIEW B 77, 195209 (2008)

respect to the valence-band maximum (VBM).

The local vibrational mode frequencies of the molecules are calculated by using the so-called frozen phonon approach,³⁰ in which we followed a practical methodology described in Ref. 31. Because C and N atoms have similar masses, we equally displaced C and N to calculate the potential energy of stretching and compressing bonds. The mass of the oscillator is taken as the reduced mass:

$$\mu = \frac{m_C m_N}{m_N + m_C}, \quad (2)$$

where m_C and m_N are the masses of C and N atoms. We find that the (harmonic) stretching vibrational frequencies of the oscillator agree very well with a full dynamic matrix calculation with the matrix constructed by displacing each and every atom in the supercell one at a time in all three principal axes directions. A test calculation (on $\text{CN}_{\text{As}}^{2+}$) shows that the agreement between the full dynamic and reduced-mass results is better than 5 cm^{-1} . An important benefit of the reduced-mass calculation (besides a significant reduction in computational effort) is that it allows us to calculate the anharmonic part of the vibration, which we found to be on the order of 20 cm^{-1} . The potential energy is evaluated at seven values of displacements, with a maximum amplitude of up to 10% of the C-N equilibrium bond distance. To test the accuracy of the approach, we calculated the stretch frequency of a C-N mode in the HCN molecule and obtained the value of 2057 cm^{-1} , which is slightly smaller than the experimental value of 2089 cm^{-1} .³² The calculated equilibrium C-N bond distance is fortuitously equal to the experimental value of 1.156 \AA . The small underestimation in vibrational frequency, which is by 32 cm^{-1} , is expected to be systematic. Therefore, we have added the value of $\omega_{\text{ER}} = 32 \text{ cm}^{-1}$ to all of our calculated frequencies as a systematic correction.

III. RESULTS AND DISCUSSION

We investigated two forms of CN molecules in GaAs: at the substitutional As site and at the interstitial site. If initially the CN molecule is symmetrically placed at the As site (in the form of a split-interstitial configuration) with its principal axis aligned along the $[100]$ direction, due to the symmetry, the orientation of the molecule will remain unchanged even when relaxation is allowed. The resulting symmetric configuration, $\text{CN}_{\text{As}}(\text{sym})$, is shown in Fig. 1(a). However, this orientation is not the lowest energy one for all charge states. Breaking the symmetry causes the molecule (in some charge states) to spontaneously rotate, without any barrier, into an asymmetric configuration [Fig. 1(b), $\text{CN}_{\text{As}}(\text{asym})$ in the $2+$ charge state].

For an interstitial CN, there are two possible sites for the zinc-blende crystal: the tetrahedral interstitial sites surrounded by either Ga [$T_d(\text{Ga})$] or As atoms [$T_d(\text{As})$]. The calculations show that CN_i energetically prefers the $T_d(\text{Ga})$ site over the $T_d(\text{As})$ site. The $T_d(\text{Ga})$ site is surrounded by four Ga atoms in a tetrahedral configuration similar to the local structure surrounding a substitutional As lattice site. Again, if the molecule is initially placed in a high-symmetry orientation, $\text{CN}_i(\text{sym})$, the orientation remains fixed by sym-

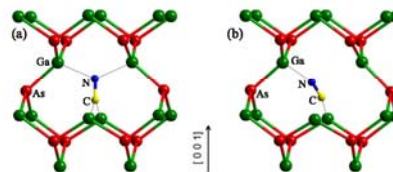


FIG. 1. (Color online) Local atomic geometry of a CN molecule substituting on an As site in GaAs: (a) symmetric configuration, $\text{CN}_{\text{As}}(\text{sym})$, and (b) asymmetric configuration, $\text{CN}_{\text{As}}(\text{asym})$. Both are shown for the $2+$ charge state.

metry, but breaking the symmetry can lead to rotation of the molecule into a lower-energy asymmetric configuration, $\text{CN}_i(\text{asym})$.

A. Substitutional CN molecules (CN_{As})

The substitutional molecule CN_{As} introduces a deep donor level (at approximately 0.25 eV) in the GaAs band gap, as shown in Fig. 2. The charge density (Fig. 3) of these levels resembles the $pp\pi^*$ molecular orbital of the CN molecule.²² The molecular orbital theory tells us that the CN molecule has the following molecular orbitals, which are in order of increasing energy: $ss\sigma$, $ss\sigma^*$, $pp\pi$ (doublet), $pp\sigma$, $pp\pi^*$ (doublet), and $pp\sigma^*$. In the neutral charge state, the CN molecule on an As site has 12 valence electrons: 9 from the CN itself and 3 more contributed from the surrounding Ga atoms. These 12 electrons occupy the CN molecular orbitals up to the lower $pp\pi^*$ level and leave the higher $pp\pi^*$ level empty. Because the lower $pp\pi^*$ level is located deep inside the GaAs band gap, CN_{As} can donate up to two electrons and become $\text{CN}_{\text{As}}^{2+}$ when the Fermi level of the system falls below the 0.25 eV donor level. The bonding between the C and N atoms in $\text{CN}_{\text{As}}^{2+}$ is a triple bond ($\text{C}\equiv\text{N}$), with a bond distance of $1.17\text{--}1.20 \text{ \AA}$ (depending on the orientation), which is in good agreement with the known triple-bond length between C and N in HCN of 1.156 \AA .³³

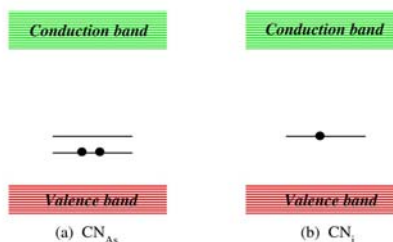


FIG. 2. (Color online) Schematic illustrations of the $pp\pi^*$ single-particle energy levels of the CN molecule in the GaAs band gap. (a) Substituting on an As site (CN_{As}) and (b) CN on an interstitial site (CN_i). The solid dots show the electron occupation for the neutral charge state.

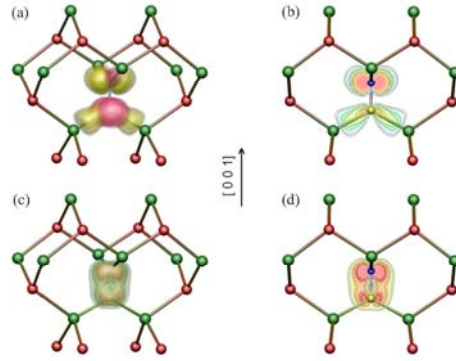


FIG. 3. (Color online) (a) Charge density of the $pp\pi^*$ states of CN_{As} that are located in the GaAs band gap. (b) Contour plot of one of the states in (a) in a (001) plane cutting through the CN molecule. (c) Charge density of one of the $pp\pi^*$ states of CN_{As} that resides below the valence-band maximum. (d) The corresponding contour plot of (c).

In the $2+$ charge state, the $pp\pi^*$ level is unoccupied; hence, the CN_{As}^{2+} has little interaction with the surrounding neighbor. The molecule can therefore rotate quite freely, and it indeed moves away from the symmetric configuration to a new orientation that has a lower energy. Our calculated energy profile for the molecule rotating from the [001] to the (near) [110] direction, which is based on the nudged elastic band (NEB) method,³⁴ is shown in Fig. 4. We can see that starting from the symmetric [001] orientation, the molecule can rotate without any barrier to a new orientation in which the molecule's principal axis is nearly parallel with the [110] direction, lowering its energy by 0.27 eV in the process. By investigating the charge density (not shown), we found that the asymmetric configuration allows better interactions

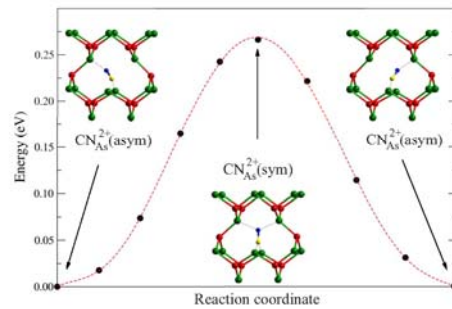


FIG. 4. (Color online) Calculated energy of CN_{As}^{2+} as the CN molecule rotates from the asymmetric to symmetric and back to an equivalent asymmetric configuration. The symmetric configuration is the saddle point along this path.

TABLE I. Calculated bond lengths d_{C-N} , stretching frequencies ω , and formation energies E_f (for the Fermi level at the VBM) of CN molecules in GaAs in the symmetric (asymmetric in parentheses) configurations. For each charge state, the lower-energy configuration is shown in boldface.

Charge state (q)	d_{C-N} (Å)	ω (cm^{-1})	E_f (eV)	
			Ga rich	As rich
CN on the As site (CN_{As})				
2+	1.20	1779	2.42	3.11
	(1.17)	(2052)	(2.15)	(2.84)
1+	1.25	1481	2.42	3.11
	(1.22)	(1734)	(2.46)	(3.15)
0	1.30	1328	2.58	3.27
	(1.25)	(1345)	(3.08)	(3.77)
1−	1.35	1173	3.13	3.82
	(1.31)	(1182)	(3.34)	(4.03)
2−	1.38	1095	4.03	4.72
	(1.40)	(1097)	(3.82)	(4.51)
CN on the interstitial site (CN_i)				
1+	1.20	1897	4.41	4.41
	(1.19)	(1934)	(3.85)	(3.85)
0	(1.25)	(1519)	(4.37)	(4.37)

between the bonding pp states of CN and two of the surrounding Ga atoms, resulting in a lower formation energy.

Starting from CN_{As}^{2+} , when the Fermi level is raised, the defect levels characteristic of $pp\pi^*$ molecular orbitals become occupied with electrons, and the charge state of CN_{As} increases from $2+$ to $1+$, 0 , $1-$, and $2-$. Because these defect states correspond to antibonding orbitals of the free molecule, occupying them leads to an increase in the CN bond length (of approximately 0.05 Å per electron added), as shown in Table I. In addition, the charge density plots [Fig. 3(a) and 3(b)] reveal that the $pp\pi^*$ states hybridize with the dangling-bond states of the surrounding Ga atoms in the directions in which the density lobes are pointing. For instance, the lower two lobes in Fig. 3(b) clearly show the bond formation between the C atom and two Ga atoms, whereas the upper two lobes still maintain the molecular $pp\pi^*$ features. Because of the possibility of bond formation with the neighboring Ga atoms, CN_{As}^{1+} , CN_{As}^0 , and CN_{As}^{1-} all favor the symmetric configuration.³⁵

CN_{As}^{2-} , on the other hand, favors an asymmetric configuration (with a different orientation from that of CN_{As}^{2+}). Because the $pp\pi^*$ states are fully occupied, the molecule tries to optimize the Coulombic interaction between these $pp\pi^*$ states and its four Ga neighbors. Since the charge distribution for the CN molecule is not symmetric (the N atom is more electronegative than the C atom), the asymmetric configuration allows the N side of the molecule to bind with three Ga atoms instead of two, making the configuration more stable.

The formation energies of CN_{As} are shown in Table I (Table II for CN in GaP) and plots as a function of Fermi level are shown in Fig. 5 for two growth conditions: Ga rich ($\mu_{Ga}=0$) and As rich ($\mu_{As}=0$). As can be seen from Eq. (1),

LIMPIJUMNONG *et al.*

PHYSICAL REVIEW B 77, 195209 (2008)

TABLE II. Calculated bond lengths d_{C-N} , stretching frequencies ω , and formation energies E_f (for the Fermi level at the VBM) of CN molecules in GaP in the symmetric (asymmetric in parentheses) configurations. For each charge state, the lower-energy configuration is shown in boldface.

Charge state (q)	d_{C-N} (Å)	ω (cm^{-1})	E_f (eV)	
			Ga rich	P rich
CN on the P site (CN_P)				
2+	1.20	1734	2.25	3.13
	(1.18)	(2028)	(2.12)	(3.00)
1+	1.25	1517	2.40	3.28
0	1.31	1352	2.75	3.63
1−	1.36	1197	3.58	4.46
	(1.33)	(1283)	(3.74)	(4.62)
2−	1.39	1113	4.77	5.65
	(1.41)	(1105)	(4.50)	(5.38)
CN on the interstitial site (CN_i)				
1+	1.21	1875	4.43	4.43
	(1.19)	(1933)	(3.96)	(3.96)
0	(1.26)	(1511)	(4.82)	(4.82)

the slope of the plot indicates the charge state of the CN molecule. In our plots, only the lowest energy charge state (at a given Fermi energy) is shown. For example, $\text{CN}_{\text{As}}(\text{asym})$ is stable in the 2+ charge state when the E_F of the system is located between 0.0 and 0.25 eV; therefore, the line has a slope of 2. For $0.25 \text{ eV} < E_F < 0.70 \text{ eV}$, the symmetric configuration becomes more stable and the neutral and 1- (for a narrow range near $E_F = 0.70 \text{ eV}$) charge states are the lowest in energy. At higher E_F , the asymmetric configuration with the 2- charge state, i.e., $\text{CN}_{\text{As}}^{2-}(\text{asym})$, becomes the most stable.³⁶ Therefore, the stable configurations in order of increasing E_F are as follows: $\text{CN}_{\text{As}}^{2+}(\text{asym})$, $\text{CN}_{\text{As}}^0(\text{sym})$, $\text{CN}_{\text{As}}^{1-}(\text{sym})$, and $\text{CN}_{\text{As}}^{2-}(\text{asym})$. $\text{CN}_{\text{As}}^{1+}$ is never stable. Because CN is substituting on the As site to form CN_{As} , its formation energy is lower in the Ga-rich condition than that in the As-rich condition. The plots also show that the formation energy of CN_{As} is always lower than that of CN_i for both the Ga- and As-rich conditions throughout the entire Fermi-energy range, with an energy difference of at least 1 eV. This implies that CN_{As} is far easier to form than CN_i .

The trends in bonding discussed above are reflected in our calculated values of vibrational frequencies, which show that the frequency is highest for $\text{CN}_{\text{As}}^{2+}$ (2052 cm^{-1} for an asymmetric configuration and 1779 cm^{-1} for a hypothetical sym-

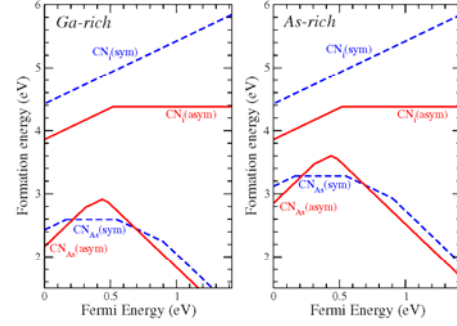


FIG. 5. (Color online) Formation energies of CN molecules in GaAs as a function of the Fermi energy. The solid lines and dashed lines represent the asymmetric and symmetric configurations, respectively.

metric configuration). This is because in the 2+ charge state, the bonding states of the molecule are all occupied and the antibonding states ($pp\pi^*$) are all empty. As electrons are added into the antibonding states of CN_{As} , the C-N bond is weakened and the frequency is reduced to 1481, 1328, 1173, and 1097 cm^{-1} for $\text{CN}_{\text{As}}^{1+}$, CN_{As}^0 , $\text{CN}_{\text{As}}^{1-}$, and $\text{CN}_{\text{As}}^{2-}$, respectively.

B. Interstitial CN molecules (CN_i)

The CN molecule has a total of nine electrons filling its molecular orbitals in the following order: $ss\sigma$, $ss\sigma^*$, $pp\pi$ (doublet), and with the last electron occupying $pp\sigma$. This leaves the $pp\sigma$ bonding state half-occupied and able to accept one more electron. Due to the strong bonding nature in the CN molecule, this $pp\sigma$ state has a low energy. When the molecule is placed in GaAs, the $pp\sigma$ state lies below the VBM and always becomes fully occupied. At the same time, the insertion of CN at an interstitial site also creates strain in nearby Ga-As bonds, leading to Ga-As bond extension (or breaking). The broken Ga-As bonds are shown in dotted lines in Fig. 6. CN_i is stable in two charge states: 1+ and neutral. We initially used symmetric configurations in our calculations [Fig. 6(a)], but this configuration can spontaneously relax into asymmetric configurations with lower energies [Fig. 6(b) and 6(c)] if symmetry breaking is allowed. The energy change as the CN_i rotates from the symmetric configuration into the asymmetric one (for 1+ charge state) calculated by using the NEB method is shown in Fig. 7. Figure 7 shows that the asymmetric configuration is favored

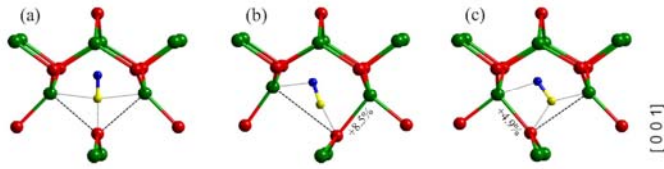


FIG. 6. (Color online) Local atomic geometry of interstitial CN molecules in GaAs: (a) $\text{CN}_i^{1+}(\text{sym})$, (b) $\text{CN}_i^{1+}(\text{asym})$, and (c) $\text{CN}_i^0(\text{asym})$.

CARBON-NITROGEN MOLECULES IN GaAs AND GaP

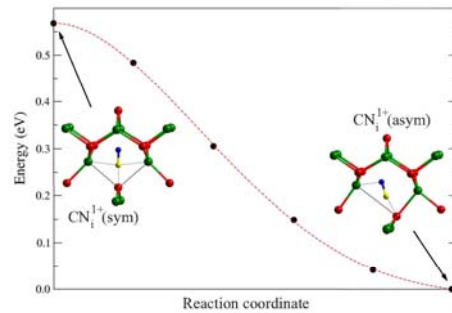


FIG. 7. (Color online) Calculated energy of CN_i^{1+} as the CN molecule rotates from a symmetric to an asymmetric configuration. The rotation occurs without any barrier and lowers the energy by almost 0.6 eV.

over the symmetric one by ~ 0.6 eV. We can clearly see in the asymmetric configuration [Fig. 6(c)] that only one of the Ga-As bonds is now broken (another bond is extended from a typical Ga-As bond). One of the two electrons released from the broken bond goes to the $pp\sigma$ state of the CN molecule, whereas another one is removed, resulting in the $1+$ charge state. As an additional electron is added (increasing the charge state of the defect from $1+$ to neutral), the additional electron goes to the $pp\pi^*$ level, which is located at approximately 0.5 eV above the VBM (see Fig. 2). This leads to the $+0$ transition level of CN_i at 0.5 eV above the VBM. The occupation of the $pp\pi^*$ level leads to the increase in the CN bond to 1.25 Å and is reflected in an enhanced binding between the molecule and its neighbors [Fig. 6(c)] compared to the $1+$ charge state [Fig. 6(b)]. Because the electron density of the $pp\pi^*$ state has four lobes pointing outward, which is similar to Fig. 3(b), when this state is occupied, the molecule can gain energy by turning the lobes to form bonds with the neighboring atoms.

Vibrational frequencies for the stretching modes of CN_i in GaAs and GaP are shown in Tables I and II. The frequency is higher for the CN_i in the $1+$ charge state, which has all the bonding states occupied and the antibonding states empty. The frequency of 1934 cm^{-1} (1897 cm^{-1} for a hypothetical symmetric configuration) is comparable to that of $\text{CN}_{\text{As}}^{2+}(\text{asym})$, which has a similar electron occupation on the molecule. For the neutral charge state CN_i , with an electron occupying the $pp\pi^*$ state, the C-N bond length increases to 1.25 Å and the vibrational frequency decreases to 1519 cm^{-1} .

C. General trends of the bond length and the vibrational frequency

Our results show that the C-N bond distance becomes larger (and the vibrational frequency becomes lower) as more electrons are added into the $pp\pi^*$ states. Our investigations of the various configurations of CN molecules in GaAs and GaP allow us to quantitatively study the relation-

PHYSICAL REVIEW B 77, 195209 (2008)

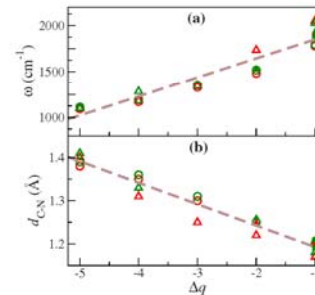


FIG. 8. (Color online) (a) Calculated vibrational frequencies and (b) C-N bond distances for various configurations of a CN molecule in GaAs and GaP as a function of charge Δq inserted into the molecule, which are measured relative to a neutral free CN molecule with nine electrons. The solid symbols are for interstitial CN and the open symbols are for substitutional CN. The colors code the host material (red for GaAs and green for GaP), whereas the symbols are used to distinguish the symmetric (circle) from the asymmetric (triangle) configurations. The CN molecule is characterized as triply, doubly, or singly bonded for $\Delta q = -1, -3$, and -5 , respectively. The dashed lines are linear fits to all of the data points.

ship between the electron occupation (of the CN molecule) and the bond length as well as the vibrational frequency. To do this, we define Δq as the additional charge being added to the CN molecule relative to the neutral free CN molecule. A free CN molecule has nine electrons, which occupy the molecular states up to half of the $pp\sigma$ state. Since this state is located below the VBM of GaAs, it is always fully occupied. This means that at least one electron from the host has to be added to the molecule ($\Delta q = -1$) and the electron occupation of the molecule becomes the same as that of a free (triple-bonded) CN^- ion. For the CN molecule in GaAs, this occupation corresponds to the lowest charge state, i.e., $\text{CN}_{\text{As}}^{2+}$ and CN_i^{1+} . As the Fermi energy is raised, electrons are inserted into the antibonding states ($pp\pi^*$ states) of the CN molecule, thus weakening the C-N bond. When two electrons are inserted into the antibonding state (i.e., CN_{As}^0), making $\Delta q = -3$, the C-N bond is reduced to a double bond instead of a triple bond. When four electrons are inserted into the antibonding states (i.e., $\text{CN}_{\text{As}}^{2-}$), making $\Delta q = -5$, the C-N bond is reduced to a single bond. Our calculations thus show that CN_{As} can have its bond strength varied from a triple bond down to a single bond depending on the electron occupation. CN_i , on the other hand, can only exhibit the bond strength of a triple bond (CN_i^{1+}) or a triple bond with one electron in the antibonding state (CN_i^0) (which can be considered as halfway between a double bond and a triple bond).

A plot of the C-N bond distance as a function of Δq is shown in Fig. 8(b). The bond distance, especially of the symmetric configurations, clearly show a linear trend with Δq . The deviations from the linear trend in the case of some of the asymmetric configurations can be attributed to the interaction with neighboring host atoms. A linear fit between the bond distance and Δq for all data points yields

LIMPIJUMNONG *et al.*PHYSICAL REVIEW B **77**, 195209 (2008)

$$d_{\text{C-N}} = -0.0496\Delta q + 1.143, \quad (3)$$

where $d_{\text{C-N}}$ is the bond distance between C and N in Å. The bond length increases by approximately 0.05 Å for every electron inserted.

The vibrational frequency decreases as the bond is extended. The relationship between the frequency and Δq is shown in Fig. 8(a). Again, a linear trend is seen. A linear fit yields

$$\omega = 207\Delta q + 2057, \quad (4)$$

where ω is the vibration frequency in cm^{-1} , i.e., the frequency is redshifted by approximately 200 cm^{-1} for every electron that is inserted. Deviations from the fit (on the order of 100 cm^{-1}) occur because the actual frequency also depends on other factors such as the detailed local geometry. Still, the linear fit in Eq. (4) nicely highlights the general trend, even if it does not provide a completely accurate prediction of the frequency.

D. Discussion and comparison with experiment

Ulrici and Clerjaud²¹ performed a polarized infrared absorption spectroscopy on C-doped dilute-nitride GaAs and GaP. They observed a sharp local vibrational mode at 2087.1 cm^{-1} (at $T=7 \text{ K}$) in GaP and a similar mode (2088.5 cm^{-1}) in GaAs. They identified it as a CN complex with a triple bond (between C and N) aligned along three equivalent $\langle 100 \rangle$ directions. Their C and N assignments were based on their observation of additional weak peaks at 2031 and 2048 cm^{-1} , which exhibit an intensity ratio and frequency shift that match the natural abundance and predicted frequency shift for C^{13} and N^{15} isotopes. The orientation of the molecule was confirmed by polarized IR absorption under different types of uniaxial stress.

An inspection of Tables I and II shows that the measured frequency of 2087 cm^{-1} is most consistent with our calculated frequencies for triply bonded CN molecules with $\Delta q = -1$. A more detailed identification runs into some complications, however. There are four configurations with triple bonds covered in our study: $\text{CN}_{\text{As}}^{2+}(\text{asym})$, $\text{CN}_{\text{As}}^{2+}(\text{sym})$, $\text{CN}_{\text{N}}^{1+}(\text{asym})$, and $\text{CN}_{\text{N}}^{1+}(\text{sym})$. (1) $\text{CN}_{\text{As}}^{2+}(\text{asym})$ provides the best matching frequency to the experiment (lower by 36 cm^{-1} , which is well within the computational error bar). However, the molecule does not align along $\langle 100 \rangle$ but, instead, prefers to align in a direction close to $\langle 110 \rangle$. (2) $\text{CN}_{\text{As}}^{2+}(\text{sym})$ has the correct orientation; however, its frequency is too low (by 309 cm^{-1}), and, even more importantly, it is not energetically stable and spontaneously rotates to $\text{CN}_{\text{As}}^{2+}(\text{asym})$, lowering the energy by 0.27 eV . Therefore, we can rule out $\text{CN}_{\text{As}}^{2+}(\text{sym})$. (3) $\text{CN}_{\text{N}}^{1+}(\text{asym})$ is a possible candidate. Its calculated vibrational frequency is not too far from the observed value (lower by 154 cm^{-1}). However, its orientation also deviated from $\langle 100 \rangle$ by 16° . In addition, the interstitial configurations are energetically unfavorable compared to those of $\text{CN}_{\text{As}}^{2+}(\text{asym})$. (4) $\text{CN}_{\text{N}}^{1+}(\text{sym})$ is an unlikely candidate because it is not energetically stable. It can spontaneously rotate to the asymmetric configuration and gain 0.6 eV . In addition, its vibrational frequency is even lower than

that of the asymmetric configuration, widening the disagreement with experiment to 191 cm^{-1} .

Our first-principles calculations of vibrational frequencies for CN molecules in various configurations in GaAs and GaP therefore generally support Ulrici and Clerjaud's²¹ assignment of the 2087 cm^{-1} mode to a triply bonded CN molecule. However, our calculations also show that the triply bonded CN molecule (in either the substitutional or interstitial configurations) does not symmetrically align in a tetrahedral site surrounded by four Ga atoms. As a result, neither CN_{As} nor CN_{N} have the C-N axis aligned in the $\langle 100 \rangle$ direction, as proposed by Ulrici and Clerjaud.²¹ However, given a rather low rotation barrier of only 0.27 eV (Fig. 4), it is possible that $\text{CN}_{\text{As}}^{2+}(\text{asym})$ is constantly rotating, resulting in an average orientation in the $\langle 100 \rangle$ direction observed in the experiment.

IV. CONCLUSIONS

We have presented first-principles results for CN molecules in GaAs and GaP. The study covered two possible lattice locations: (1) CN molecules substituting for anions ($\text{CN}_{\text{As}(\text{or P})}$) and (2) interstitial CN molecules at the T_d site surrounded by four Ga atoms (CN_i). All possible charge states and various orientations were considered. The calculated formation energies show that the molecule favors substituting for the anion site over the interstitial configuration for all equilibrium growth conditions with a margin of at least 1 eV . The calculations predict the CN molecule to produce a level with a strong $pp\pi^*$ molecular orbital characteristic at approximately $0.5\text{--}0.8 \text{ eV}$ above the VBM. In p -type conditions, where the Fermi level is located below this $pp\pi^*$ level, the molecules are triply bonded and form donor defect centers (double donor $\text{CN}_{\text{As}}^{2+}$ and single donor CN_i^{1+}). The calculations with full relaxation show that triply bonded $\text{CN}_{\text{As}}^{2+}$ and CN_i^{1+} do not symmetrically orient in the Ga tetrahedron but, instead, are tilted in order to gain better interactions with neighboring Ga atoms. The calculated vibration frequencies of the triply bonded $\text{CN}_{\text{As}}^{2+}$ and CN_i^{1+} are in reasonable agreement with the measurement by Ulrici and Clerjaud supporting their identification that the bonding is triple-bond type. Although neither CN_{As} nor CN_i have the C-N bond oriented along the $\langle 100 \rangle$ directions, as proposed by Ulrici and Clerjaud,²¹ the low rotation barrier of $\text{CN}_{\text{As}}^{2+}$ makes it possible that the molecule might be constantly rotating, leading to an average orientation in the $\langle 100 \rangle$ direction. At higher Fermi levels, the CN_i^{1+} can accept an electron and becomes CN_i^0 , whereas $\text{CN}_{\text{As}}^{2+}$ can accept one, two, three, or four electrons (depending on the Fermi level) and becomes $\text{CN}_{\text{As}}^{1+}$, CN_{As}^0 (metastable), $\text{CN}_{\text{As}}^{1-}$, or $\text{CN}_{\text{As}}^{2-}$, respectively. We found that the C-N bond length and vibrational frequency linearly change (to a good approximation) with the number of electrons added into the antibonding states of the molecule.

ACKNOWLEDGMENTS

This work was supported in part by the MRSEC Program of the National Science Foundation under Award No.

Manuscript Published in Physical Review B

CARBON-NITROGEN MOLECULES IN GaAs AND GaP

PHYSICAL REVIEW B **77**, 195209 (2008)

DMR05-20415, by the NSF IMI Program under Award No. DMR 04-09848, and by the UCSB Solid State Lighting and Display Center. This work also made use of the CNSI Computing Facility under NSF Grant No. CHE-0321368. S.L.

and P.R. thank the Thailand Research Fund (Grants No. BRG5180001 and No. PHD/0203/2546), AOARD/AFOSR (Grant No. FA4869-08-1-4007), and the California NanoSystems Institute for the hospitality.

- ¹K. M. Yu, W. Walukiewicz, J. Wu, D. E. Mars, D. R. Chamberlin, M. A. Scarpulla, O. D. Dubon, and J. F. Geisz, *Nat. Mater.* **1**, 185 (2002).
- ²W. Shan, W. Walukiewicz, J. W. Ager, E. E. Haller, J. F. Geisz, D. J. Friedman, J. M. Olson, and S. R. Kurtz, *Phys. Rev. Lett.* **82**, 1221 (1999).
- ³I. A. Buyanova, M. Izadifard, W. M. Chen, H. P. Xin, and C. W. Tu, *Phys. Rev. B* **69**, 201303(R) (2004).
- ⁴N. Q. Thitih, I. P. Vorona, I. A. Buyanova, W. M. Chen, S. Limpijumnong, S. B. Zhang, Y. G. Hong, C. W. Tu, A. Utsuni, Y. Furukawa, S. Moon, A. Wakahara, and H. Yonezu, *Phys. Rev. B* **70**, 121201(R) (2004).
- ⁵G. Pettinari, F. Masia, A. Polimeni, M. Felici, A. Frova, M. Capizzi, A. Lindsay, E. P. O'Reilly, P. J. Klar, W. Stolz, G. Bais, M. Piccin, S. Rubini, F. Martelli, and A. Franciosi, *Phys. Rev. B* **74**, 245202 (2006).
- ⁶G. Pettinari, A. Polimeni, F. Masia, R. Trotta, M. Felici, M. Capizzi, T. Niebling, W. Stolz, and P. J. Klar, *Phys. Rev. Lett.* **98**, 146402 (2007).
- ⁷G. Ciatto, F. Boscherini, A. A. Bonapasta, F. Filippone, A. Polimeni, and M. Capizzi, *Phys. Rev. B* **71**, 201301(R) (2005).
- ⁸P. R. C. Kent and A. Zunger, *Phys. Rev. B* **64**, 115208 (2001).
- ⁹M.-H. Du, S. Limpijumnong, and S. B. Zhang, *Phys. Rev. Lett.* **97**, 075503 (2006).
- ¹⁰M.-H. Du, S. Limpijumnong, and S. B. Zhang, *Phys. Rev. B* **72**, 073202 (2005).
- ¹¹K. Kim and A. Zunger, *Phys. Rev. Lett.* **86**, 2609 (2001).
- ¹²A. M. Teweldeberhan and S. Fahy, *Phys. Rev. B* **72**, 195203 (2005).
- ¹³A. Amore Bonapasta, F. Filippone, and P. Giannozzi, *Phys. Rev. B* **68**, 115202 (2003).
- ¹⁴A. Janotti, S. B. Zhang, S.-H. Wei, and C. G. Van de Walle, *Phys. Rev. Lett.* **89**, 086403 (2002).
- ¹⁵X. Li, B. Keyes, S. Asher, S. B. Zhang, S.-H. Wei, T. J. Coutts, S. Limpijumnong, and C. G. Van de Walle, *Appl. Phys. Lett.* **86**, 122107 (2005).
- ¹⁶R. E. Welser, R. S. Setzko, K. S. Stevens, E. M. Rehder, C. R. Lutz, D. S. Hill, and P. J. Zampardi, *J. Phys.: Condens. Matter* **16**, S3373 (2004).
- ¹⁷W. Songprakob, R. Zallen, W. K. Liu, and K. L. Bacher, *Phys. Rev. B* **62**, 4501 (2000).
- ¹⁸K. H. Tan, S. F. Yoon, Q. F. Huang, R. Zhang, Z. Z. Sun, J. Jiang, W. Feng, and L. H. Lee, *Phys. Rev. B* **67**, 035208 (2003).
- ¹⁹J. R. L. Fernandez, F. Cerdeira, E. A. Meneses, M. J. S. P. Brasil, J. A. N. T. Soares, A. M. Santos, O. C. Noriega, J. R. Leite, D. J. As, U. Köhler, S. Potthast, and D. G. Pacheco-Salazar, *Phys. Rev. B* **68**, 155204 (2003).
- ²⁰B.-H. Cheong and K. J. Chang, *Phys. Rev. B* **49**, 17436 (1994).
- ²¹W. Ulrici and B. Clerjaud, *Phys. Rev. B* **72**, 045203 (2005).
- ²²S. Limpijumnong, X. N. Li, S. H. Wei, and S. B. Zhang, *Appl. Phys. Lett.* **86**, 211910 (2005).
- ²³E.-C. Lee, Y. S. Kim, Y. G. Jin, and K. J. Chang, *Phys. Rev. B* **64**, 085120 (2001).
- ²⁴P. Fons, H. Tampo, A. V. Kolobov, M. Ohkubo, S. Niki, J. Tomimaga, R. Carboni, F. Boscherini, and S. Friedrich, *Phys. Rev. Lett.* **96**, 045504 (2006).
- ²⁵A. Janotti and C. G. Van de Walle, *Phys. Rev. B* **76**, 165202 (2007).
- ²⁶LDA provides a lattice constant of bulk GaP that is slightly in better agreement with that of experiment. On the other hand, generalized gradient approximation (GGA) provide a slightly better lattice constant for GaAs. Test calculations show that the choice of LDA/GGA only slightly affects the numerical value of energy and vibration frequency but does not change the main conclusions.
- ²⁷D. Vanderbilt, *Phys. Rev. B* **41**, 7892 (1990).
- ²⁸G. Kresse and J. Furthmüller, *Comput. Mater. Sci.* **6**, 15 (1996).
- ²⁹S. B. Zhang and J. E. Northrup, *Phys. Rev. Lett.* **67**, 2339 (1991).
- ³⁰J. Ashkenazi, *Phys. Rev. B* **26**, 1512 (1982).
- ³¹S. Limpijumnong, J. E. Northrup, and C. G. Van de Walle, *Phys. Rev. B* **68**, 075206 (2003).
- ³²K. Kim and W. T. King, *J. Chem. Phys.* **71**, 1967 (1979).
- ³³G. Herzberg, *Molecular Spectra and Molecular Structure: Electronic Spectra and Electronic Structure of Polyatomic Molecules* (Van Nostrand, New York, 1966).
- ³⁴H. Jónsson, G. Mills, and K. W. Jacobsen, in *Classical and Quantum Dynamics in Condensed Phase Simulations*, edited by B. J. Berne, G. Cicciotti, and D. F. Coker (World Scientific, Singapore, 1998), p. 385.
- ³⁵CN_{AS} in the +1 and 0 charge states is stable in the symmetric configuration. Test calculations for 1+ showed that a dimer initially tilted by as much as 15° away from the symmetric direction, i.e., the [001] direction, spontaneously rotated back after relaxations. The asymmetric configurations are only metastable. The (higher-energy) metastable asymmetric configuration for each charge state is found by initially aligning the CN molecule along the [110] direction and allowing relaxation of its neighbors before letting the molecule itself relax. The metastable asymmetric configurations are higher in energy than the symmetric ones by 0.1 and 0.5 eV for the 1+ and neutral charge states, respectively. The dimer qualitatively behaves the same in GaP except that none of the metastable asymmetric configurations exists.
- ³⁶Although the calculated LDA band gap (at the Γ point) for GaAs is only 0.6 eV, our calculations are performed at special k points wherein the lowest conduction band occurs at 1.08 eV above the VBM. Any defect levels that lie below 1.08 eV are therefore accounted for and can be properly occupied.

Abstract submitted for the First National Symposium on Physics Graduate Research,

Chaiya Phum (2006)

A nitrogen-carbon molecule in GaAs : A first principles study

โมเลกุลไนโตรเจน-คาร์บอนในแกเลียมอาร์เซไนด์ : การศึกษาแบบเฟิสต์-พริ้นซิเพิล

Sukit Limpijumnong and Pakpoom Reunchan*

*School of Physics, Institute of Science, Suranaree University of Technology
and National Synchrotron Research Center, Nakhon Ratchasima, Thailand*

First-principles calculation shows that NC molecule prefers to occupy the anion (As or P) site over the interstitial site in GaAs. Both CN molecules occupying the anion site and the interstitial site maintain their molecular characteristics rather well. The C-N bond distances and vibration frequencies are comparable to those of a free molecule. The calculated vibration frequencies of the CN molecules occupying the anion sites in GaAs are in a good agreement (within a computational error bar) with the recent infrared spectroscopy measurement [W. Ulrici and B. Clerjaud, Phys. Rev. B 72, 045203 (2005)].

การศึกษแบบเฟิสต์-พริ้นซิเพิล แสดงให้เห็นว่าโมเลกุลไนโตรเจน-คาร์บอนมักจะไปอยู่แทนที่ตำแหน่งของแอนไอออนมากกว่าตำแหน่งของช่องว่างในผลึกแกเลียมอาร์เซไนด์ ในทั้งสองตำแหน่งโมเลกุลไนโตรเจน-คาร์บอน ยังคงรักษาคุณสมบัติของโมเลกุลไว้ ความยาวพันธะและความถี่ของการสั่นยังอยู่ในช่วงที่เปรียบเทียบกับโมเลกุลอิสระได้ ความถี่ในการสั่นที่คำนวณได้ของโมเลกุลไนโตรเจน-คาร์บอนที่ไปแทนที่ตำแหน่งแอนไอออนในผลึกแกเลียมอาร์เซไนด์สอดคล้องกับผลการทดลองการวัดอินฟราเรด-สเปกโตรสโกปีเมื่อเร็ว ๆ นี้ [W. Ulrici and B. Clerjaud, Phys. Rev. B 72, 045203 (2005)].

PACS numbers: 61.72.Ji, 78.30.Fs, 63.20.Pw

Keywords: first-principles, complexes, local vibration modes

Abstract submitted for the Siam Physics Congress 2008, Nakhon Ratchasima (2008)

SPC2008
NAKHON RATCHASIMA, THAILAND

Mutual Passivation of Electrically Active and Isovalent Impurities in GaAsN Alloys

**Pakpoom Reunchan,^{1,2} Anderson Janotti,¹
Sukit Limpijumnong,^{1,2} and Chris G. Van de Walle¹**

¹ Department of Materials, University of California, Santa Barbara, CA 93106

² School of Physics, Suranaree University of Technology and National
Synchrotron Research Center, Nakhon Ratchasima, Thailand

Abstract

Recent experiments found that Si can reverse the band-gap-narrowing effect induced by nitrogen in GaAs; simultaneously, the electrical activity of Si as a shallow donor is deactivated [K.M. Yu *et al.*, Nat. Mater. **1**, 185 (2002)]. The process is known as “mutual passivation”. The formation of a substitutional pair ($\text{Si}_{\text{Ga}}\text{-N}_{\text{As}}$) was proposed to be the cause of the mutual passivation. However, using first-principles calculations we find that the Si_{Ga} and N_{As} do not bind into the $\text{Si}_{\text{Ga}}\text{-N}_{\text{As}}$ pair. Si and N actually much more prefer to bind to each other and share an As-site in the form of a $(\text{Si-N})_{\text{As}}$ “split interstitial” complex, which has a low formation energy in *n*-type GaAsN alloys. The $(\text{Si-N})_{\text{As}}$ pair creates a deep level in the band gap which acts as a deep acceptor; simultaneously the band gap is restored back to that of GaAs.

Keyword: passivation, complex, GaAsN alloys, first principles calculations

Abstract submitted for the RGJ-Ph.D. Congress IX, Chon Buri (2008)

A carbon-nitrogen molecule in GaAs: a first principles study

Pakpoom Reunchan^{a,b}, Sukit Limpijumnong^{a,b}, Anderson Janotti^a, and Chris G. Van de Walle^a

^a*Department of Materials, University of California, Santa Barbara, CA 93106*

^b*School of Physics, Suranaree University of Technology and National Synchrotron Research Center, Nakhon Ratchasima, Thailand*

Introduction and Objective

Small amount of N can strongly affect the electronic properties of GaAs, thus it is important to study defects and impurities in GaAsN alloys. Because carbon is a common impurity in many semiconductors, including GaAs, the complex between C and N is studied in detail.

Methods

The CN defects are studied using first principles supercell approach [1]. The calculations are performed based on the density functional theory (DFT) with the local density approximation (LDA) [2]. The supercell size of 64 atoms is used and all atoms are allowed to relax to their equilibrium.

Results

Energetically, CN molecule prefers to occupy an As site (CN_{As}) over an interstitial site (CN_i). Under *p*-type conditions, CN_{As} is stable in 2+ charge state ($\text{CN}_{\text{As}}^{2+}$). We found that the molecule is the most stable in asymmetric configuration which has energy lower than the symmetric configuration by 0.26 eV. The vibration frequency of the asymmetric $\text{CN}_{\text{As}}^{2+}$ is 2020 cm^{-1} , in agreement with the experimental value to within the computational error bar [3-4].

Conclusion

Based on first principles calculations, we found that a CN molecule is the most stable when substituting on an As-site (CN_{As}) in GaAs and is stable in 2+ charge state under *p*-type conditions. The detail investigation of the configuration shows that the molecule prefers to rotate into an asymmetric configuration. The calculated vibrational frequency of the molecule is in good agreement with the value from an available infrared absorption experiment [5].

Keywords: density functional theory, GaAs, CN molecule, complex

Selected References:

1. A. Janotti, P. Reunchan, S. Limpijumnong, and C. G. Van de Walle, *Phys. Rev. Lett.* **100**, 045505 (2008).
2. W. Kohn and L. J. Sham, *Phys. Rev.* **140** A1133 (1965); G. Kresse and J. Furthmüller, *Comput. Mater. Sci.* **6**, 15 (1996).
3. S. Limpijumnong, X. N. Li, S. H. Wei, and S. B. Zhang, *Appl. Phys. Lett.* **86**, 211910 (2005).
4. S. Limpijumnong, J. E. Northrup, and C. G. Van de Walle, *Phys. Rev. B.* **68**, 075206 (2003).
5. W. Ulrici and B. Clerjaud, *Phys. Rev. B.* **72**, 045203 (2005).

Abstract submitted for the 34th Congress on Science and Technology of Thailand,
Bangkok (2008)

คาร์บอน-ไนโตรเจนโมเลกุลในแกเลียมอาเซไนด์

CARBON-NITROGEN MOLECULE IN GALLIUM ARSENIDE

ภาณุภูมิ เรือนจันทร์,^{1,2} สุกิจ ลิ้มปิจนงค์,^{1,2} Anderson Janotti,¹ และ Chris G. Van de Walle¹

Pakpoom Reunchan,^{1,2} Sukit Limpijumnong,^{1,2} Anderson Janotti,¹ and Chris G. Van de Walle¹

¹Department of Materials, University of California, Santa Barbara, CA 93106

²School of Physics, Suranaree University of Technology and National Synchrotron Research Center, Nakhon Ratchasima, Thailand

บทคัดย่อ : คุณสมบัติทางไฟฟ้าของแกเลียมอาเซไนด์สามารถถูกเปลี่ยนแปลงได้อย่างมากด้วยการเจือด้วยไนโตรเจนในปริมาณน้อยๆ ดังนั้นจึงเป็นที่สนใจในวงกว้างในการศึกษาความบกพร่องและสารเจือ GaAsN ในอัลลอย สำหรับคาร์บอนนั้น เป็นสารเจือที่พบได้ในสารกึ่งตัวนำทั่วไป รวมถึงแกเลียมอาเซไนด์ด้วย ดังนั้น ความบกพร่องแบบซับซ้อนระหว่างคาร์บอนและไนโตรเจนจึงน่าจะเกิดได้ทั่วไป ในงานวิจัยนี้ความบกพร่องดังกล่าวจึงได้ถูกศึกษาโดยใช้การคำนวณแบบเฟิร์สพริ้นซิเปิล โดยการจำลองความบกพร่องในผลึกทำโดยใช้ซูเปอร์เซลล์ขนาด 64 อะตอมและทุกอะตอมถูกปล่อยให้เคลื่อนเข้าสู่ในสภาพสมดุล พบว่าคาร์บอน และ ไนโตรเจน ชอบที่จะจับตัวกันเป็น CN โมเลกุล และ โมเลกุลนี้ชอบที่จะอยู่แทนที่ตำแหน่งของอาร์เซนิกอะตอม (CN_{As}) มากกว่าที่จะไปอยู่ที่ตำแหน่งช่องว่าง (CN_i) ซึ่ง ในสถานะที่ GaAs มีสภาพเป็นตัวนำชนิด p (p -type) CN_{As} จะมีขั้วประจุเสถียร $2+$ ความถี่การสั่นที่คำนวณได้ของ CN_{As}^{2+} คือ 2052 cm^{-1} ซึ่งสอดคล้องกับผลการทดลองของการดูดกลืนแสงในย่านอินฟราเรด

Abstract: Small amount of N can strongly affect the electronic properties of GaAs, thus it is of great current interests to study defects and impurities in GaAsN alloys. Carbon is a common impurity in many semiconductors, including GaAs. Thus, the complexes between carbon and nitrogen are highly probable. In this work, the complex is studied using first principles supercell approach. The supercell size of 64 atoms is used and all atoms are allowed to relax to their equilibrium positions. We found that carbon and nitrogen prefer to bind each other and form a CN molecule. Energetically, the CN molecule prefers to occupy an As site (CN_{As}) over an interstitial site (CN_i). Under p -type conditions, CN_{As} is stable in $2+$ charge state (CN_{As}^{2+}). The vibration frequency of CN_{As}^{2+} is 2052 cm^{-1} , in good agreement with the value from an infrared absorption experiment.

Keyword: first principles, GaAs, CN molecule, complex

References:

1. Sukit Limpijumnong, Pakpoom Reunchan, Anderson Janotti, and Chris G. Van de Walle, Phys. Rev. **B** 77, 195209 (2008).
2. W. Ulrici and B. Clerjaud, Phys. Rev. **B** 72, 045203 (2005).

Abstract submitted for the Siam Physics Congress 2009, Phetcha Buri (2009)

SPC2009
CHA-AM, PHETCHBURI, THAILAND

Poster Presentation

Vacancy Defects in Indium Oxide

***Pakpoom Reunchan,^{1,2} Sukit Limpijumnong,^{1,2}
Anderson Janotti,¹ and C.G. Van de Walle¹***

¹Materials Department, University of California, Santa Barbara, California 93106

²School of Physics, Suranaree University of Technology and Synchrotron Light
Research Institute, Nakhon Ratchasima 30000, Thailand

Abstract

First-principles density functional theory is used to investigate the electronic behavior of oxygen and indium vacancies in In_2O_3 . Based on the recently revised In_2O_3 band gap of 2.9 eV, oxygen vacancy is found to be a deep donor and have high formation energy in *n*-type materials. It is thus unlikely to be a source of *n*-type conductivity that commonly observed in as-grown In_2O_3 . Indium vacancy acts as triple acceptor with high formation energy in p-type materials. Somewhat it can play a role as a compensation center for *n*-type doping.

Keyword: vacancy defects, indium oxide, first-principles calculations

Abstract submitted for the Junior Research Group seminar 2009, Pohang, South
Korea (2009)

Diatomic Molecules in Dilute Nitrides: A First-Principles Study

Pakpoom Reunchan and Sukit Limpijumnong

*Research Center in Computation and Theoretical Physics/TheP Center, School of Physics, Suranaree
University of Technology, Nakhon Ratchasima 30000, Thailand
Synchrotron Light Research Institute, Nakhon Ratchasima 30000, Thailand*

Based on first-principles density functional calculations we investigated behavior of electrically active impurities incorporated in dilute GaAsN alloys. We found that both C and Si are not likely to present as ordinary substitutional defects but form bond to N into diatomic molecules. The formation energy calculations show that the molecule favors substituting for an anion site over being an interstitial under all equilibrium growth conditions. N changes the behavior of C and Si in GaAsN alloys in more dramatic way. The $(\text{C-N})_{\text{As}}$ acts as a donor in p -type materials and as an acceptor when Fermi level is raised up to n -type region. The $(\text{Si-N})_{\text{As}}$ is found to be a deep-acceptor split interstitial and also explain the GaAs band gap recovery and donor compensation in experimental observation of mutual passivation effect in dilute nitrides.

Abstract submitted for the International Conference on Materials for Advanced
Technologies 2009, Singapore (2009)

**FIRST PRINCIPLES STUDY OF GALLIUM-FRENKEL PAIRS IN GALLIUM
NITRIDE**

Pakpoom Reunchan and Sukit Limpijumnong

*Research Center in Computation and Theoretical Physics/ThEP Center, School of Physics, Suranaree
University of Technology, Nakhon Ratchasima 30000, Thailand*

Synchrotron Light Research Institute, Nakhon Ratchasima 30000, Thailand

Based on first-principles density functional calculations, we investigated defect complexes between a gallium interstitial and a gallium vacancy (Ga-Frenkel pairs) in GaN. We found that when a Ga interstitial is directly placed next to a Ga vacancy, the complex is not stable against spontaneous recombination, i.e., the Ga interstitial occupies the vacancy. The first stable complex occurs when the Ga interstitial is placed on the next interstitial site away from the vacancy. The complex is bound with a high binding energy and maintains the neutral charge state at almost entire Fermi range. The binding energy is reduced when the separation (between the Ga interstitial and the Ga vacancy) is increased. The energy profiles for the recombination of the defect complexes are also calculated and the recombination barrier is determined. Our results indicated that the Ga-frenkel pairs are unlikely to form in nature but can be stable in low-temperature electron irradiated-GaN samples.

The work was partially supported by AOARD/AFOSR (Grant No.FA4869-08-1-4007) and Thailand Research Fund (Grants No. BRG5180001 and No. PHD/0203/2546). The authors thank Prof. David C. Look for suggesting the research topic to us and for helpful discussions.

CURRICULUM VITAE

Mr. Pakpoom Reunchan was born on June 22nd, 1981. He finished his high school from Benjamachutit Ratchaburi. After that he received full scholarship for the one who has talents in science and technology (DPST) to study physics at Kasetsart University. He received his B.Sc. in physics (second-class honors) in 2003. In the same year, he joined the Ph.D. program at Suranaree University of Technology. He was granted by the Thai Research Fund for a Royal Golden Jubilee scholarship (RJG) for his Ph.D. program under the supervision of Prof. Dr. Sukit Limpijumnong on the first year. His works focus on applying first-principles methods to study defects in semiconductors. During Sep 2006- June 2007, he did a practical training at Materials Department University of California Santa Barbara under supervision of Dr. Anderson Janotti and Prof. Dr. Chris. G. Van de Walle. He has contributed in a number of national/international conferences where he got two awards for the outstanding oral presentation. He has got academic award for the outstanding research from Suranaree University of Technology in 2008. He has also contributes in three publications in high impact journals as the co-author.